NUREG/CR-0011

LMFBR FUEL ANALYSIS
TASK A: OXIDE FUEL DYNAMICS

Final Report

October 1, 1976 - September 30, 1977

V. K. Dhir
J. Doshi
M. Frank
B. Hauss
W. E. Kastenberg
K. Wong

University of California, Los Angeles

Prepared for

U. S. Nuclear Regulatory Commission

DISCLAIMER

NOTICE

This report was prepared as an account of work sponsored by the United States Government. Neither the United States nor the United States Nuclear Regulatory Commission, nor any of their employees, nor any of their contractors, subcontractors, or their employees, makes any warranty, express or implied, nor assumes any legal liability or responsibility for the accuracy, completeness or usefulness of any information, apparatus, product or process disclosed, nor represents that its use would not infringe privately owned rights.

Available from
National Technical Information Service
Springfield, Virginia 22161
Price: Printed Copy $7.25 ; Microfiche $3.00

The price of this document for requesters outside of the North American Continent can be obtained from the National Technical Information Service.

NUREG/CR-0011

LMFBR FUEL ANALYSIS
TASK A: OXIDE FUEL DYNAMICS

Final Report
October 1, 1976 - September 30, 1977

V. K. Dhir
J. Doshi
M. Frank
B. Hauss
W. E. Kastenberg
K. Wong

Manuscript Completed: October 1977
Date Published: February 1978

University of California, Los Angeles
Department of Chemical, Nuclear, and Thermal Engineering
Los Angeles, CA 90024

Prepared for
Division of Project Management
Office of Nuclear Reactor Regulation
U. S. Nuclear Regulatory Commission
Under Contract No. NRC-03-77-001

Task A

Oxide Fuel Dynamics

The study presented in Task A deals with several areas of uncertainty in the analysis of the unprotected overpower transient for the Clinch River Breeder Reactor. These areas of uncertainty include the time, place, and mode of fuel pin failure; pre-failure fuel motion; fuel freezing, plugging, and plate-out following pin failure; and the potential for re-criticality.

Internal molten fuel motion prior to pin failure was found to be sensitive to ramp rate and burnup. The strain-limit fuel failure criterion was found to be inappropriate for analysis based on existing data. The coupling of pre-transient- and transient-induced stresses tended to force the failure location towards the core midplane.

Analysis of post-failure thermal hydraulics continues to exhibit a tendency for fuel freezing and channel plugging. Lastly, several configurations of partially disrupted cores exhibit a propensity for re-criticality.

Blank Page

PREFACE

The report presented here represents a summary of work accomplished as part of the Technical Assistance Program, U.S. Nuclear Regulatory Commission, Division of Project Management. In particular, this final report for the period October 1, 1976 - September 30, 1977, (TASK A: OXIDE FUEL DYNAMICS) is concerned with oxide fuel behavior in LMFBR's during postulated unprotected overpower transients.

The help of Drs. J. F. Meyer and T. Speis of the Nuclear Regulatory Commission Staff is greatly acknowledged. The models and computer code used in the analysis of fuel freezing and plugging were developed under the support of the Division of Reactor Safety Research, NRC. The models and computer code used in the evaluation of internal fuel motion were developed under the support of the Electric Power Research Institute as part of the Ph.D. dissertation of Michael Frank.

The report presented here is the fifth in a series of final reports as follows:

1. "Transient Analysis of LMFBR Oxide Fuel Elements During Accidents," R. C. Erdmann, UCLA-ENG-7362, August 1973.
2. "Transient Analysis of LMFBR Oxide Fuel Elements During Accidents," W. E. Kastenberg, UCLA-ENG-7468, August 1974.
3. "Preliminary Analysis of the Transient Overpower Accident for CRBRP," W. E. Kastenberg and M. Frank, UCLA-ENG-7557, July 1975.
4. "LMFBR Fuel Analysis, Task A: Oxide Fuel Dynamics," W. E. Kastenberg, NUREG-0146, January 1977.

Blank Page

ABSTRACT

The study presented in this report deals with several areas of uncertainty in the analysis of the unprotected overpower transient for the Clinch River Breeder Reactor. These areas of uncertainty include the time, place, and mode of fuel pin failure; pre-failure fuel motion; fuel freezing, plugging, and plate-out following pin failure; and the potential for re-criticality.

Internal molten fuel motion prior to pin failure was found to be sensitive to ramp rate and burnup. The strain-limit fuel failure criterion was found to be inappropriate for analysis based on existing data. The coupling of pre-transient- and transient-induced stresses tended to force the failure location towards the core midplane.

Analysis of post-failure thermal hydraulics continues to exhibit a tendency for fuel freezing and channel plugging. Lastly, several configurations of partially disrupted cores exhibit a propensity for re-criticality.

Blank Page

TABLE OF CONTENTS

LIST OF FIGURES

Blank Page

LIST OF TABLES

1.0 INTRODUCTION

The transient overpower accident (TOP) is postulated to be initiated by a continuous ramp reactivity insertion accompanied by failure of all plant protective systems (failure to scram). This reactivity insertion causes the power to rise while the coolant maintains steady flow. Early analysis of the TOP was based on postulated ramp rates, varying between \$15/sec and \$50/sec [1-3]. Attempts at mechanistically describing this initiating ramp rate yielded TOP analyses based on a range of 50¢/sec to \$15.0/sec [4-6]. Ramp rates in this range were associated, for example, with a bubble moving through the most reactive portion of the core [4] or for the ejection of a control rod [5,6].

For the Clinch River Breeder Reactor Plant (CRBRP), the PSAR argues that only moderate reactivity insertions could be realistically postulated to occur rapidly [7]. In particular, the reactivity insertions selected for initiators in CRBRP, are those corresponding to a continuous rod withdrawal at full power. The design value specified in the PSAR and used in subsequent analysis [7,8] is 2.4¢/sec, and the total magnitude of reactivity insertion is limited to the maximum expected worth of one control rod, or \$3.20, with an uncertainty of ±15%.

For accident evaluation purposes, Appendix F of the PSAR (as amended) considers a range of initiators, which includes 2.4¢/sec, 10¢/sec and 50¢/sec. Analysis of the response of CRBRP to initiating ramp rates as low as 1¢/sec have also been carried out [9,10] with the SAS-3A computer code [11].

For initiating ramp rates on the order of \$5.0/sec or greater, the power rises rapidly in the reactor and the fuel heats up nearly adiabatically. Doppler feedback keeps the net reactivity below prompt critical,

until sufficient energy generated in the fuel causes clad failure. For these rather large ramp rates, most models predict midplane clad failures [12-14]. Midplane failures usually lead to termination of the transient by hydrodynamic disassembly of the core [4-7]. This hydrodynamic disassembly occurs because midplane failures lead to sodium voiding in the central core zones and the initial fuel motion is towards the midplane.

For initiating ramp rates below 50¢/sec, the description of events becomes less clear. These "mild" ramp rates cause a much slower progression of events. Such an expanded time scale may heighten the importance of various pre-failure as well as post-failure phenomena which are neglected in current TOP computer codes (i.e., SAS-3A [11], MELT III [15], and HOPE [16]).

Pre-failure phenomena which have been neglected and have been identified as having the possibility of being important include a) pre-failure fuel motion, b) fission gas behavior, including gas pressure communication with the plenum, c) fuel cracking and healing and d) heat transfer, including pre-failure sodium boiling [10,17]. Post-failure phenomena which have been identified as having the possibility of being important, include a) freezing, plugging and plate-out of fuel, b) fuel remelting and c) potential for recriticality. In this context, the degree of coolability following the transient has been treated, but only superficially [8,18,19].

This report summarizes the results of studies conducted in support of the U.S. Nuclear Regulatory Commission's review of the PSAR for the CRBRP. In particular, it deals with several areas of uncertainty pertaining to the unprotected overpower transient. These areas of uncertainty

include the time, place and mode of fuel pin failure and the phenomena associated with transient overpower accidents initiated by slow or mild ramp rates.

In Chapter 2, the question of fuel pin motion prior to clad failure is addressed. A model developed for GCFR fuel pins (which are manufactured with annular pellets) is employed to examine CRBRP fuel pins [20]. This phenomenon is associated with slow ramp rates.

In Chapter 3, fuel pin failure models are addressed. Calculations based on a clad failure criterion developed by Dr. Ira Levy at the Battelle Pacific Northwest Laboratories [17], are presented. In addition, preliminary calculations based on a time-dependent version [20] of Dr. Sun's model [21], for calculating clad and fuel, stress and strain are presented. This is a generic question for the TOP.

In Chapter 4, the question of fuel freezing, plugging and plate-out is addressed. In addition, the degree of thermal loading,core coolability and potential for reactivity insertion is discussed. The work presented is based on the Ph.D. dissertation of Dr. Kin Wong [22]. The analysis presented is of generic importance, but may be particularly important for slow ramp rates.

Chapter 5 contains a discussion of potential recriticality. Preliminary results are presented for several configurations which might arise. This work, while also of a generic nature, has particular importance for slow ramp rates. Chapter 6 contains a summary and conclusions.

1.1 References for Chapter 1.0

1. Lorenzini, P. G. and G. F. Flannagan, "An Evaluation of Fuel-Coolant interactions During Disassembly of an LMFBR," USAEC-CONF-710302, March 1971.

2. Mills, J. C. and W. E. Kastenberg, "An Axial Kinetics Model for LMFBR Disassembly Accidents," USAEC-CONF-710302, March 1971.

3. Mills, J. C. and W. E. Kastenberg, "An Evaluation of Fuel-Coolant Interactions on Kinetics During Fast Reactor Disassembly Accidents," Proceedings of the International Conference on Fast Reactors for Safe and Reliable Operation, Karlsrühe, Germany, October 1972.

4. Heusener, G., G. Kessler, et.al., "Analysis of Hypothetical Accidents for SNR-300" KFK-1834, Nuclear Research Center, Karlsrühe, West Germany, September 1973.

5. Waltar, A. E., N. P. Wilburn, et.al., "An Analysis of the Unprotected Transient Overpower Accident in the FTR" HEDL-TME-75-50, Hanford Engineering and Development Laboratory, June 1975.

6. Kastenberg, W. E. and M. V. Frank, "Preliminary Analysis of the Transient Overpower Accident for CRBRP," UCLA-ENG-7557, July 1975.

7. Preliminary Safety Analysis Report, Clinch River Breeder Reactor, Project Management Corporation, (1975), Docket No. 50-537.

8. Amendments 5, 19, and 23. Preliminary Safety Analysis Report, Clinch River Breeder Reactor, Project Management Corporation, (1975), Docket No. 50-537.

9. Bohl, W. R., et.al., "An Analysis of Transient Undercooling and Transient Overpower Accidents without Scram in the Clinch River Breeder Reactor," ANL/RAS 75-29, Argonne National Laboratory, July 1975.

10. Haas, P. M., T. Ginsberg, and T. P. Henry, "Analysis of Low Ramp TOP Accidents in the EOEC Core of the CRBR," Technical Note: BNL 21000, Brookhaven National Laboratory, November 3, 1975.

11. Dunn, F. E., W. R. Bohl, and T. J. Heames, "The SAS 3A LMFBR Accident Analysis Computer Code," ANL/RAS 75-17. Argonne National Laboratory, 1975.

12. Smith, L. L. and M. G. Stevenson, "Effect of Reactivity Insertion Rate on Fuel Pin Failure Threshold," Trans. Amer. Nuc. Soc. Vol. 17, November 1973, pp. 284-285.

13. Scott, J. H., et.al., "Microstructural Dependence of Failure in Mixed-Oxide LMFBR Fuel Pins," CONF-740401, Beverly Hills, California 1974.

14. Rumble, E. T., et.al., "Fuel Movement Investigations During LMFBR Overpower Excursions Using a New Model," CONF-740401, Beverly Hills, California, 1974.

15. Waltar, A. E., W. L. Partain, et.al., "MELT-III - A Neutronics, Thermal-Hydraulics Computer Program for Fast Reactor Safety Analysis," HEDL-TME-74-77, Hanford Engineering and Development Laboratory, December 1974.

16. Rumble, E. T., "HOPE, A Hypothetical Overpower Excursion Model for Liquid Metal-Cooled Fast Breeder Reactors," Ph.D. dissertation in Engineering, UCLA, June 1974.

17. Kastenberg, W. E., "LMFBR Fuel Analysis, Task A: Oxide Fuel Dynamics," Final Report to the USNRC, NUREG-0146, January 1977.

18. Partain, W. L. and A. E. Waltar, "Effects of Fuel Density Gradients and Molten Fuel Freezing During a Fast Reactor Excursion," Trans. Amer. Nuc. Soc., Vol. 17, No. 1 p. 361-362 (November 1973).

19. Waltar, A. E. et.al., "Consequences of Channel Plugging During Fast Reactor Overpower Excursions," Trans. Amer. Nuc. Soc., Vol. 19, p. 282, (June 1975).

20. Frank, M. V., "Some Aspects of Fuel Rod Behavior During a Fast Reactor Overpower Transient," Ph.D. in Engineering, UCLA, December 1977 (expected).

21. Sun, Y. and D. Okrent, "A Simplified Method of Computing Clad and Fuel Strain and Stress During Irradiation," NUREG-0260, June 1977.

22. Wong, K. W., "A Mechanistic Study of Fuel Freezing, Channel Plugging, and Continued Coolability During Fast Reactor Overpower Excursions," NUREG-0310, July 1977.

Blank Page

2.0 PRE-FAILURE FUEL MOTION

2.1 Introduction

Pre-failure axial fuel motion within the central cavity is potentially important in slow overpower transients from a reactivity-power perspective. Fast overpower transients have minimal axial fuel motion within the central cavity prior to failure. This will be demonstrated herein.

Experimental evidence [1,2] suggests that axial motion is forced by gravity, fuel thermal expansion, gas bubble addition and expansion in molten fuel, and a pressure differential (if there is communication between the central cavity and the plenum). A model which analytically incorporates the first three mechanisms has been suggested [3] and is described in detail for the GCFR fuel pin [4]. The current study has modified the model in order to describe fuel motion within a central cavity which has developed as a result of restructuring only. The fuel column does not have a prefabricated central cavity.

2.2 Description of the Model

The current model attempts to quantify the following sequence of events, which may be typical of slow overpower transient conditions in LMFBR type fuel pins.

1. Molten fuel flow is initiated when either of two conditions are met:
   (a) The central cavity closes at any axial location due to molten fuel melting (motion up or down), or
   (b) The fuel weight vector in the downward direction exceeds the restraining force created by the surface energy of

the molten fuel/cavity gas interface.

2. Molten fuel is assumed to flow as a slug under gravity to the bottom of the cavity.
3. Upon reaching the cavity bottom, the molten fuel continues to backfill the cavity. Downward flow is terminated when the lower boundary of the slug reaches the bottom of the cavity. Backfill is enhanced by thermal expansion and phase change expansion.
4. The upper boundary of the molten fuel continues to rise until the fuel pin fails or the cavity is calculated to be completely filled. Cladding failure was suppressed for this study. Therefore, the calculations terminated via the filling mechanism.

The velocity of gravity-driven slug flow is given in Reference [4]. However, the molten mass distribution therein assumed "layer" flow. The model has been modified to include the mass distribution of a molten fuel "slug." The molten mass distribution after motion begins is computed by assuming that all molten fuel backfills the available central cavity space from the location of the lower slug boundary. The displacement of this boundary is found by integrating the slug flow velocity. The initial slug boundaries are found by filling the central cavity upward and downward from the location of the initial cavity closure. The total mass of molten fuel and the location of its production are determined by an independent transient temperature routine also documented in Reference [4].

The JANE code has incorporated the above model. It is presently a program which calculates the thermal, mechanical, fission gas and fuel motion response of a single fast reactor fuel pin to an input power rise

of the form

$$\frac{P(t)}{P_o} = e^{t/\tau},$$

where

P_o = the initial multiple of nominal full power operation,

$P(t)$ = the transient multiple of nominal full power operation,

t = time (s), and

τ = the power transient time constant.

Reactivity effects are not appropriate in a single pin model; therefore, they have not been included in this study. Efforts are planned to extend JANE to multiple channel or whole core capability. Reactivity effects due to doppler, coolant density, thermal expansion, and fuel motion will be included.

The potential for axial molten fuel motion in the central cavity prior to failure has been investigated with the JANE code for low and high burnup CRBR type fuel pins. Three ramp rates have been simulated. Values of τ = 4.34 and 35.518 are roughly equivalent to a power rise due to a 10¢/s and 2.4¢/s reactivity insertion, respectively. A value of τ = 126.7 is roughly equivalent to a calculated power rise due to a 1¢/s reactivity insertion.

2.3 Results

Table 1 is the matrix of cases (this and subsequent tables are found at the end of this chapter). Table 2 presents some relevant input quantities. Table 3 is a summary of the results. In all cases attempted for this study, the cavity closes at the hottest axial location (the axial interval which spans the midplane) prior to satisfaction of the

surface tension criterion. However, this conclusion is sensitive to the assumed value of the molten fuel-to-solid fuel contact angle. A sensitivity study on contact angle has not been performed. The major conclusions of this study are not sensitive to the mode of initiation.

The average flowing fuel velocity ranges from 24 to 9 cm/s and decreases with decreasing heat-up rate (increasing τ). The asymptotic slug flow velocity is proportional to the square of the flowing slug radius. This radius is larger for higher radial melt fractions. Tables 4 through 9 show that decreasing heat-up rates produce a decreasing average melt fraction in the rod during the time of flow. The average melt radius is therefore smaller, yielding a smaller flowing slug radius. As seen in Figures 2.1 through 2.6, the flow velocity increases rapidly at first. Then the acceleration attenuates. In fact, Cases M5 and M6 are calculated to reach an asymptotic velocity soon after flow initiates. The reason for this behavior is as follows. As flow proceeds downward, the fuel slug encounters a narrower cavity. This is especially true of the low heat-up rate cases which do not exhibit melting near the cavity bottom. The velocity is proportional to the factor

$$1 - \frac{32}{\lambda^4} \exp\left(-\lambda^2 \nu t / R^2\right),$$

where

λ = the root of the zeroth order ordinary Bessel function, J_o,

ν = the kinematic viscosity of the fuel, and

R = the radius of the slug or cavity.

The exponential term reduces to 0.001 within 0.050 seconds for the slug radii representative of Cases M5 and M6. This term reduces to 0.001 in about 0.2 seconds for the slug radii representative of the other cases.

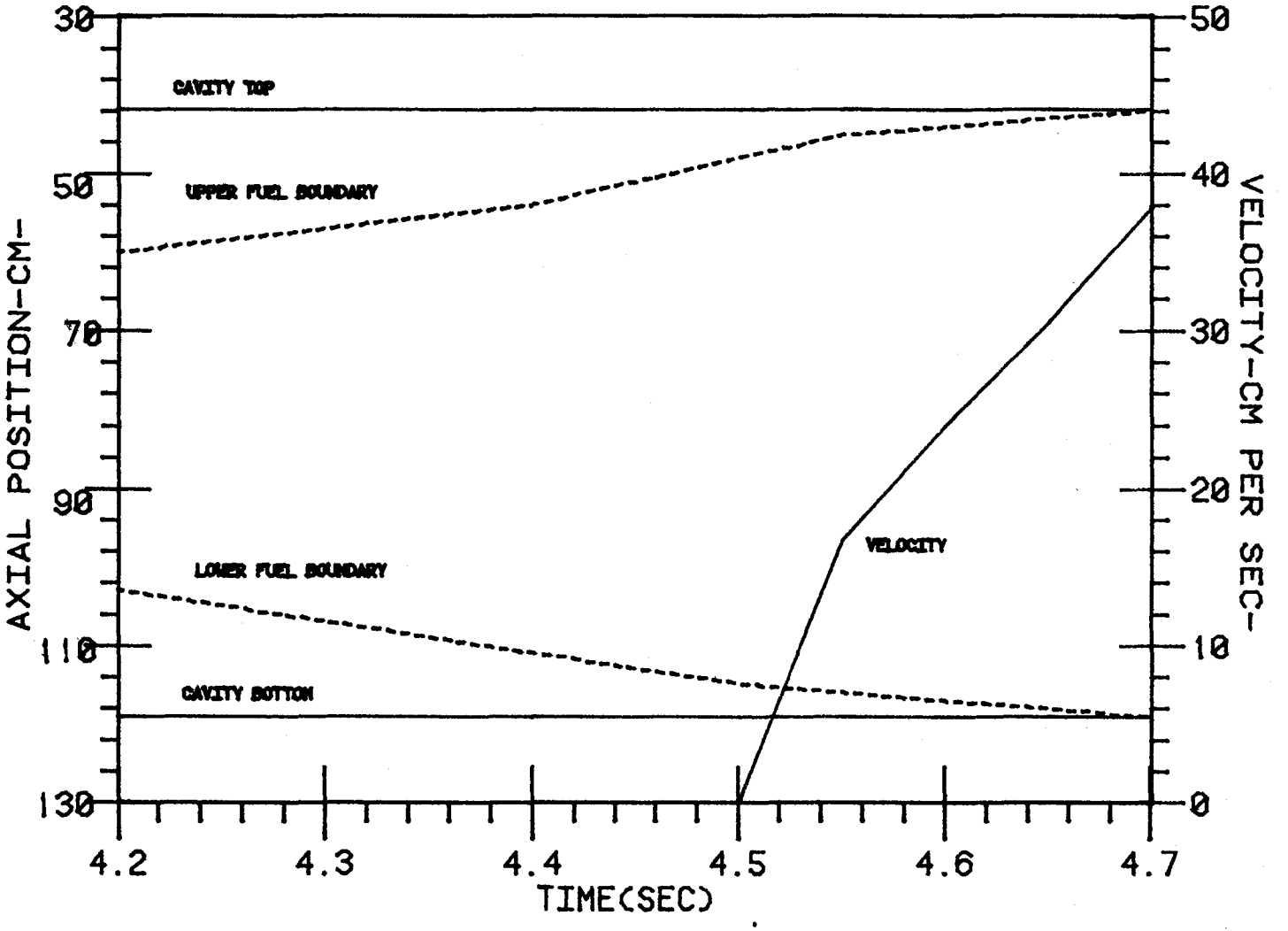

Figure 2.1. Molten Fuel Axial Boundaries and Velocity (Case M1).

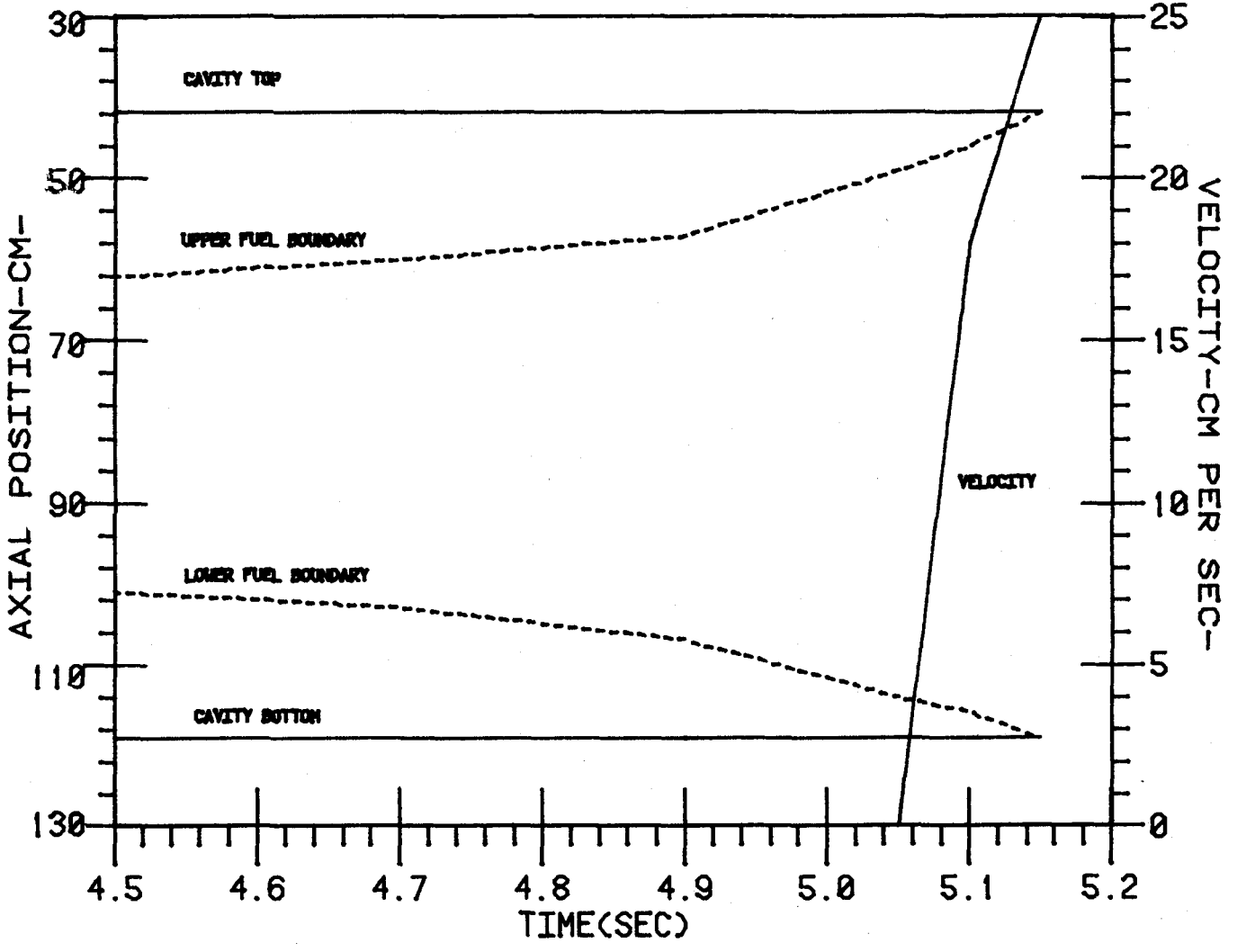

Figure 2.2. Molten Fuel Axial Boundaries and Velocity (Case M2).

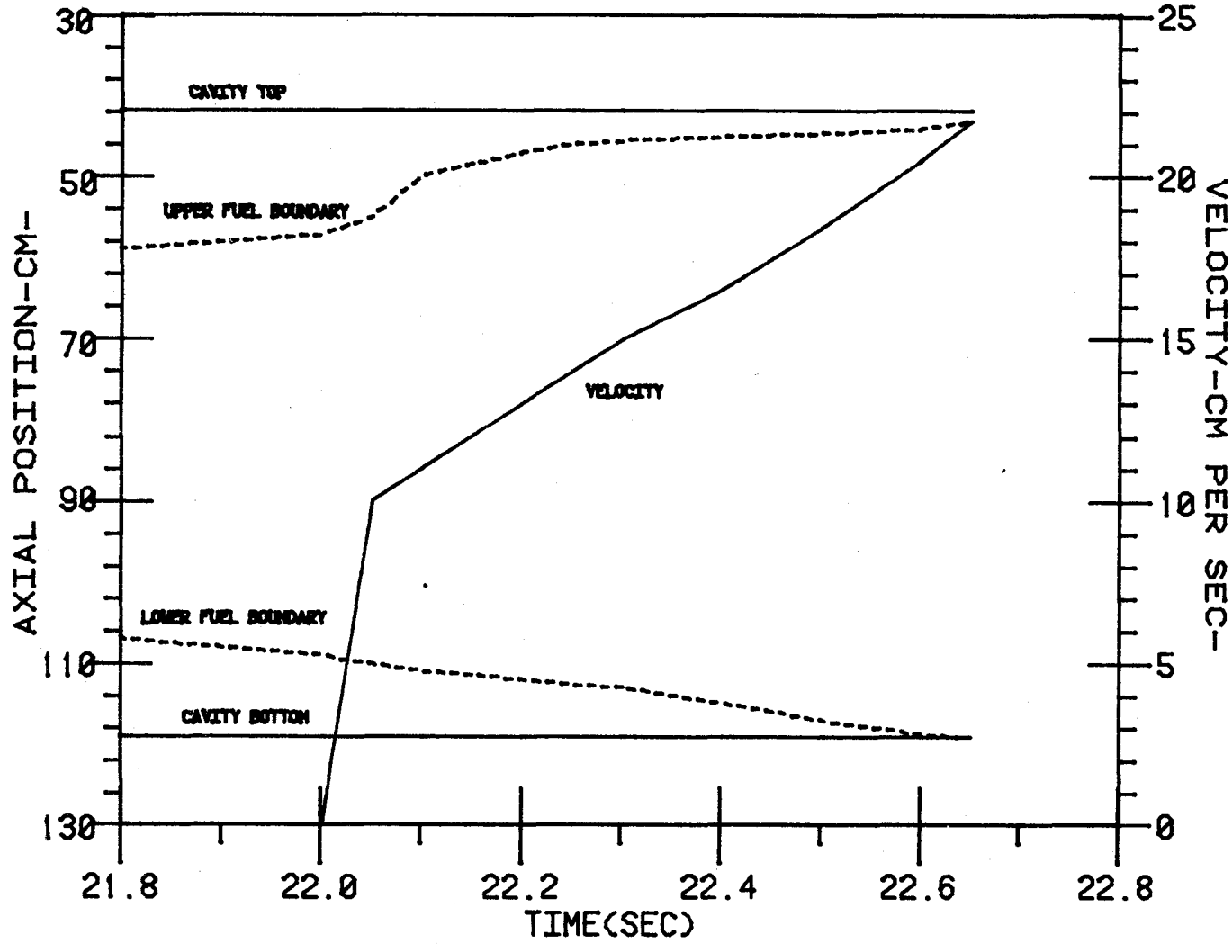

Figure 2.3. Molten Fuel Axial Boundaries and Velocity (Case M3).

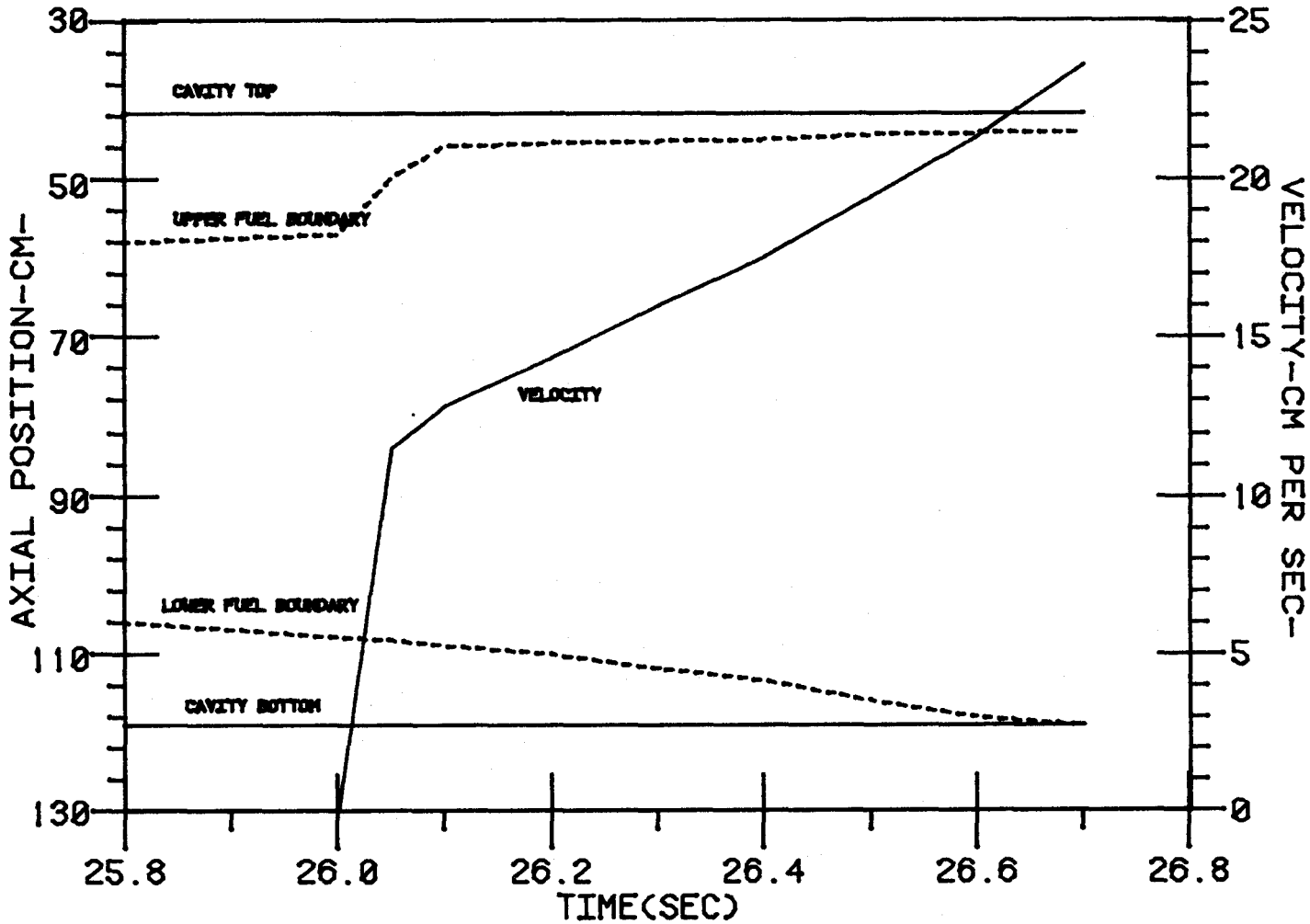

Figure 2.4. Molten Fuel Axial Boundaries and Velocity (Case M4).

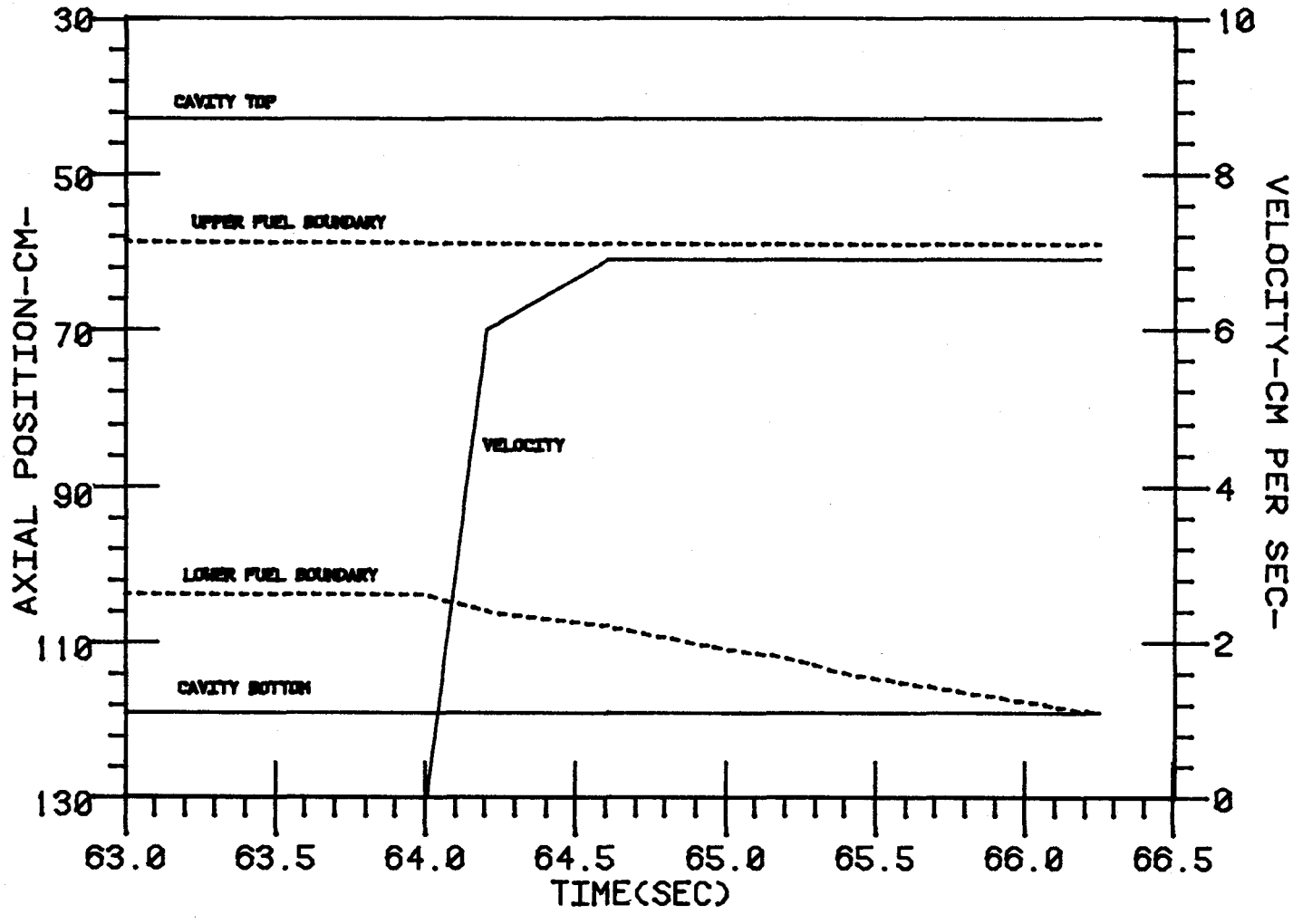

Figure 2.5. Molten Fuel Axial Boundaries and Velocity (Case M5).

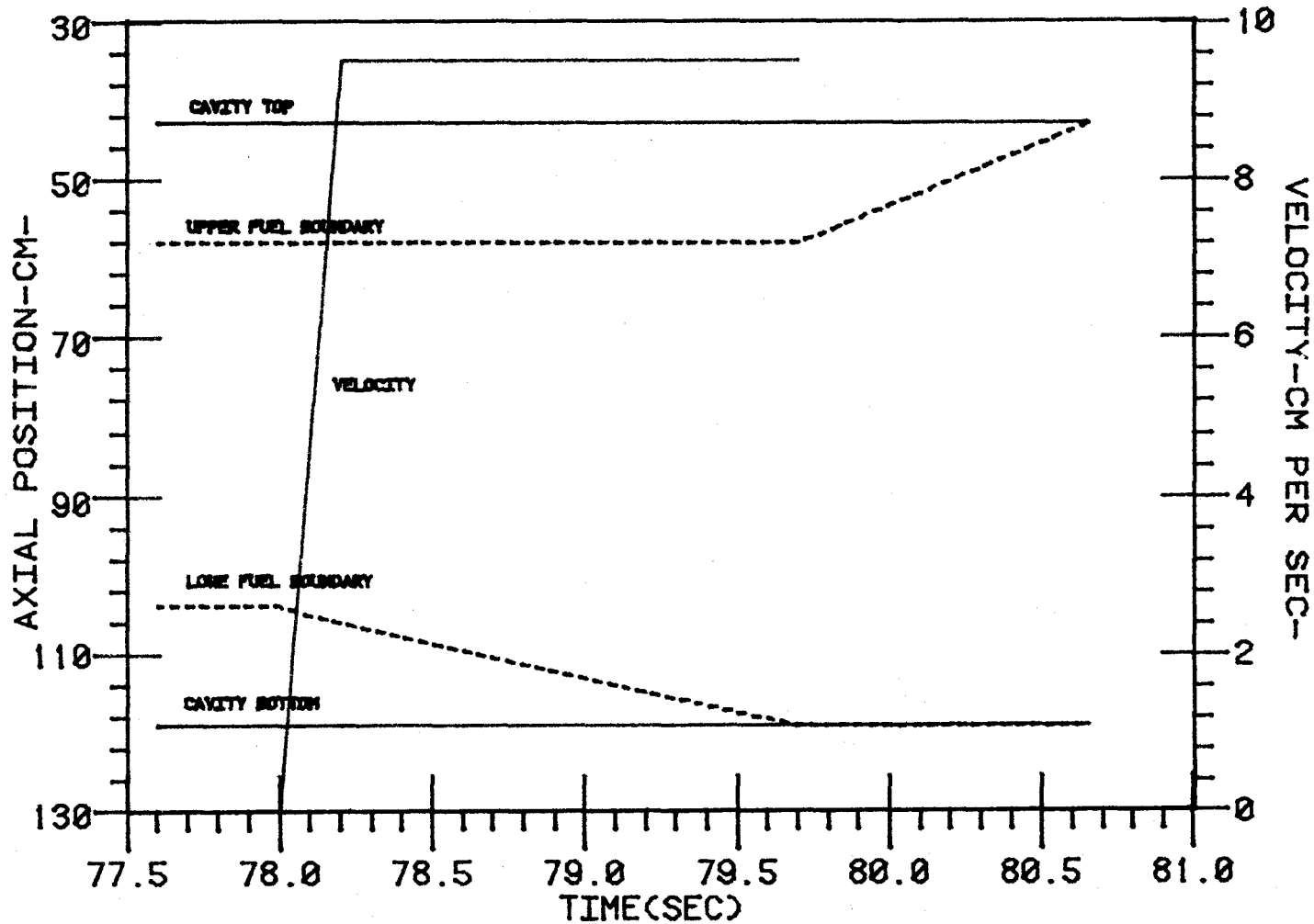

Figure 2.6. Molten Fuel Axial Boundaries and Velocity (Case M6).

Tables 4 through 9 illustrate the downward mass redistribution due to axial fuel motion. This net downward displacement is more pronounced for the slower heat-up rates. Figures 2.3 to 2.6 show that the flowing slug of Cases M3 through M6 reaches the bottom of the cavity prior to the filling up of the cavity with molten fuel. Tables 6 through 9 show that downward flow occurs prior to significant melting near the cavity bottom. Case M2 was terminated by cavity fill-up before the slug could reach the cavity bottom (Figure 2.2) by gravity-driven flow. The net displacement caused by gravity-driven flow was only 2 cm. Fuel was calculated to melt and fill the cavity voids as flow progressed. Case M1 was terminated by cavity fill-up at about the same time as the gravity-driven slug reached the bottom of the cavity (Figure 2.1). In both cases, fuel melting rates rather than fuel motion were the dominant mechanism of molten fuel redistribution.

The burnup dependence is induced by two factors, as illustrated in Table 2. First, the lower restructuring transition temperatues at high burnup causes the JANE code to calculate a larger cavity volume. Second, the lower fraction of reactor power attributed to the core at higher burnup causes the code to compute lower initial fuel temperatures. Both of these factors contribute to a delayed fuel initiation for the high burnup cases (M2, M4, and M6). The time delay causes a steeper slope on the assumed exponential heat-up. Therefore, during the time of flow, for each value of τ the fuel motion in the high burnup cases responds to a slightly higher heat-up rate than its low burnup companion. This explains the higher rate of increase in average melt fraction for Cases M2, M4, and M6 and why the cavity filled in Case M2 prior to significant fuel motion. The larger cavity volume produces a larger average flow velocity for the

high burnup cases (Table 3). The net result is that for high burnup, low ramp rate cases (M4 and M6) the time between flow termination and cavity fill-up is larger than for the low burnup companion cases (M3 and M5).

The major conclusion of this study is that the potential for significant reactivity changes due to axial fuel motion prior to failure increases with decreasing ramp rate and decreasing burnup. Next year's effort will attempt to extend JANE to treat whole core transients and estimate the magnitude of possible reactivity effects.

Table 1. Fuel Motion Case Matrix.

	Ramp Rate			
	τ (s)	4.34	35.518	126.7
	$\Delta\rho$ (¢/s)	10	2.4	1
Burnup (MWD/T)				
1,000		Case M1	Case M3	Case M5
38,000		Case M2	Case M4	Case M6

Table 2. Relevant Input Quantities.

Quantity	Burnup (MWD/T)	
	1,000	38,000
Columnar grain zone transition temperature (°C)	1,807	1,560
Equiaxed grain zone transition temperature (°C)	1,531	1,360
Fraction of reactor power produced in the core (total reactor power = 975 MW)	0.937	0.841
Peak linear power density (W/cm)	402	361
Columnar grain boundary at peak location (cm)	0.114	0.139
Equiaxed grain boundary at peak location (cm)	0.166	0.166
Outer fuel radius at peak location (cm)	0.250	0.249
Central cavity length (cm)	76.2	76.2
Central cavity volume (cm^3)	0.237	0.272
Fuel surface tension* (dynes/cm)	441	441
Fuel contact angle* (radians)	0.62	0.62
Fuel melting temperature (°C)	2,745	2,745

*For fuel motion initiation criterion.

Table 3. Fuel Motion Results Summary.

Case	Peak Steady State Power (W/cm)	Time of Incipient Melting (s)	Time of Fuel Flow Initiation (s)	Time of Flow Termination (s)	Peak Melt Radius at Flow Initiation (cm)	Plug Flow or Layer Flow Criterion Met?	Average Flow Velocity (cm/s)
M1	402	3.15	4.50	4.7	0.14	Plug	23
M2	361	3.8	5.05	5.15*	0.14	Plug	15
M3	402	14.0	22.00	22.65	0.14	Plug	15
M4	361	18.0	26.00	26.70	0.14	Plug	17
M5	402	43.5	64.00	66.25	0.14	Plug	7
M6	361	58.0	78.00	79.70	0.14	Plug	9

*Flow terminated because cavity had filled with molten fuel.

Table 4. Molten Fuel Mass and Melt Fraction Progression for Case M1.

Core Axial Position from Top of Upper Axial Blanket (cm)[1]	Time (s)							
	4.4		4.5[2]		4.6		4.7[3]	
	Mass (g)	Melt Fraction	Mass (g)	Melt Fraction	Mass (g)	Melt Fraction	Mass (g)	Melt Fraction
50.8	0.05	0.002	0.19	0.007	0.52	0.017	0.94	0.03
66.0	4.51	0.17	5.39	0.20	6.19	0.23	6.84	0.26
81.3	6.77	0.25	7.66	0.29	8.63	0.33	9.20	0.35
96.5	5.17	0.19	6.21	0.23	6.76	0.25	7.71	0.29
111.8	0.15	0.006	0.42	0.016	0.77	0.030	1.38	0.05
Total Mass /Average Melt Fraction	16.65	0.09	19.87	0.11	22.87	0.12	26.07	0.14

Notes: (1) Locations are at midplanes of axial intervals; each interval is 15.25 cm.

(2) Flow begins.

(3) Flow ends.

Table 5. Molten Fuel Mass and Melt Fraction Progression for Case M2.

Core Axial Position from Top of Upper Axial Blanket (cm)[1]	Time (s)							
	4.4		4.5[2]		4.6		4.7[3]	
	Mass (g)	Melt Fraction	Mass (g)	Melt Fraction	Mass (g)	Melt Fraction	Mass (g)	Melt Fraction
50.8	0.00	0.00	0.01	0.0005	0.23	0.008	0.68	0.02
66.0	1.56	0.06	4.42	0.16	5.84	0.22	6.42	0.24
81.3	3.46	0.13	6.60	0.25	7.99	0.30	8.81	0.33
96.5	1.88	0.07	4.99	0.19	6.44	0.24	7.12	0.26
111.8	0.00	0.00	0.06	0.002	0.43	0.016	0.80	0.03
Total Mass /Average Melt Fraction	6.90	0.04	16.08	0.09	20.93	0.11	23.83	0.13

Notes: (1) Locations are at midplanes of axial intervals; each interval is 15.25 cm.

(2) Flow begins.

(3) Flow ends.

Table 6. Molten Fuel Mass and Melt Fraction Progression for Case M3.

Core Axial Position from Top of Upper Axial Blanket (cm)[1]	Time (s)							
	22.0[2]		22.4		22.65[3]		22.75	
	Mass (g)	Melt Fraction	Mass (g)	Melt Fraction	Mass (g)	Melt Fraction	Mass (g)	Melt Fraction
50.8	0.01	0.0003	0.19	0.003	0.28	0.007	0.33	0.008
66.0	4.84	0.18	5.71	0.21	6.25	0.23	6.47	0.24
81.3	7.86	0.30	8.32	0.32	8.78	0.33	9.04	0.34
96.5	5.94	0.22	6.73	0.25	7.47	0.28	7.80	0.30
111.8	0.11	0.004	0.35	0.01	0.66	0.02	0.78	0.02
Total Mass /Average Melt Fraction	18.76	0.10	21.30	0.11	23.44	0.12	24.42	0.13

Notes: (1) Locations are at midplanes of axial intervals; each interval is 15.25 cm.

(2) Flow begins.

(3) Flow ends.

Table 7. Molten Fuel Mass and Melt Fraction Progression for Case M4.

Core Axial Position from Top of Upper Axial Blanket (cm)[1]	Time (s)							
	26.0[2]		26.4		26.7[3]		26.9	
	Mass (g)	Melt Fraction	Mass (g)	Melt Fraction	Mass (g)	Melt Fraction	Mass (g)	Melt Fraction
50.8	0.00	0.00	0.24	0.003	0.37	0.008	0.44	0.013
66.0	5.30	0.20	6.02	0.23	6.75	0.26	7.33	0.28
81.3	7.87	0.30	8.39	0.32	9.00	0.34	9.61	0.37
96.5	5.85	0.22	6.86	0.26	7.77	0.29	0.94	0.03
111.8	0.09	0.01	0.33	0.01	0.72	0.02	0.94	0.03
Total Mass /Average Melt Fraction	19.12	0.10	21.84	0.12	24.61	0.13	26.64	0.14

Notes: (1) Locations are at midplane of axial intervals; each interval is 15.25 cm.

(2) Flow begins.

(3) Flow ends.

Table 8. Molten Fuel Mass and Melt Fraction Progression for Case M5.

Core Axial Position from Top of Upper Axial Blanket (cm)[1]	Time (s)							
	64.0[2]		65.0		66.25[3]		66.50	
	Mass (g)	Melt Fraction	Mass (g)	Melt Fraction	Mass (g)	Melt Fraction	Mass (g)	Melt Fraction
50.8	0.00	0.00	0.00	0.00	0.00	0.00	0.13	0.00
66.0	3.80	0.14	5.48	0.20	5.46	0.20	5.43	0.20
81.3	7.94	0.30	8.20	0.31	8.19	0.31	8.16	0.31
96.5	4.98	0.19	5.53	0.21	6.62	0.25	6.89	0.26
111.8	0.00	0.00	0.09	0.00	0.21	0.00	0.21	0.00
Total Mass /Average Melt Fraction	16.72	0.09	19.30	0.10	20.48	0.11	20.82	0.11

Notes: (1) Locations are at midplane of axial intervals; each interval is 15.25 cm.

(2) Flow begins.

(3) Flow ends.

Table 9. Molten Fuel Mass and Melt Fraction Progression for Case M6.

Core Axial Position from Top of Upper Axial Blanket (cm)[1]	Time (s)							
	78.0[2]		79.0		79.6[3]		80.7	
	Mass (g)	Melt Fraction	Mass (g)	Melt Fraction	Mass (g)	Melt Fraction	Mass (g)	Melt Fraction
50.8	0.00	0.00	0.00	0.00	0.00	0.00	0.16	0.00
66.0	4.05	0.15	5.41	0.20	5.38	0.20	5.43	0.21
81.3	7.65	0.29	8.25	0.32	8.21	0.32	8.32	0.32
96.5	4.57	0.17	5.73	0.21	5.78	0.22	6.93	0.26
111.8	0.00	0.00	0.17	0.00	0.28	0.00	0.30	0.00
Total Mass /Average Melt Fraction	16.27	0.09	19.56	0.10	19.65	0.11	21.14	0.11

Notes: (1) Locations are at midplane of axial intervals; each interval is 15.25 cm.

(2) Flow begins.

(3) Flow ends.

2.4 References for Chapter 2.0

1. Hikido, T., and J. H. Field, General Electric, GEAP-13542, 1968.
2. Roberts, J. T. A., B. J. Wrona, et al., Nucl. Techn. 27:267, 1975.
3. Frank, M. V., and W. E. Kastenberg, ANS Trans. 26:378, 1977.
4. Frank, M. V., Ph. D. in Engineering, UCLA, to be published.

3.0 FUEL PIN FAILURE MODELS

3.1 Introduction

A generic problem for the analysis of transient overpower accidents is a description of the time, place and mode of fuel pin failure. It is well known that the ultimate course of the accident is profoundly affected by time, place and mode of pin failure [1-3]. At present, two approaches appear to be emerging for the prediction of fuel pin failure.

In the first approach, integral type information obtained from the TREAT [4,5] experiments has been employed to obtain correlations for failure prediction. The second is an attempt to determine, from both experiments and analysis, the various phenomena affecting clad failure, and then to model them.

In TREAT, thirteen-inch sections of LMFBR fuel pins, representing various stages of irradiation and linear power rating, are pulsed to failure. The microstructure is generally uniform in the axial direction and the spatial energy deposition is fairly non-prototypical. In spite of these shortcomings, there are arguments for using these results for the prediction of pin failure [6-10].

As a first approach to the correlative technique, it was argued that the failure threshold was related to "thermal upset" and that this thermal upset could be measured by a "failure enthalpy' [7]. To improve upon this, a new correlation based upon a "damage parameter" was recently presented [8,9,10]. The correlation is used by computing the value of the parameter at several axial pin locations as the transient proceeds. Pin failure is assumed at the location and time for which the parameter first achieves the failure criterion value. The pin failure criterion (0.38×10^{-2}) is the average of the parameter values calculated for a

series of tests. Various factors such as clad strength, transient time, fuel conditions and enthalpy deposition make up the damage parameter.

Some of the basic limitations are 1) the damage parameter has been correlated for only a very narrow range of experimental values [11], 2) the experiments used are non-prototypical, and 3) it appears that even some of the experiments do not correlate well (low power, highly irradiated and high power, low irradiated pin segments).

In the second approach to predicting clad failure, an attempt is made to mechanistically model all the clad-loading mechanisms and calculate the axial (and temporal) distribution of stress and/or strain. Comparison of this calculation with experimentally determined clad failure data may yield the time, place and mode of pin failure in these experiments [12-14].

A variety of mechanisms have been postulated to occur in the fuel which can cause it to strain the clad. Included are:

1. Differential thermal expansion between fuel and clad,
2. Volumetric growth or swelling of fuel due to intragranular precipitation and growth of fission gas bubbles,
3. Hydraulic pressure in the cavity, due to fuel which expands during melting, and
4. Release of retained fission gas into the central pin cavity prior to and upon fuel melting.

In addition, pin failure for fresh fuel has been postulated to occur by either molten fuel contacting clad (clad melt through) or clad melting under dry-out conditions.

Most computer models use a "sealed bottle" cavity approach in modelling the central cavity for computing a "primary" stress on the clad, in addition to calculating a "secondary" stress due to thermal differential

expansion. This "sealed bottle" is defined by the amount of molten fuel and any free space (such as the central void formed during steady state) which exists in the pin during the transient. This bottle or cavity contains molten fuel, fission gas released during steady state and fission gas released during the transient. The bottle or cavity is sealed in that communication with the fission gas plenum, the fuel/clad gap (if it exists) and the microstructure is neglected. From the cavity volume and a calculated average temperature, the pressure and hence the stress on the clad can be computed. It is usually assumed that the fuel is strengthless (or becomes so after a threshold has been reached), with the pressure transmitted to the clad via the ratio of melt radius to solid radius and use of the thin membrane approximation [15]. The secondary loading due to differential thermal expansion is usually neglected when the fuel becomes strengthless.

Although volumetric growth or swelling of fuel due to intragranular precipitation and growth of fission gas has been studied in some detail [16-20], it has been incorporated in only one code [21] developed in West Germany and only parametric results have been obtained thus far [22,23].

Having obtained the primary loadings, these codes then compare the clad stress to either an ultimate stress [24], some plastic yield stress (a given percent permanent deformation) [15], or a burst stress [25]. If the clad stress in any node reaches one of these limits, the pin is assumed to have failed. Recently, a failure criterion based on the Larson-Miller parameter and a stress-rupture life fraction rule has been introduced [26,27].

Since a large degree of uncertainty does exist, other failure criteria have been employed. These include fuel node melt fraction and

the onset of melting of the unrestructured fuel (fission gas bearing portion). In addition to changing the course of a transient overpower accident by arbitrarily changing the failure location, changes in the failure criterion can produce similar results. Kuczera and Royal [22,23] have shown that by changing from a burst pressure criterion to a melt fraction or onset of melting criterion the accident moved from a hydraulic nuclear shutdown to a hydrodynamic disassembly. In addition, use of a high temperature brittle fracture criterion on the clad (caused by differential expansion and/or fuel swelling) resulted in a disassembly for the same case as a burst pressure criterion which resulted in hydraulic sweepout.

Experimental programs for determining clad failure data have also been initiated [28,29,30]. Recently, Levy at the Battelle Pacific Northwest Laboratories (PNL) has developed a "strain-failure" criterion [31] based on the clad burst tests [32]. This criterion was implemented into the HOPE computer code [15] and preliminary results were presented previously [33].

In this Chapter, two aspects of fuel pin failure are treated. First, further studies employing the (PNL) "strain failure" criterion are reported. Second, an attempt has been made to derive a consistent model for treating fuel and clad, stress and strain between steady state and transient conditions. The model used was developed by Frank [34] for GCFR fuel pins, and is an extension of Sun's work on steady state fuel and clad, stress and strain [35].

3.2 The PNL Strain-Limit Failure Model

In the TASK A final report - July 1, 1975 - September 30, 1976 [33], a new criterion to define clad failure, "the strain-failure limit", was

introduced. As an initial approach to evaluating this technique, a "simplified failure model" was developed and incorporated into the HOPE computer code [15] for testing, the results being presented in the 1975-76 TASK A final report. Because of the simplistic nature of the model employed, however, no conclusions concerning the validity of the strain-failure method could be drawn. The work presented here describes the incorporation of a completed strain-limit model into HOPE (correcting the deficiencies of the earlier simplified model) and summarizes test data obtained for a sample $3/sec reactor transient. The results are presented in two phases. First, a description of each modification made in the simplified failure model and its effect on transient clad failure is discussed. Then, an overall evaluation of the failure model, as incorporated in the HOPE code, is summarized in order to point out any obvious errors in the method.

Several important differences exist between the strain-failure model currently being incoporated into HOPE and the earlier model examined in last year's TASK A report. These differences are related to inadequacies in the earlier model [33]. First, instead of using clad-strength parameters (i.e., σ_{PEL} (PEL strength (ksi) of cladding), σ_{YS} (0.2% offset yield strength (ksi) of cladding) and $\sigma_{0.0}$ (value of cladding strength (ksi) at 0% plastic strain extrapolated from slope of stress-strain curve beyond 0.2% YS)) computed for some average clad-fluence, the spatial variation of clad strength due to radially and axially dependent clad-fluences is now incorporated into the model. This spatial dependence is obtained by modifying the average clad-fluence with respect to radial and axial power shapes (already existing in HOPE), and then using polynomials developed for σ_{PEL}, σ_{YS} and $\sigma_{0.0}$ versus transient clad temperature, at

selected fluences (0.0, 1.5, 4.0 and $\geq 6 \times 10^{22} n/cm^2$), with a linear interpolation of the polynomials between the various fluence levels.

To study the affect of this modification on the rate of clad-strain accumulation, one must consider not only the explicit dependence of the clad-strength in the expressions for the plastic strain,

$$\varepsilon_{P(1)}(\%) = C(\sigma - \sigma_{PEL}), \quad \text{for} \quad \sigma_{PEL} \leq \sigma \leq \sigma_{YS}$$

$$\varepsilon_{P(2)}(\%) = D(\sigma - \sigma_{0.0}), \quad \text{for} \quad \sigma > \sigma_{YS} ,$$

but also the implicit effect of the "strength" on the temperature dependent parameters C and D, where

$$C(\%\ /KSI) = \frac{0.1732}{\sigma_{YS} - \sigma_{PEL}} \quad \text{and} \quad D(\%\ /KSI) = \frac{0.1732}{\sigma_{YS} - \sigma_{0.0}} \cdot$$

*

Let's begin by examining the effect of the spatially dependent fluence on the clad strength. More specifically, consider the yield strength of the cladding (as a function of position) versus time in the transient. In Figures 3.1 and 3.2, values of the yield strength computed for an average fluence of $4.0 \times 10^{22} n/cm^2$ are compared to the yield strengths obtained by using the true spatially dependent clad-fluence. To get a variety of clad-fluence and temperature rate conditions, several

---

*In the PNL report (BNW-LM-TN-77-4), the temperature-dependent parameters $\frac{1}{C}$ and $\frac{1}{D}$ are given simply as polynomials; however, the coefficients of the various powers of temperature in these polynomial expressions are just

$$a_{i,C(\%\ /KSI)} = \frac{a_{i,\sigma_{YS}} - a_{i,\sigma_{PEL}}}{0.1732} \quad \& \quad a_{i,D(\%\ /KSI)} = \frac{a_{i,\sigma_{YS}} - a_{i,\sigma_{0.0}}}{0.1732}$$

so that the values of C and D obtained are identical to those calculated from the above algorithm.

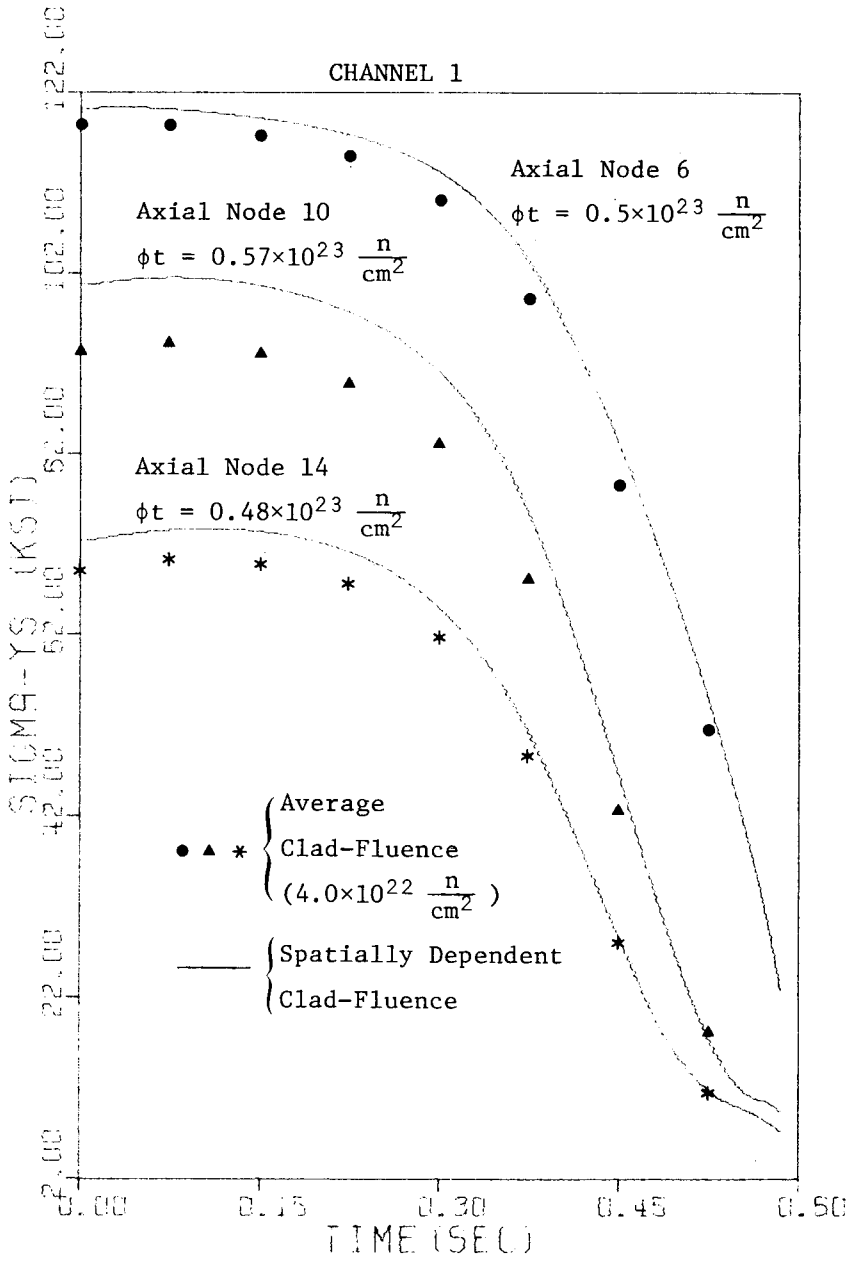

Figure 3.1. σ_{YS}(KSI) (as determined from both the spatially dependent and average clad-fluence) vs. Time for Axial Nodes 6, 10 and 14 of Channel 1 - \$3/s Initiating Ramp

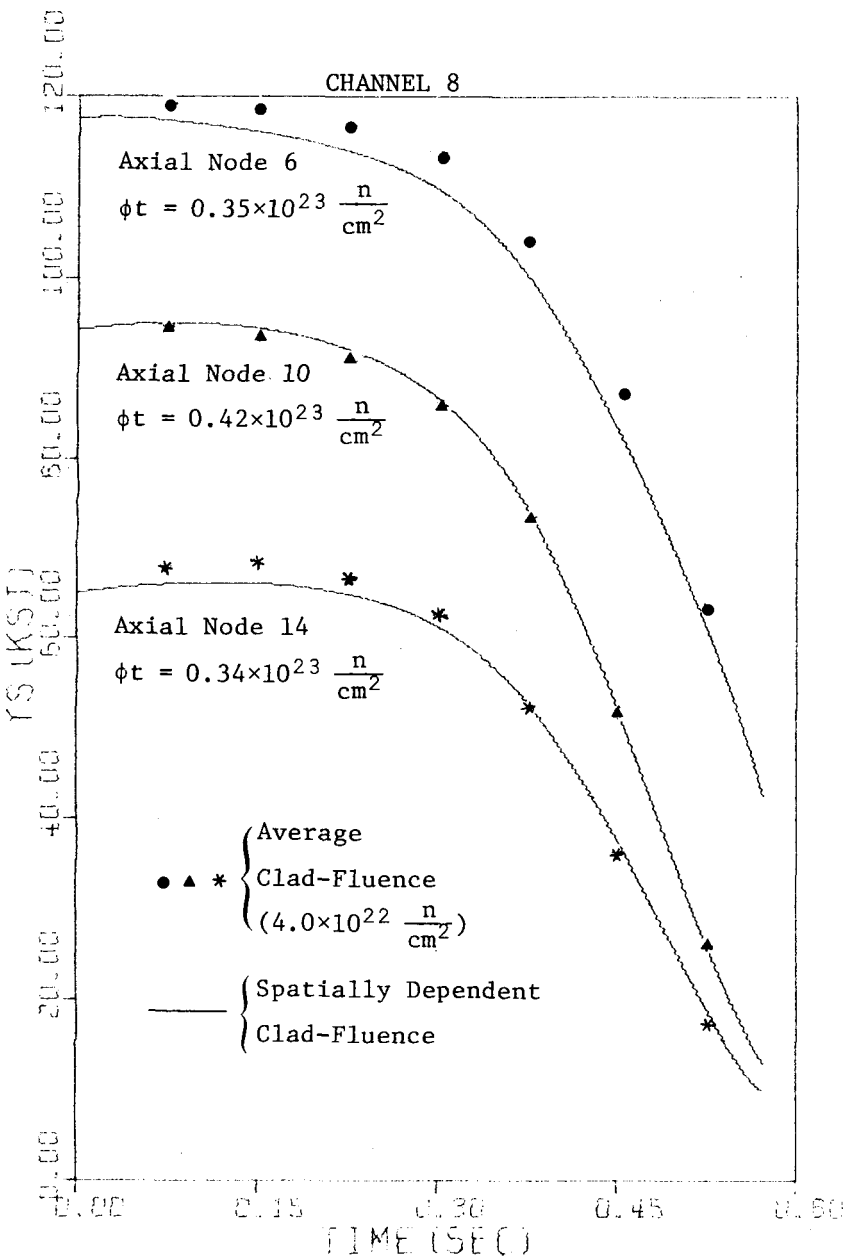

Figure 3.2. σ_{YS}(KSI) (as determined from both the spatially dependent and average clad-fluence) vs. Time for Axial Nodes 6, 10 and 14 of Channel 8 - \$3/s Initiating Ramp

axial locations (axial nodes 6, 10, and 14) and two radial core positions (channels 1 and 8) are considered. One result which is obvious from these graphs is that at the onset of the transient (when clad-temperatures are relatively low) the yield strength of the clad is directly proportional to the amount of radiation it receives; that is, clad-nodes seeing fluences above the average ($4 \times 10^{22} n/cm^2$) have yield strengths which are noticeably higher than those predicted assuming the average fluence, and similarly for nodes with spatially dependent fluences below the average. The explanation for this effect, as described in BNW-LM-TN-77-4, is that irradiation increases the inherent strength of the matrix of the cladding grain (i.e., radiation hardening), thus increasing the yield strength of the clad.

Towards the end of the transient, when clad-temperatures are high, the effect of irradiation on the clad yield strength appears to be negligible; that is, differences between the yield stress calculated for the average and spatially dependent clad-fluence are less than the uncertainties to which these values are known. The most likely reason for this is that at high temperatures the yield strength is much more sensitive to temperature than to radiation effects, and since the spread in clad-fluence over the active part of the reactor core is fairly small (i.e., approx. 3.44×10^{22} to $5.74 \times 10^{22} n/cm^2$), there is effectively no difference between yield strengths obtained using the average fluence and those calculated using the spatially dependent fluence. This is an important result since, looking at Figure 3.3, there is essentially no stress in the clad until very late in the transient (approx. 0.55 seconds into the transient). This means that as far as clad-failure is concerned

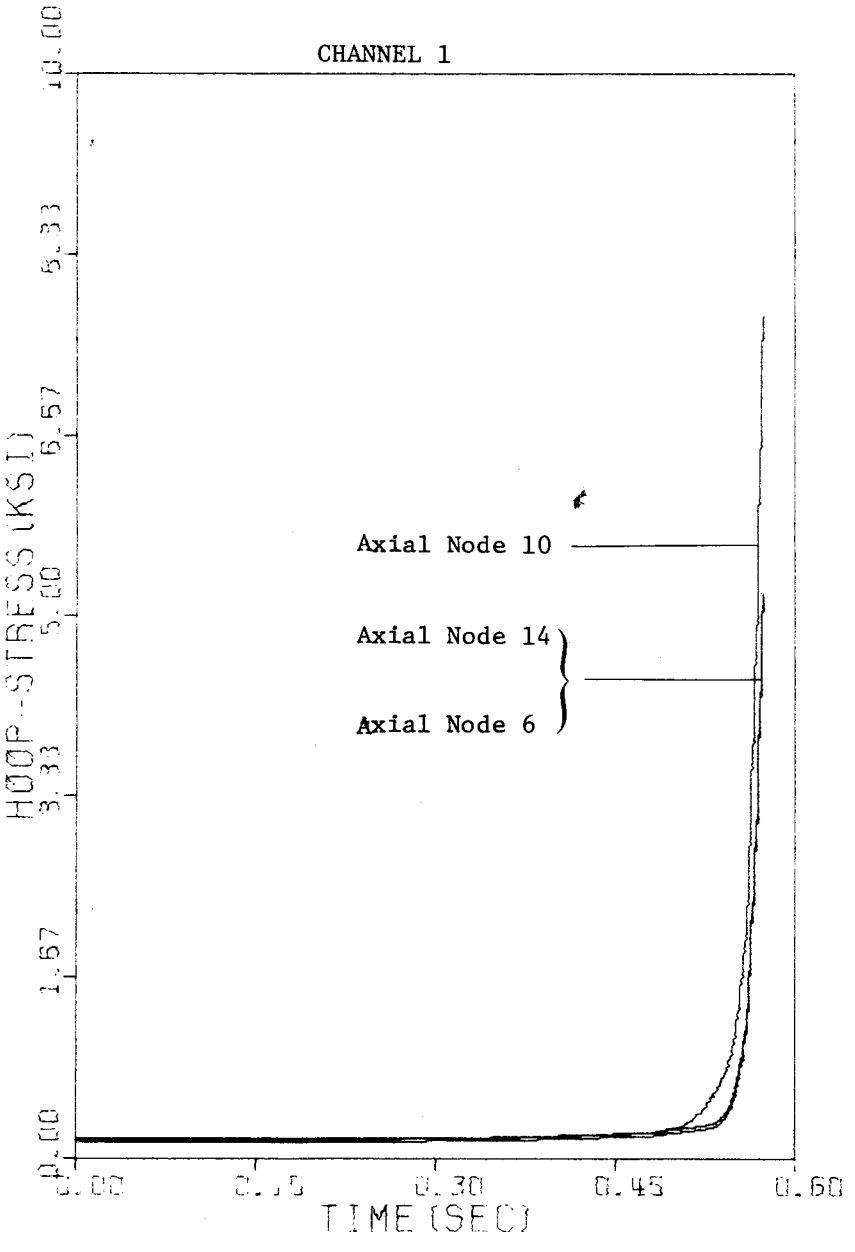

Figure 3.3. Clad-Hoop-Stress(KSI) vs. Time for Axial Nodes 6, 10 and 14 of Channel 1 - $3/s Initiating Ramp

(neglecting for the moment the parameters C and D), there is effectively no difference between using yield strengths obtained from the spatially dependent fluence and those computed from some appropriate average fluence.

Looking at the time-histories of σ_{PEL} and $\sigma_{0.0}$ (Figures 3.4 and 3.5, respectively), we find that these parameters behave in roughly the same fashion as the yield stress - σ_{YS}; that is, at low clad-temperatures they are directly proportional to the fluence seen by the clad* while at high temperatures they appear to be insensitive to irradiation effects. Therefore, just as in the case of σ_{YS}, values of σ_{PEL} and $\sigma_{0.0}$ calculated for the average clad-fluence can be used with about the same accuracy as values of these parameters obtained from the spatially-dependent fluence.

Because of the nature of σ_{PEL}, σ_{YS} and $\sigma_{0.0}$ at high temperatures, the only way in which the spatially dependent fluence can affect the location of clad-failure is through the temperature-dependent constants C and D. These constants, however, are given by the expressions

$$C(\%/KSI) = \frac{0.1732}{\sigma_{YS}-\sigma_{PEL}} \quad \text{and} \quad D(\%/KSI) = \frac{0.1732}{\sigma_{YS}-\sigma_{0.0}} \quad ,$$

so that late in the transient one would expect that they too should be insensitive to variations in clad-fluence. This behavior can, in fact, be seen in Figure 3.6, where values of D(%/KSI) computed from the average

*In the graph of $\sigma_{0.0}$ vs. Time (Fig. 3.5), one finds that in axial node 6 below approximately 0.375 seconds the value of $\sigma_{0.0}$ calculated from the average clad-fluence is greater than that obtained from the larger spatially dependent fluence. This appears to be in contradiction with the above results. However, below 0.375 seconds, the clad-temperature in this node is well below 755°K, which, according to BNW-LM-TN-77-4, is the lower limit of the range for which the polynomial fits of $\sigma_{0.0}$ are valid. Thus, the conclusions stated above remain intact.

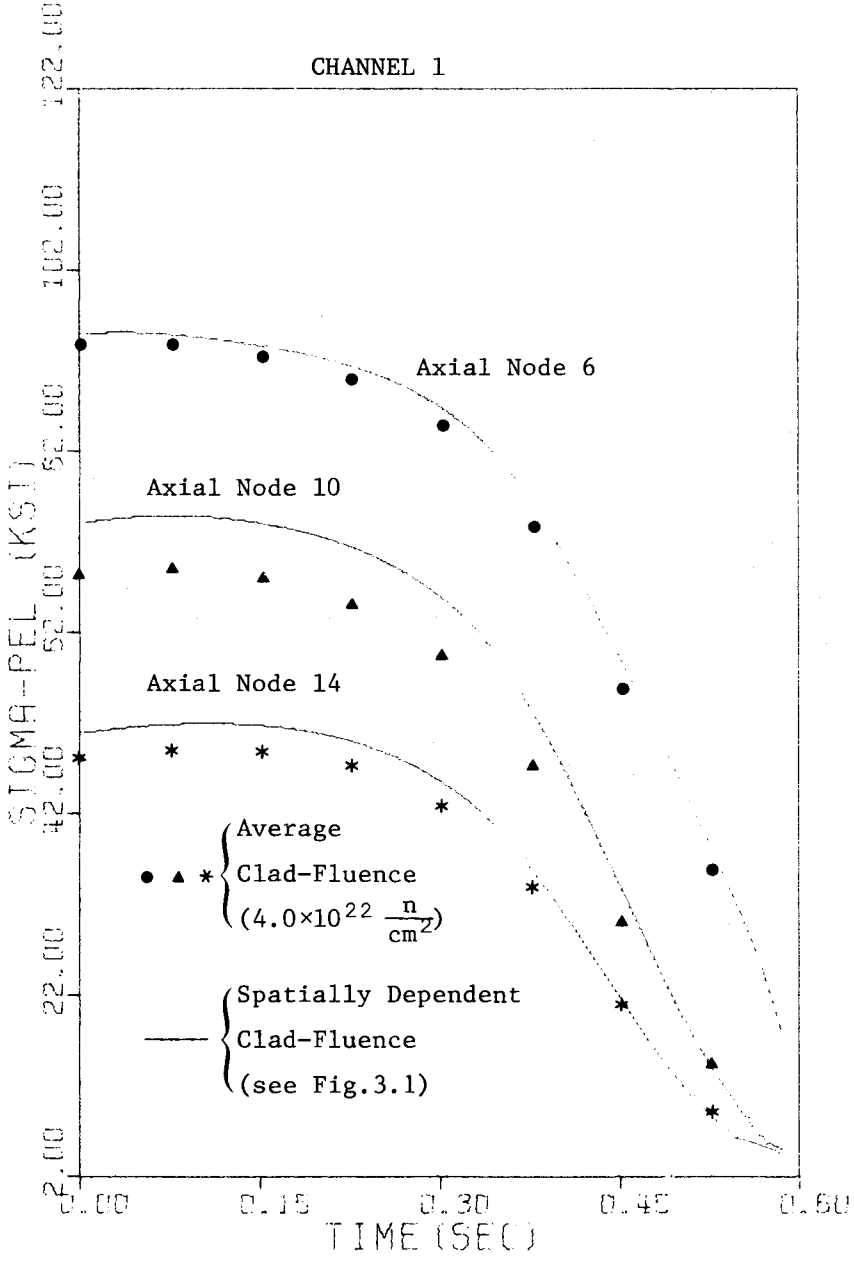

Figure 3.4. σ_{PEL}(KSI) (as determined from both the spatially dependent and average clad-fluence) vs. Time for Axial Nodes 6, 10 and 14 of Channel 1 - \$3/s Initiating Ramp

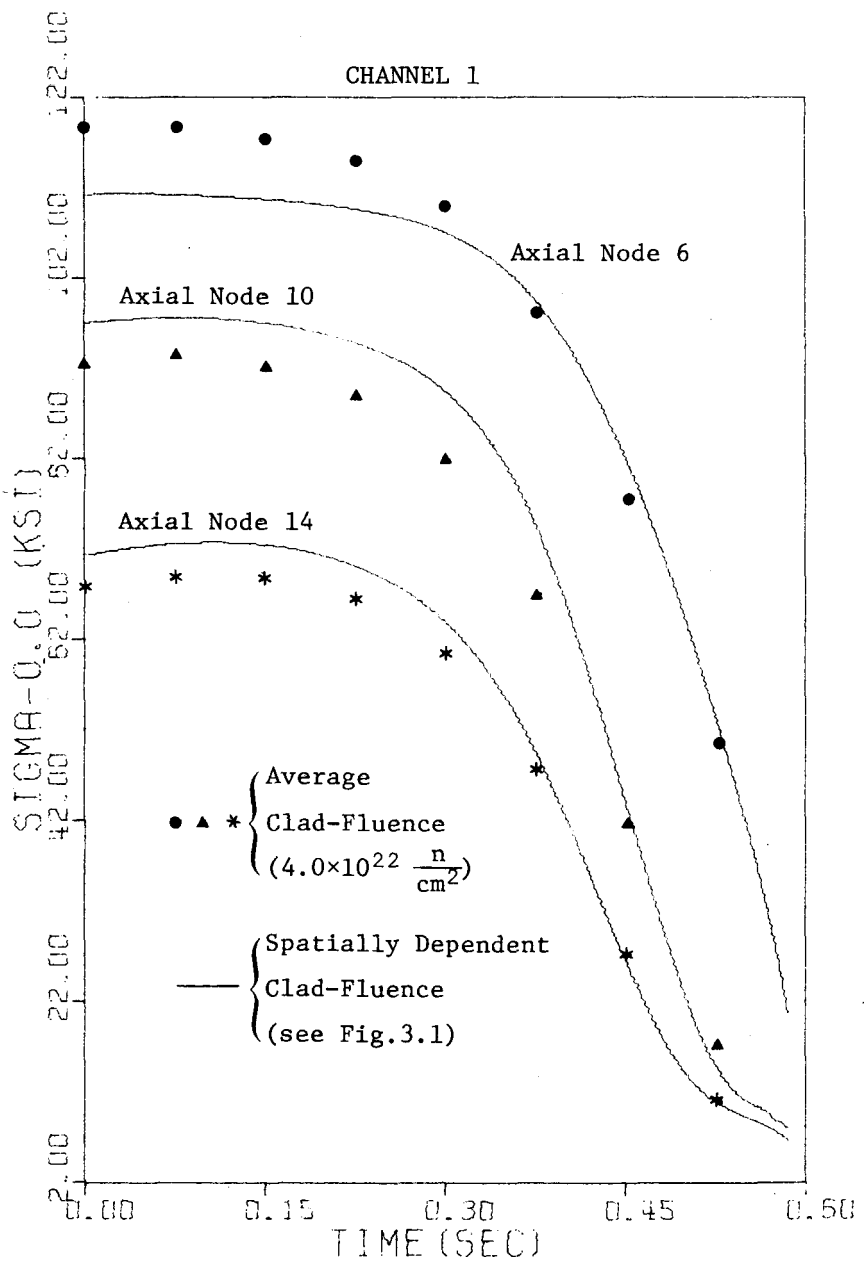

Figure 3.5. $\sigma_{0.0}$(KSI) (as determined from both the spatially dependent and average clad-fluence) vs. Time for Axial Nodes 6, 10 and 14 of Channel 1 - $3/s Initiating Ramp

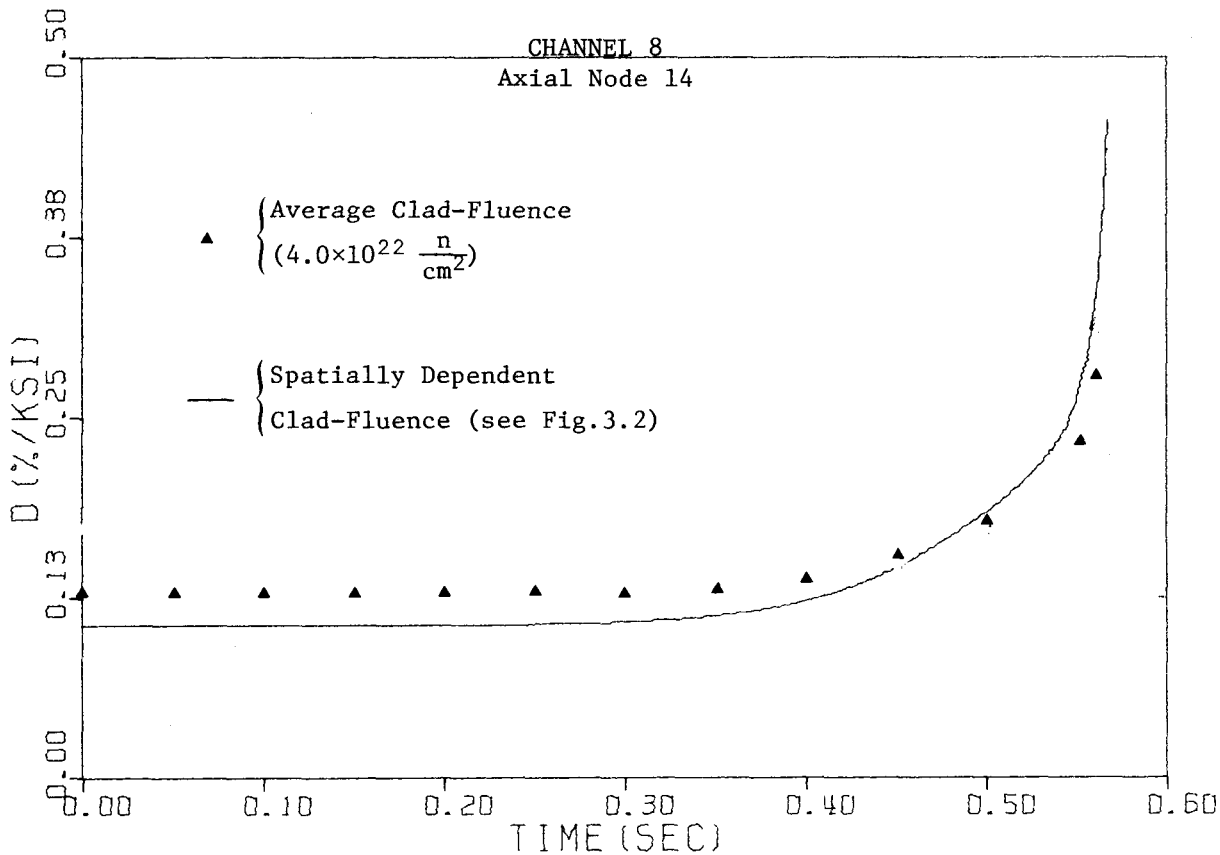

Figure 3.6. D(%/KSI) (as determined from both the spatially dependent and average clad-fluence) vs. Time for Axial Node 14 of Channel 8 - $3/s Initiating Ramp

and spatially dependent clad-fluence (for axial node 14 of channel 8) are compared. However, by choosing another clad position, say axial node 10 of channel 1, one can obtain a totally different perspective on the behavior of this constant (see Figure 3.7). One now finds that there is absolutely no correlation between the value of D calculated from the spatially-dependent and average clad-fluence. In fact, as depicted in Figure 3.7, the constant appears to have an erratic and unrealistic behavior. Upon checking other clad positions, one finds roughly the same effect. The cause of this unrealistic behavior in the parameters C and D will be discussed later. For now, it is only necessary to say that there is no definable behavior for these constants as a function of clad-fluence, so that one cannot expect to obtain improved estimates of the clad-failure location by incorporating spatially dependent clad-fluence into the PNL failure model.

The second major difference between the current strain-failure model and the earlier simplified model is in the correlation used in calculating the plastic strain generated at a given time step. It was originally assumed that the clad stress generated at a given clad node would only slightly (if at all) exceed the yield stress of the node before pin failure occurred, so that a simplified correlation for the plastic strain,

$$\varepsilon_{plastic}(\%) = \varepsilon_{P(1)}(\%) = C(\sigma-\sigma_{PEL}), \quad \text{for } \sigma > \sigma_{PEL},$$

could be employed. This assumption, however, was found to be incorrect, and a complete algorithm for calculating clad-strain is now used; that is,

$$\varepsilon_{plastic}(\%) = \varepsilon_{P(1)}(\%) \quad \text{or} \quad \varepsilon_{P(2)}(\%),$$

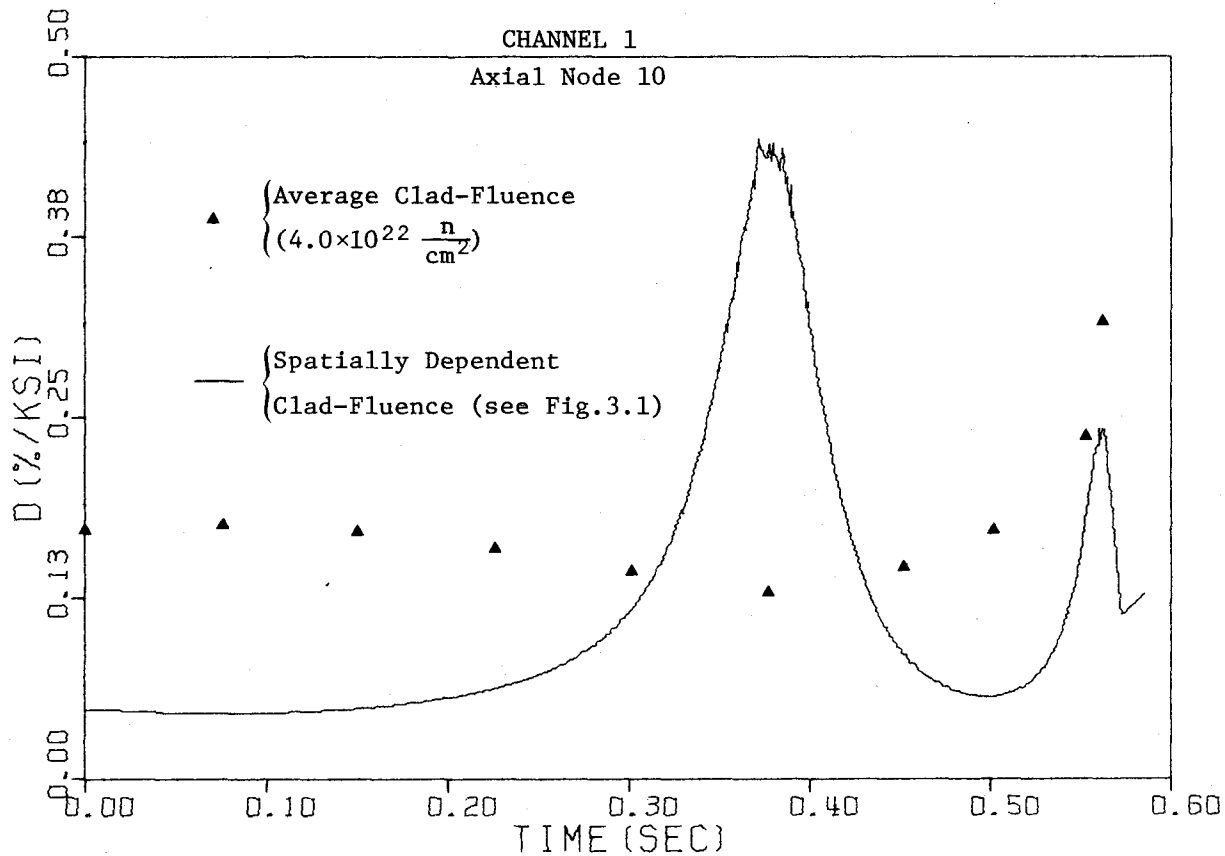

Figure 3.7. **D(%/KSI) (as determined from both the spatially dependent and average clad-fluence) vs. Time for Axial Node 10 of Channel 1 - $3/s Initiating Ramp**

where

$$\varepsilon_{P(1)}(\%) = C(\sigma-\sigma_{PEL}), \quad \text{for} \quad \sigma_{PEL} < \sigma \leq \sigma_{YS}, \text{ and}$$

$$\varepsilon_{P(2)}(\%) = D(\sigma-\sigma_{0.0}), \quad \text{for} \quad \sigma > \sigma_{YS}.$$

The meaning of the various terms in the above expressions is described in BNW-LM-TN-77-4.

The effect of this change in the correlation on the rate of strain accumulation is clearly evident in the graph of "Clad-Strain vs. Time" (Figure 3.8). Since the loading on the clad between 0.57 and 0.59 seconds is increasing in a fairly uniform manner (see Figure 3.3), the abrupt change of slope in the clad-strain can only be due to the presence of the new strain algorithm with the hoop-stress increasing beyond σ_{YS}. This hypothesis was in fact verified by comparing values of the clad hoop-stress and yield stress (as a function of time in the transient) for the respective clad nodes. Therefore, the new strain algorithm has the effect of increasing the rate of clad-strain accumulation. In terms of the effect on the course of the transient, then, the change in correlation should lead to earlier failure times than those computed with the old strain-correlation. Unfortunately, no conclusions can be drawn as to the effect of the new strain algorithm on the location of clad-failure, since this requires a highly accurate knowledge of the behavior of the constants C and D both with clad-position and time in the transient, and as will be shown presently, this is not always possible to obtain.

Finally, it was found in the preliminary studies of the "strain-failure limit" model that a method was needed for obtaining strain-failure

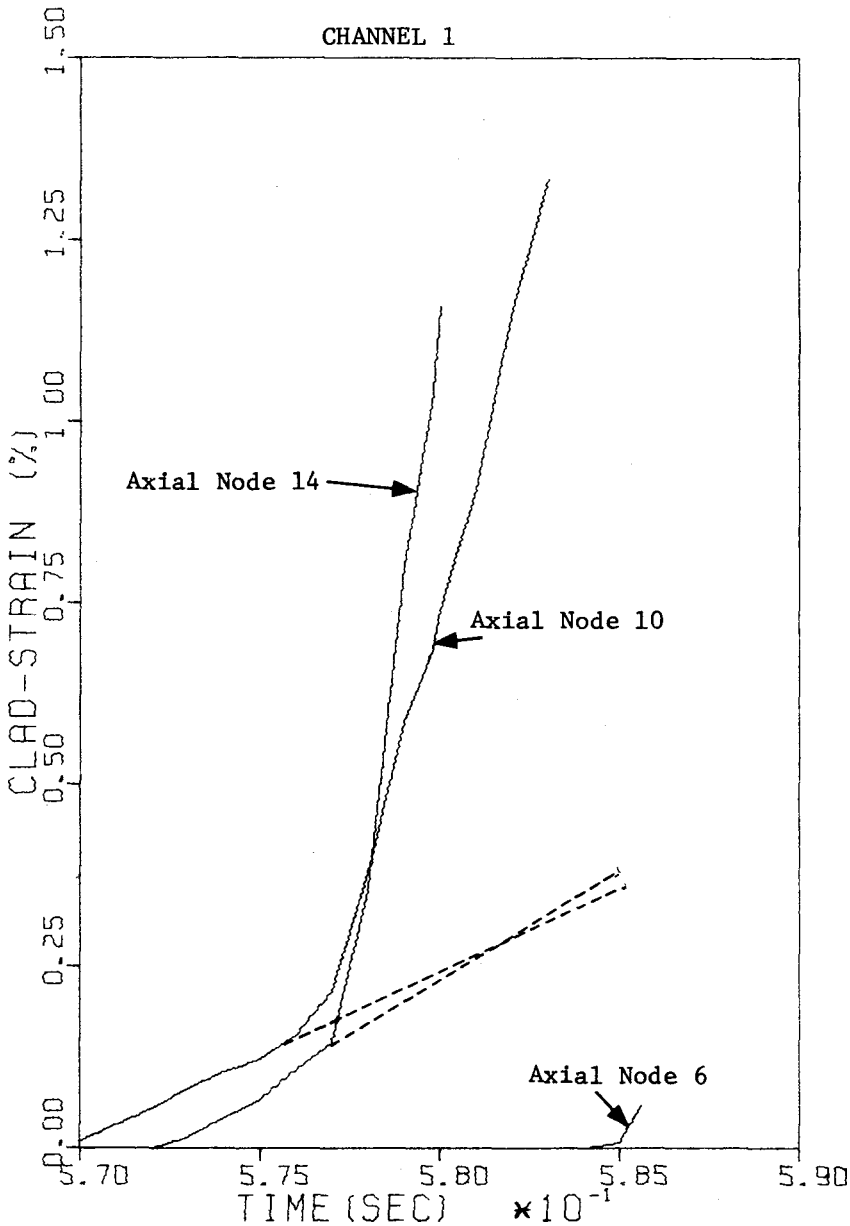

Figure 3.8. Clad-Strain(%) vs. Time for Axial Nodes 6, 10 and 14 of Channel 1 Between 0.57 and 0.59 Seconds - $3/s Initiating Ramp

limits for each clad node and at each time step as a function of the strain rate (interpolating between the 10^{o} F/s and 200^{o} F/s strain-limit data sets). To accomplish this, a linear interpolation of the failure limit is assumed between the two temperature rise-rate data sets. This interpolation procedure is conveniently represented by the "Strain-Failure Limit Correlation" discussed in the PNL report (BNW-LM-TN-77-4); that is,

$$Y(\%) = (-1.301 \times 10^{-6}z + 3.090 \times 10^{-4})x + (2.474 \times 10^{-3}z - 0.1298),$$

where

y = failure strain(%),

z = heating rate, ^{o}F/s, and

x = steady-state, mid-wall cladding node temperature ($^{\circ}$F),

It is further assumed in the PNL report that the indicated failure strain can continue to increase with temperature ramp rate until it reaches the maximum uniform strain value exhibited by unirradiated cladding with strain rate (approximately 4%). This occurs roughly between the temperature ramp rates of 3,024 to 8,516^{o} F/s.* Whether this assumption is valid still requires verification, as it appears that it could lead to fuel and clad failure conditions which are non-physical since the time to failure is increased (see Fig. 3.9).

*It was stated in BNW-LM-TN-77-4 that for transients $\leq$ \$3/s the temperature ramp rate will probably be below 200-300^{o} F/s. In actuality, the temperature ramp rate for a \$3/s input reactivity ramp (towards the end of the transient) is on the order of 5,000^{o} F/s.

Not much can be concluded about the incorporation of the strain-limit correlation into the strain-failure model. Because of the size of the transient (i.e., \$3/sec), all the clad-nodes in the reactor core reach their maximum strain-limit value (either that given by the 200^{o} F/sec data set or the maximum value for unirradiated cladding) early in the transient. Thus, using the strain-failure limit correlation does not give any difference in results than if these maximum strain-limits had been used at the onset of the transient. In order to further study the effect of incorporating the new strain-limit correlation into the failure model, a transient on the order of \$.10 to \$.50/sec would have to be run.

The results obtained from the sample \$3/sec reactor transient show that the strain-failure model is not useable in its present form. To understand why this is so, one only has to look at the values of the temperature-dependent parameters C and D (as a function of time) obtained from the model (Figures 3.10 and 3.11, respectively). One would expect these constants to be monotonically increasing functions of clad-temperature and, hence, of time. Instead, these parameters exhibit an erratic and unrealistic behavior, so that their use in predicting the clad plastic-strain is totally unjustified. The explanation for this phenomena can best be understood by realizing how the values of C and D are obtained. First, curve fits to σ_{PEL}, σ_{YS} and $\sigma_{0.0}$ are obtained from a limited number of experimental data points. These fits are satisfactory only in providing approximate values of the clad strength (i.e., σ_{PEL}, σ_{YS} and $\sigma_{0.0}$), to within a few KSI. However, the algorithms used to calculate the constants C and D require an

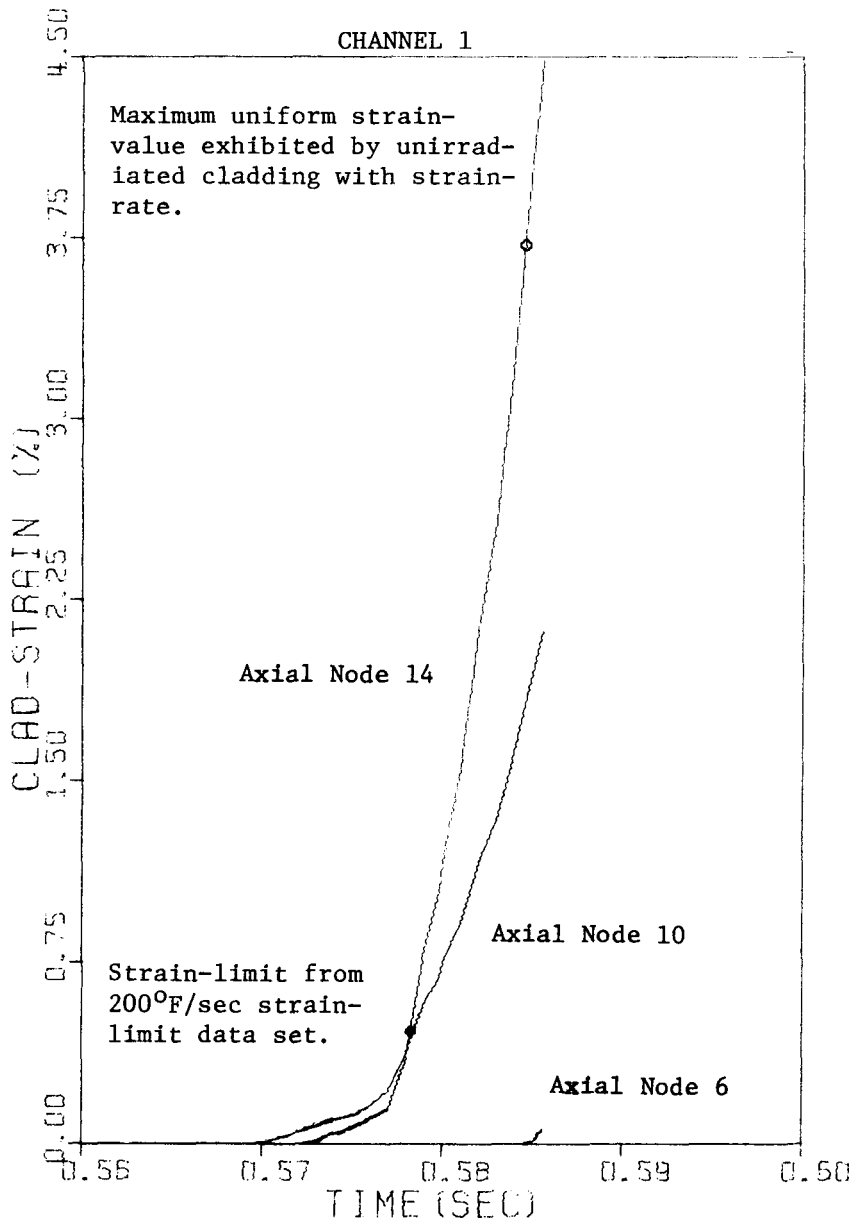

Figure 3.9. Clad-Strain(%) vs. Time for Axial Nodes 6, 10 and 14 of Channel 1 Between 0.56 and 0.60 Seconds - $3/s Initiating Ramp

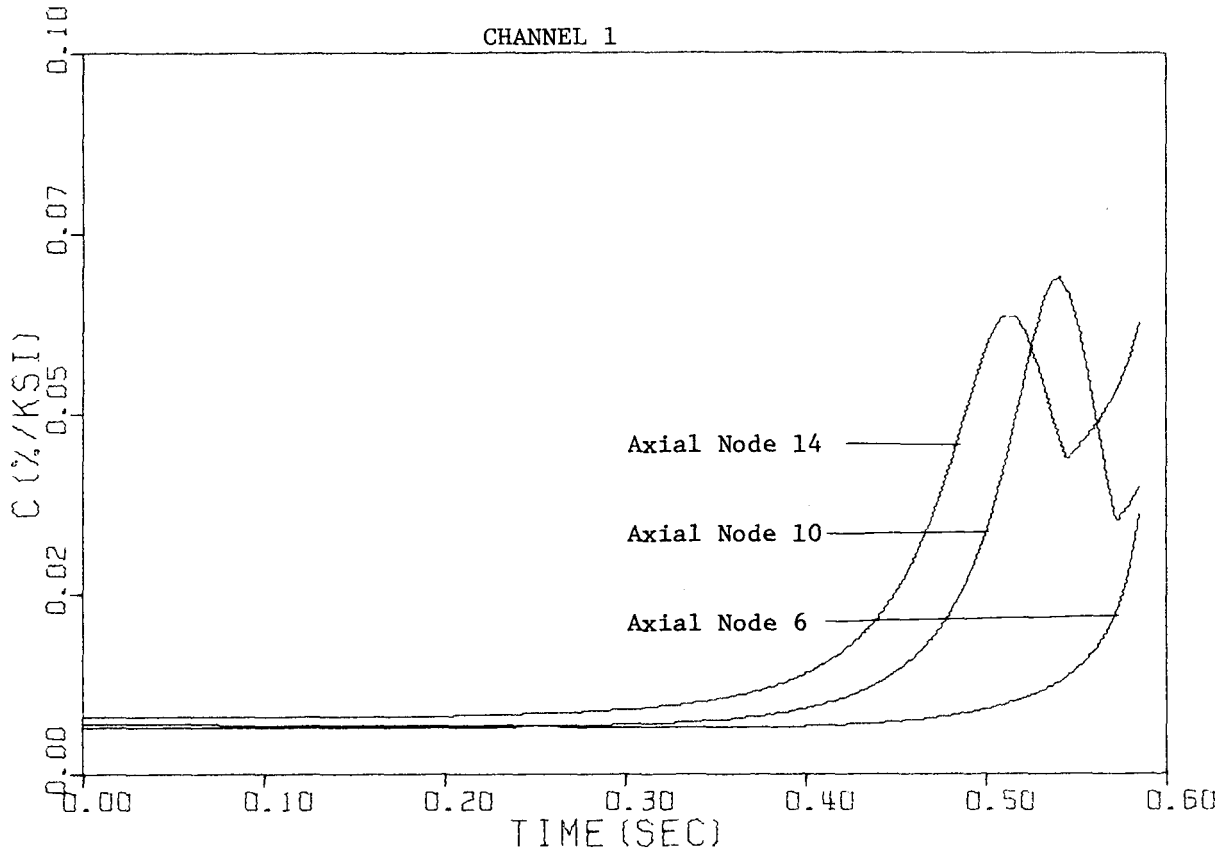

Figure 3.10. C(%/KSI) (as determined from the spatially dependent clad-fluence) vs. Time for Axial Nodes 6, 10 and 14 of Channel 1 - $3/s Initiating Ramp

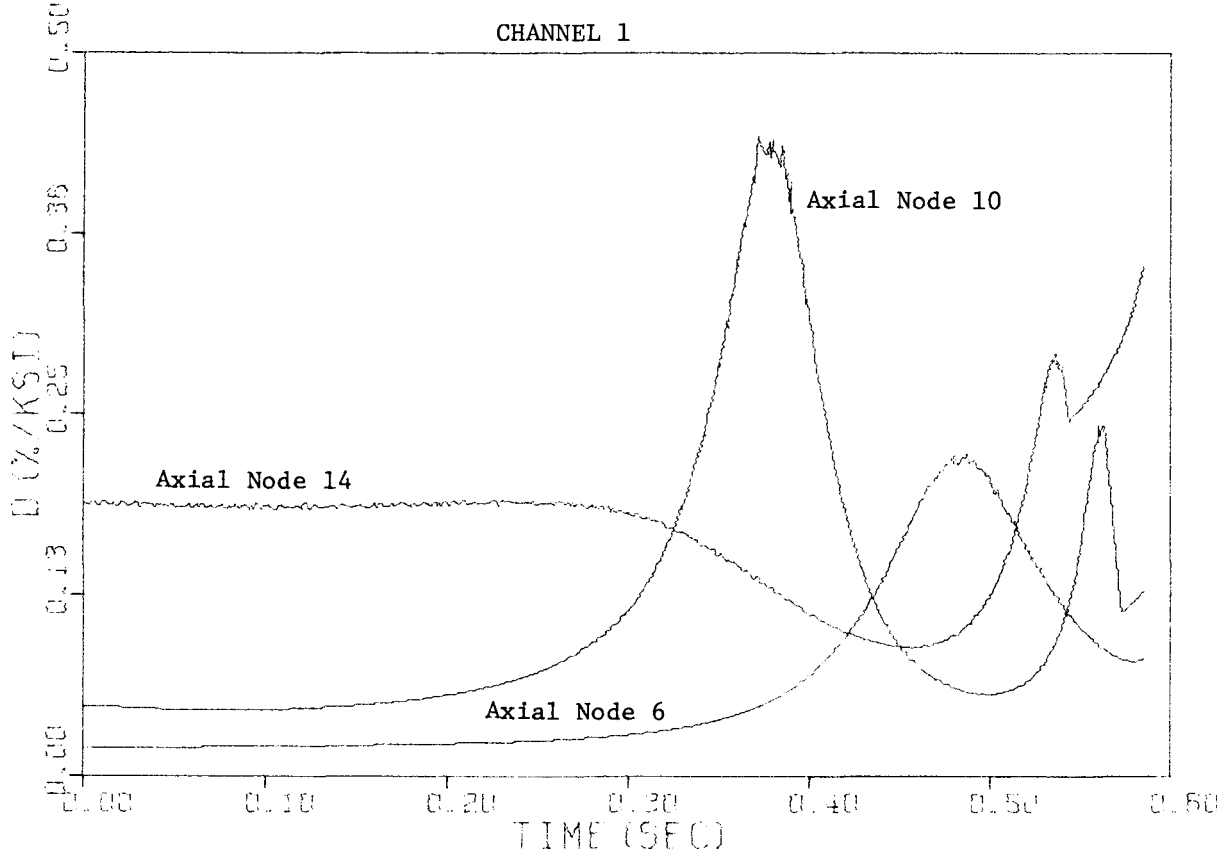

Figure 3.11. D(%/KSI) (as determined from the spatially dependent clad-fluence) vs. Time for Axial Nodes 6, 10 and 14 of Channel 1 - $3/s Initiating Ramp

extremely accurate knowledge of these clad-strength parameters. This can easily be seen by looking at the graphs comparing σ_{PEL}, σ_{YS} and $\sigma_{0.0}$ for axial nodes 6, 10 and 14 (Figures 3.12 - 3.14). We see in these graphs, for example, that the values of σ_{YS} and $\sigma_{0.0}$ are extremely close, in some cases much closer than the accuracy to which either of these values is known. This means that the value of D, given by

$$D(\%/KSI) = \frac{0.1732}{\sigma_{YS}-\sigma_{0.0}} ,$$

may not be controlled by any physical considerations or conditions of the clad, but rather only by the arbitrary error introduced by the curve fits of the parameters σ_{YS} and $\sigma_{0.0}$, thus making the value of D obtained unuseable. The same argument applies to the calculation of the constant C, although the problem does not arise until later in the transient when the closeness of σ_{PEL} and σ_{YS} magnifies the uncertainty in their values.

Therefore, since the values of C and D obtained from the model can take on erroneous values at any given time during the transient, there is no way that the strain failure method, as it now stands, can be used with any degree of confidence to predict clad failure.

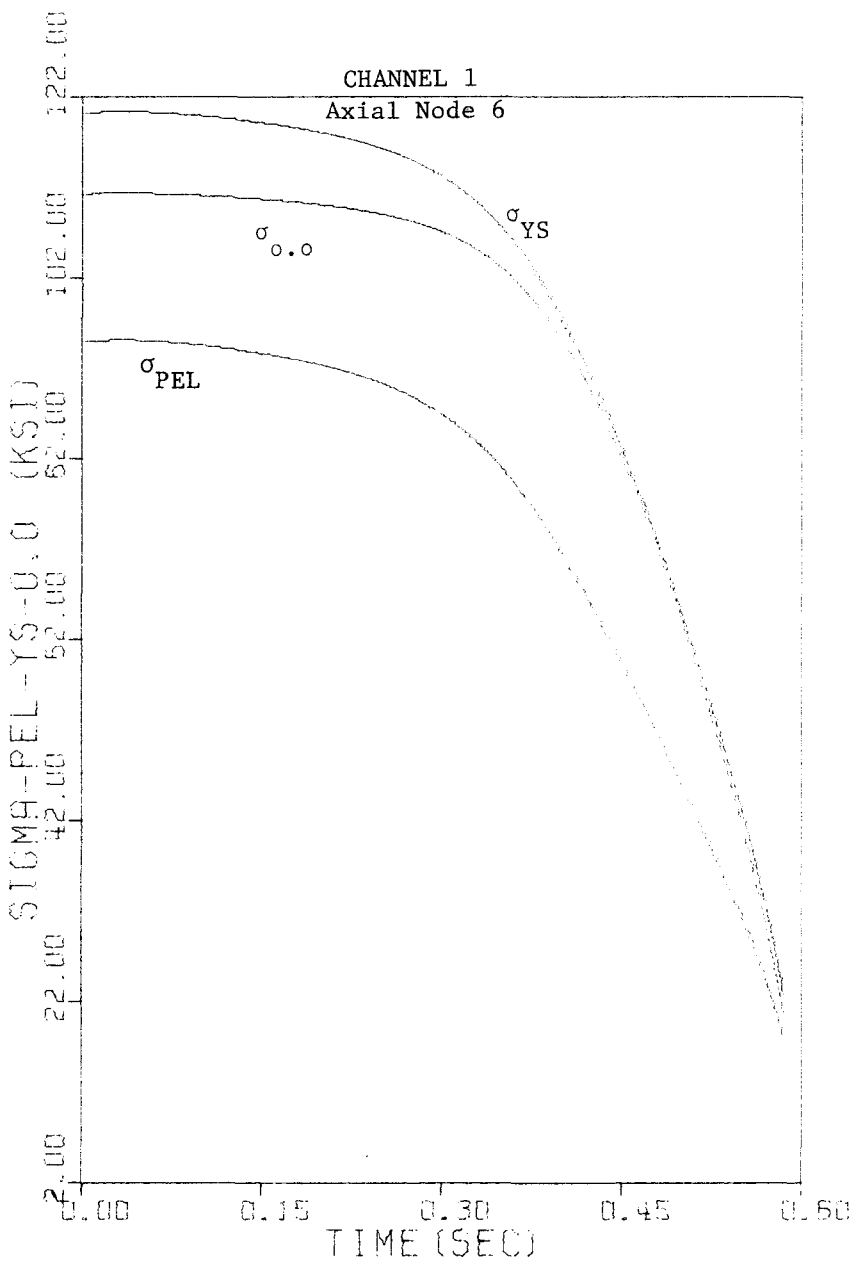

Figure 3.12. Clad-Strength Parameters (as determined from the spatially dependent clad-fluence) vs. Time for Axial Node 6 of Channel 1 - $3/s Initiating Ramp

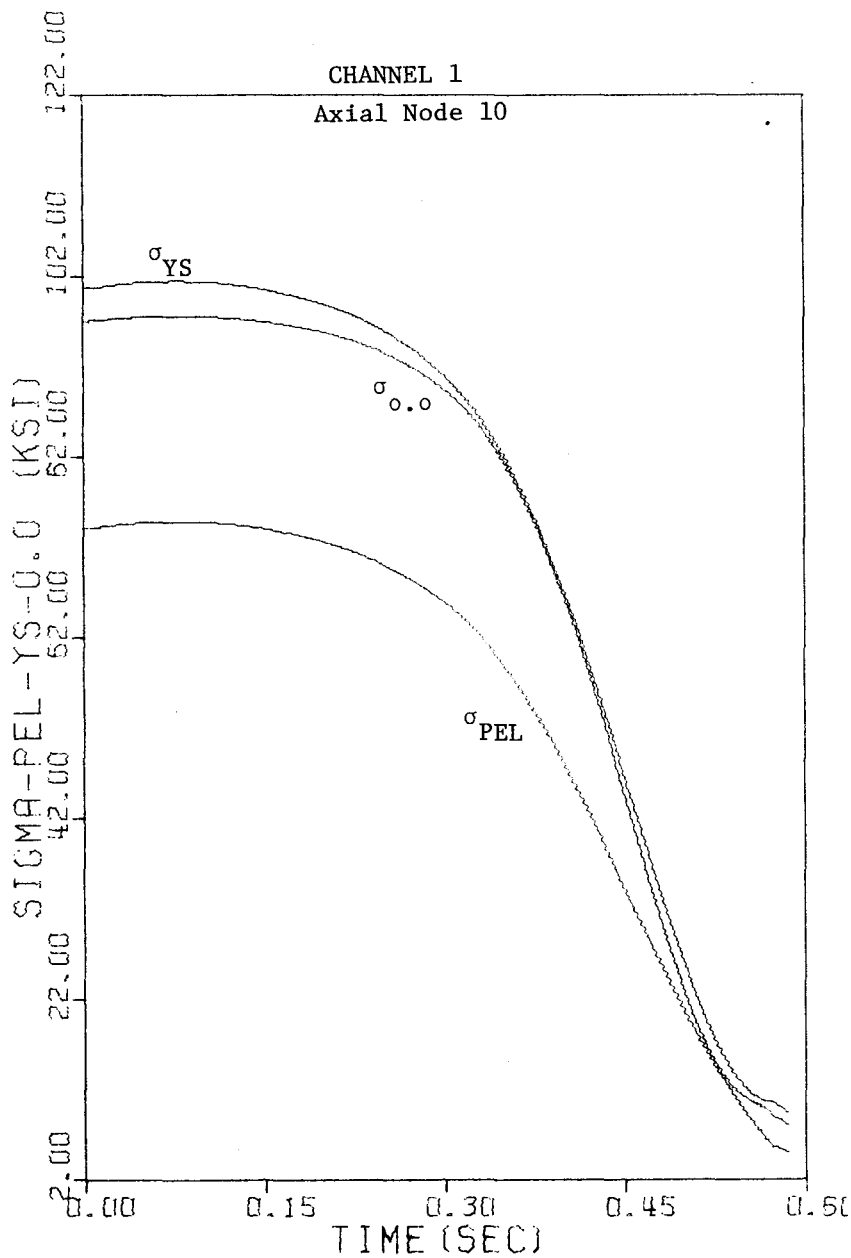

Figure 3.13. Clad-Strength Parameters (as determined from the spatially dependent clad-fluence) vs. Time for Axial Node 10 of Channel 1 - $3/s Initiating Ramp

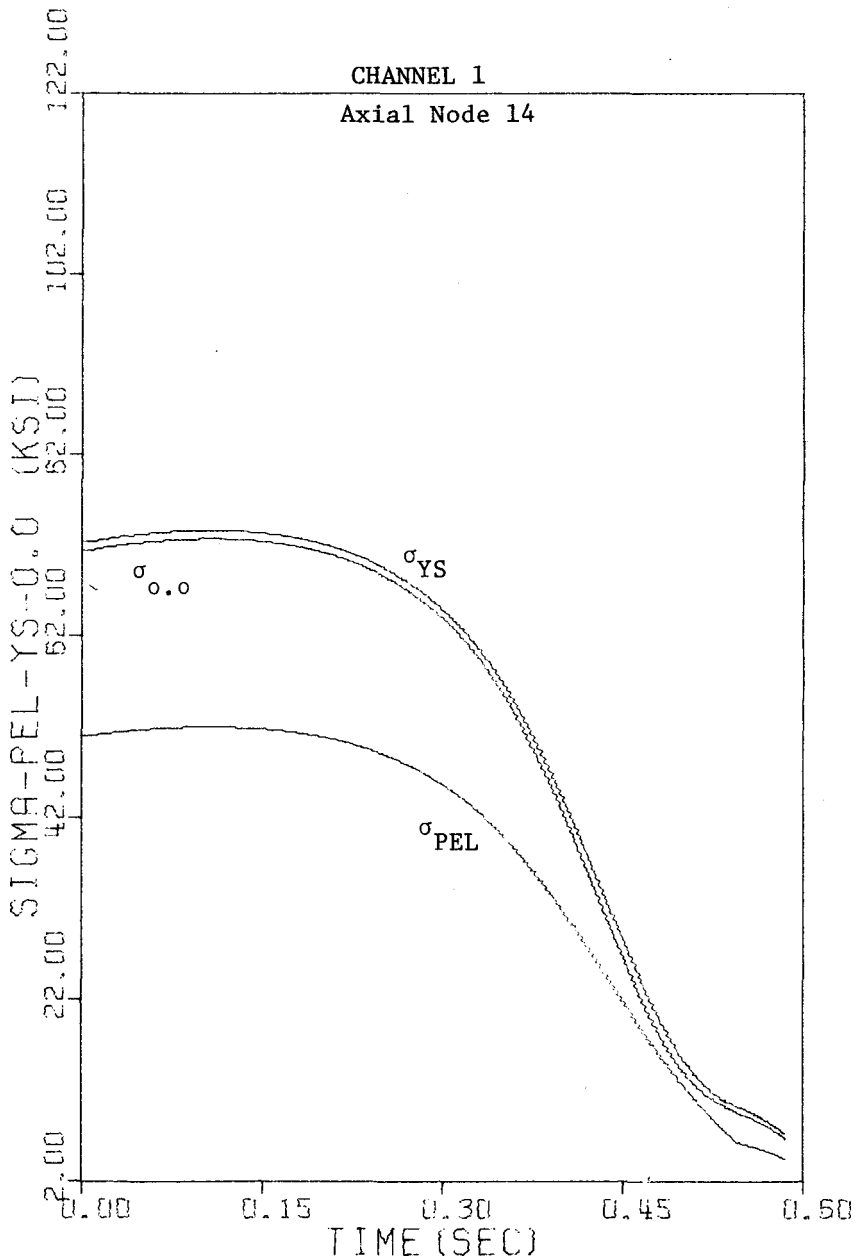

Figure 3.14. Clad-Strength Parameters (as determined from the spatially dependent clad-fluence) vs. Time for Axial Node 14 of Channel 1 - $3/s Initiating Ramp

3.3 Fuel Failure Prediction

This section briefly summarizes the failure prediction model developed for the JANE code. The model is described in more detail in References [34] and [36]. The results of using the JANE code to predict clad failure in two example type fuel pins are presented below.

In principle, from a knowledge of the fuel pin geometry, the material properties, the temperature distribution, and fission gas behavior, one can predict the distributions of stress and strain in the fuel and cladding as well as the fuel/cladding interaction. In computer codes such as DEFORM [37] and LIFE [38], such computations invølve a considerable amount of computer time in order to deal with the detailed axial, radial, and temporal variations in fuel pin behavior. This report utilizes a simplified approach for such predictions during slow overpower transient conditions, based on an extension of the models employed in the KRASS code [39]. KRASS was developed for the prediction of steady state behavior.

A summary of the assumptions of this method will serve to illuminate the simplifications:

1. The mechanical equations are quasi-static.
2. The plane strain approximation is used.
3. Axisymmetry is assumed and local effects are neglected.
4. The fuel/clad mechanical interaction is treated approximately by means of a free body force balance.
5. Microscopic phenomena such as transient fission gas swelling and hot pressing in the fuel must be characterized macroscopically.
6. The continuous-body, cylindrical-geometry stress equilibrium equation applies.

7. Current time-step strain calculations use previous time-step stresses.

The inelastic strains, including the creep strain, that accumulate in one time step, are determined from existing empirical formulae and the previous time step stress condition. A system of displacement-inelastic strain and stress-inelastic strain relations [40] has been used, such that the stress variation and the boundary movements that are induced by the inelastic strains can be determined. Creep is the only inelastic phenomenon that is considered in the fuel. The dilatational strains considered in both the fuel and clad are thermal-gradient and pressure induced. Transient fission gas bubble swelling and hot pressing are also considered in the fuel. The transition from elastic to plastic deformation is considered in the clad only, and is determined simply by using the Tresca yield criterion with a temperature- and fluence-dependent yield stress. Once the criterion is met, the clad is considered perfectly plastic. Pressure displacements in the plastic regime are found by using an effective plastic modulus to simulate the true stress-true strain curve.

The fuel is considered to be a brittle material and is, therefore, divided into two regions. Below the brittle-ductile transition temperature, the material has strength and deforms elastically. Above the brittle-ductile transition temperature, the fuel is considered strengthless. The ductile region transmits the cavity pressure, as a hydrostatic pressure, to the interface of the two regions.

When the maximum tensile stress from all contributors exceeds the fracture strength of the fuel, the brittle region is assumed to crack. In this event, which occurs soon after the TOP begins, the fuel is

assumed to immediately displace, so that the gap closes. Another major assumption in this simplified approach is that deformation of cracked fuel continues as if the fuel had not fractured. The strength of cracked fuel actually lies somewhere between strengthless and that of uncracked fuel [41].

This method has been coupled to the fission gas release and fuel motion models introduced previously [36]. Several simulated transients in a single GCFR fuel pin have been performed. The transients are induced by an exponential power rise such that an order of magnitude power increase is achieved in 10 seconds. The results are presented in Table 1. Cases S1, S2, and S4 assume steady state irradiation has closed the gap and has provided a non-zero pre-transient stress/strain state. Case S3 is identical to Case S1, except that the gap is initially open and no pre-transient stresses or strains have been applied. Case S2 includes fission gas release through molten fuel [36] and Case S4 additionally includes molten fuel motion. Case S1 has no molten fuel motion and gas release bypasses the molten fuel. In all cases the failure time and location are governed by the approach to the yield stress. Case S3 differs only slightly because fuel cracking closed the gap very early in the transient.

From these results, it therefore appears that under the present assumptions, the pre-transient stress/strain state does not govern the failure time and location. Due to the overriding importance of the stress approach to yielding in the clad, temperature-dependent yield stresses developed under transient temperature rise conditions should be derived. This work also points out the need for high-stress, high-temperature fuel and clad creep rate data.

Table 1.

Failure Prediction Study-- Results Summary [36].

Case	Failure Time (s)	Yield Time[1] (s)	Failure Location[2] (cm)	Cavity Pressure[3] (MPa)	Fuel/Clad Mechanical Interaction Pressure[3] (MPa)	Outer Clad Hoop Strain[3] (ΔD/D)	Clad Outer Radius[3] (cm)	Average Clad Hoop Stress (MPa)	Outer Clad Temperature (° C)	Peak Melt Fraction[3,4]	Melt Fraction at Failed Location
S1	5.5500	5.5250	128.67	68.3	57.2	0.01399	0.3650	219.6	903.6	0.248	0.0
S2	5.5547	5.5437	128.67	63.0	55.8	0.01398	0.3649	219.6	904.1	0.250	0.0
S3	5.6875	5.6750	128.67	71.9	48.3	0.01436	0.3648	150.9	929.7	0.302	0.007
S4[5]	------	------	128.67	61.6	55.8	0.0085	0.3648	219.6	900.1	0.234	0.0

Note: (1) Tresca criterion met and plastic deformation begins.

(2) Midplane of axial section number 8.

(3) At failure; failure is defined as having a permanent deformation greater than 0.005 ΔD/D.

(4) Fraction of mass in axial section which is molten.

(5) This case was not carried out to failure-- run termination time is 5.5187 seconds.

Two simulated transients in a single CRBR-type fuel pin have been performed. The transients were induced by the exponential power rise described in the previous chapter with $\tau = 4.34$ at a burnup of 38,000 MWD/T. The case description is presented in Table 2 and the results summary is found in Table 3. These two cases have been studied to determine the effect of steady-state irradiation induced fuel and clad pre-stressing and pre-straining on failure time and location during a TOP. Case FP1 uses the stress/strain state of the fuel rod, as calculated by the KRASS code, for initial stress/strain conditions. At this burnup, KRASS has calculated a completely closed gap in the core region. Case FP2 has identical input, except that the fuel and clad are stress free and irradiation-induced displacements are not considered. The initial gap width is simply due to the relative fuel and clad thermal expansion.

Table 3 shows that the open gap case fails 89 milliseconds sooner than the pre-stressed case, and that pre-stressing had no detectable effect on failure location. The reason for this is twofold. First, fuel cracking closes the gap very early in the transient. The gap of Case FP2 is calculated to be fully closed in the core region at 1.75 seconds after the start of the transient. The detailed results show that the transient-developed mechanical interaction pressure between the fuel and clad is 20 times larger than the steady-state induced pressure at the axial interval which exhibited first failure (node 6). Second, case FP2's cavity pressure is significantly larger than for the pre-stressed case FP1. Case FP1 has used a larger initial fuel radius because of the steady-state irradiation effect. Since the linear power densities are input to the JANE code, this result causes the code to calculate a 5% lower volumetric

Table 2. Failure Prediction Study-- Case Description.

Case	Peak Steady State Power (W/cm)	Burnup (MWD/T)	Transient Time Constant (s)	Initial Gap?*
FP1	361	38,000	4.34	No
FP2	361	38,000	4.34	Yes

*Yes denotes that the gap is assumed to be open upon initiation of the transient, and that there is no steady-state pre-stressing or pre-straining due to steady-state irradition.

No denotes that the gap is closed due to steady-state irradiation, and pre-stressing and pre-straining from the KRASS code.

Table 3. Failure Prediction Study-- Results Summary.

Case	Failure Time (s)	Yield Time[1] (s)	Failure Location (s)	Cavity Pressure[3] (MPa)	Fuel/Clad Mechanical Interaction Pressure[3,7] (MPa)	Total Outer Clad Hoop Strain[3,4,7] (ΔL/L)	Clad Outer Radius[3,7] (cm)	Average Clad Hoop Stress[3,7] (MPa)	Outer Clad Temperature[3,7] (°C)	Peak Melt Fraction[3,5,7]	Melt Fraction (3,7)
FP1	5.088	5.055	81.3[2]	11.4	84.8	0.0.48	0.2591	483	840	0.28	0.28
FP2	4.994	4.998	81.3	16.3	86.2	0.0149	0.2591	489	832	0.33	0.33

Notes: (1) Tresca yield criterion met; plastic deformation begins.

(2) Midplane of axial interval number 6 which extends ±7.6 cm from this location; 81.3 cm is the core midplane.

(3) At time of failure.

(4) Elastic plus plastic strain at failure; failure is defined as having a permanent deformation greater than 0.005 ΔD/D.

(5) Fraction of mass in axial section which is molten.

(6) This case was not carried out to failure; the computer run terminated at a simulated time of 5.5187 seconds.

(7) At failure location.

power density for Case FP1. The lower power density causes a 0.2 second delay in the onset of fuel melting in the uppermost and lowermost nodes within the central cavity (nodes 4 and 8). Since very large axial node intervals were used (15.25 cm), the cavity volume decreases rapidly with the onset of fuel melting in these two nodes. The pressure, in turn, increases rapidly. At about 5 seconds Case FP2 exhibits a 33% smaller cavity volume than Case FP1. The remainder of the pressure difference is caused by a larger fission gas release from axial intervals 4 and 8, due to the larger melt fraction.

It should be noted that the calculated failure locations are within the axial intervals whose midplane is the core midplane. Because of the very large axial intervals, the transient pressure rise is probably overestimated. Decreasing the interval size would not only delay failure but may shift the failure location. Failure location primarily depends on the interplay of differential thermal expansion, cavity pressure transmitted to the clad, fuel and clad creep relaxation, and clad strength. The first three are embodied in the fuel/clad mechanical interaction pressure shown in Figure 3.15. Four locations are shown which represent the four axial intervals from the core midplane to the core top. In general, failure occurs at the location which reaches the clad yield point first when using a permanent deformation failure criterion. The interplay between clad pressure and clad strength (or yield stress) is accounted for in the Tresca yield criterion, for which the transient values are shown in Figures 3.16 and 3.17. Since the yield stress, and therefore the yield criterion, is a strong function of temperature, failure location is biased toward the hotter, weaker clad above the core midplane. Decreasing the axial intervals, thereby providing a more realistic

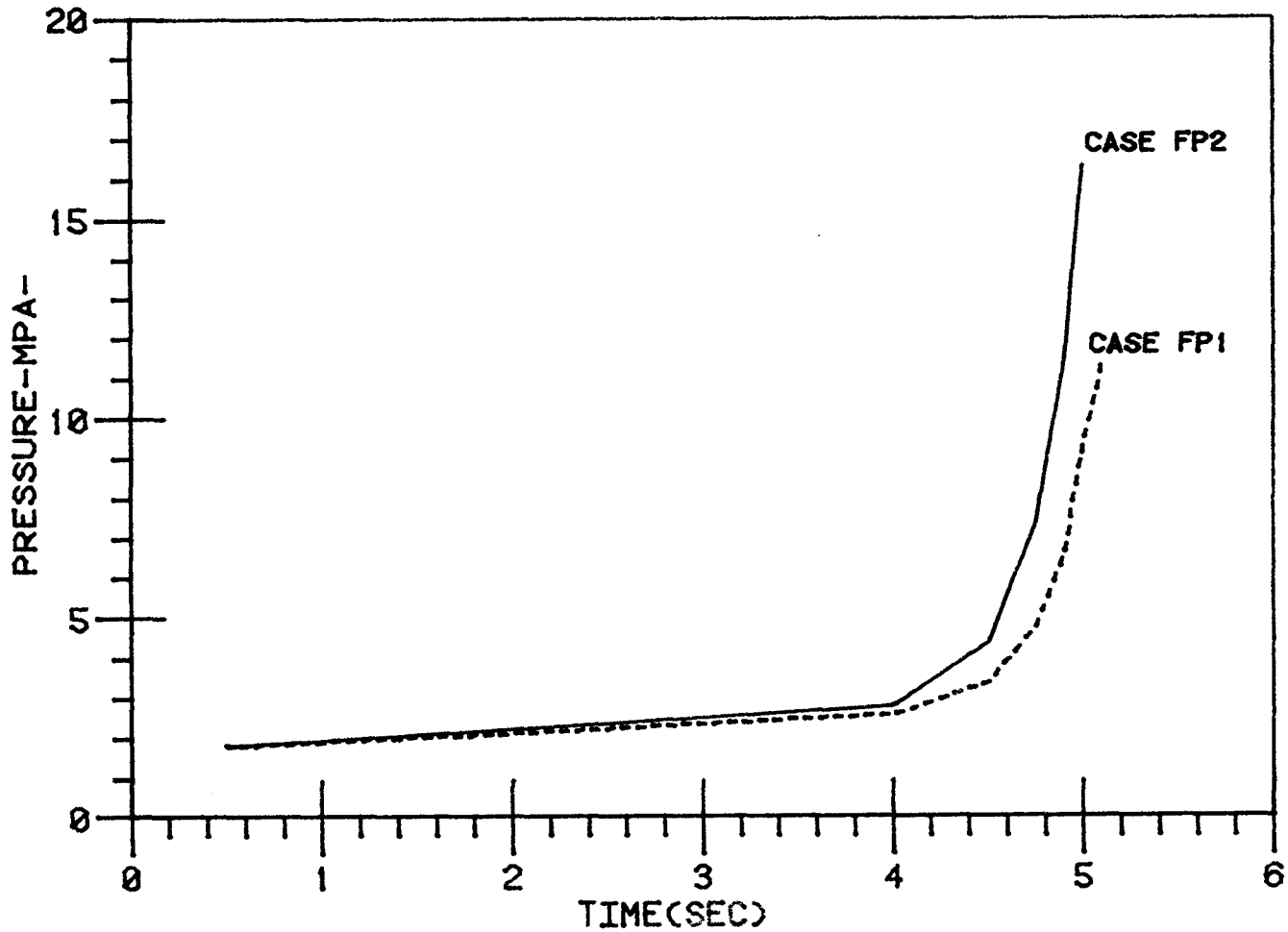

Figure 3.15. Cavity Pressures for Failure Prediction Study.

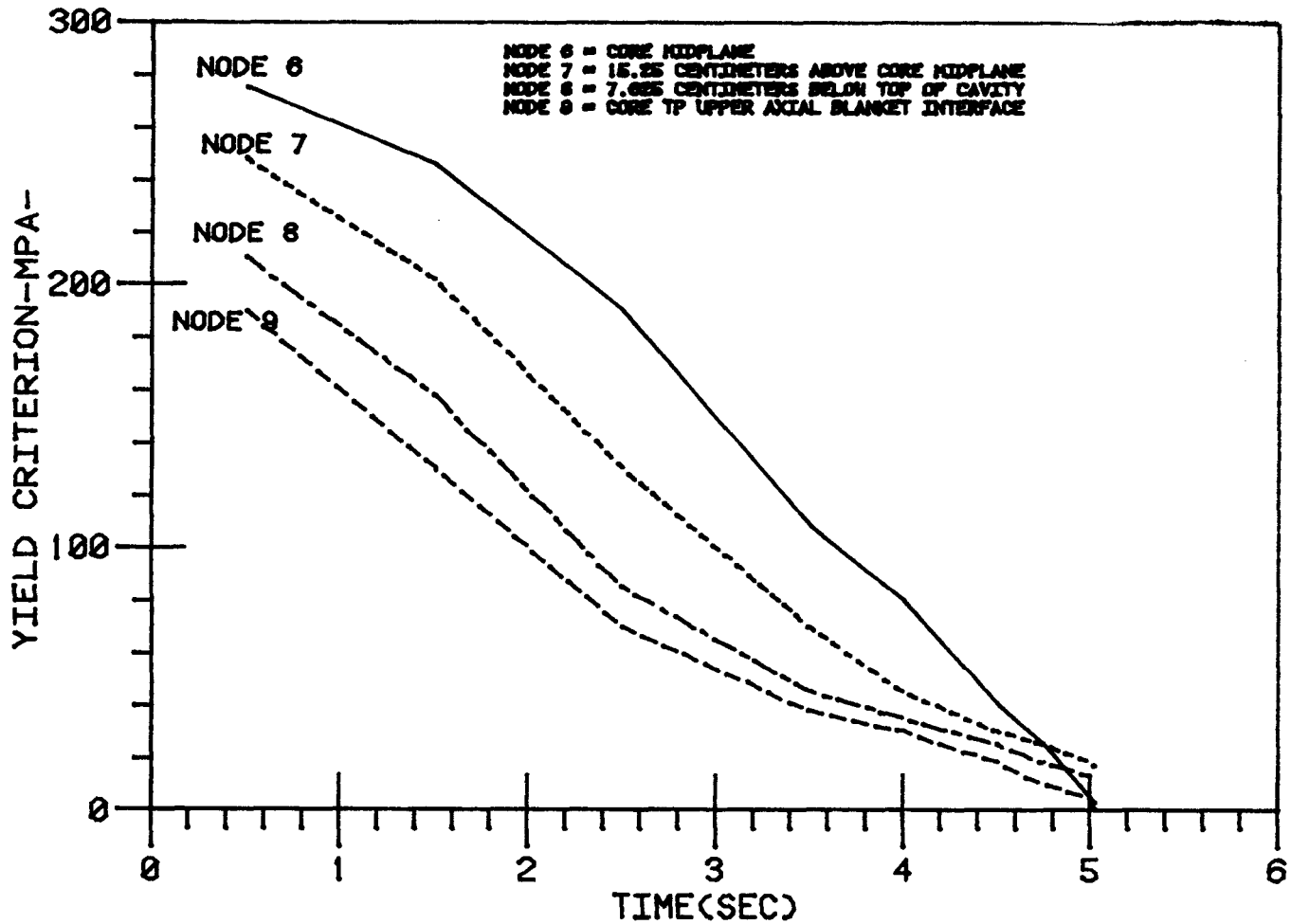

Figure 3.16. Tresca Yield Criterion in Clad (Case FP1).

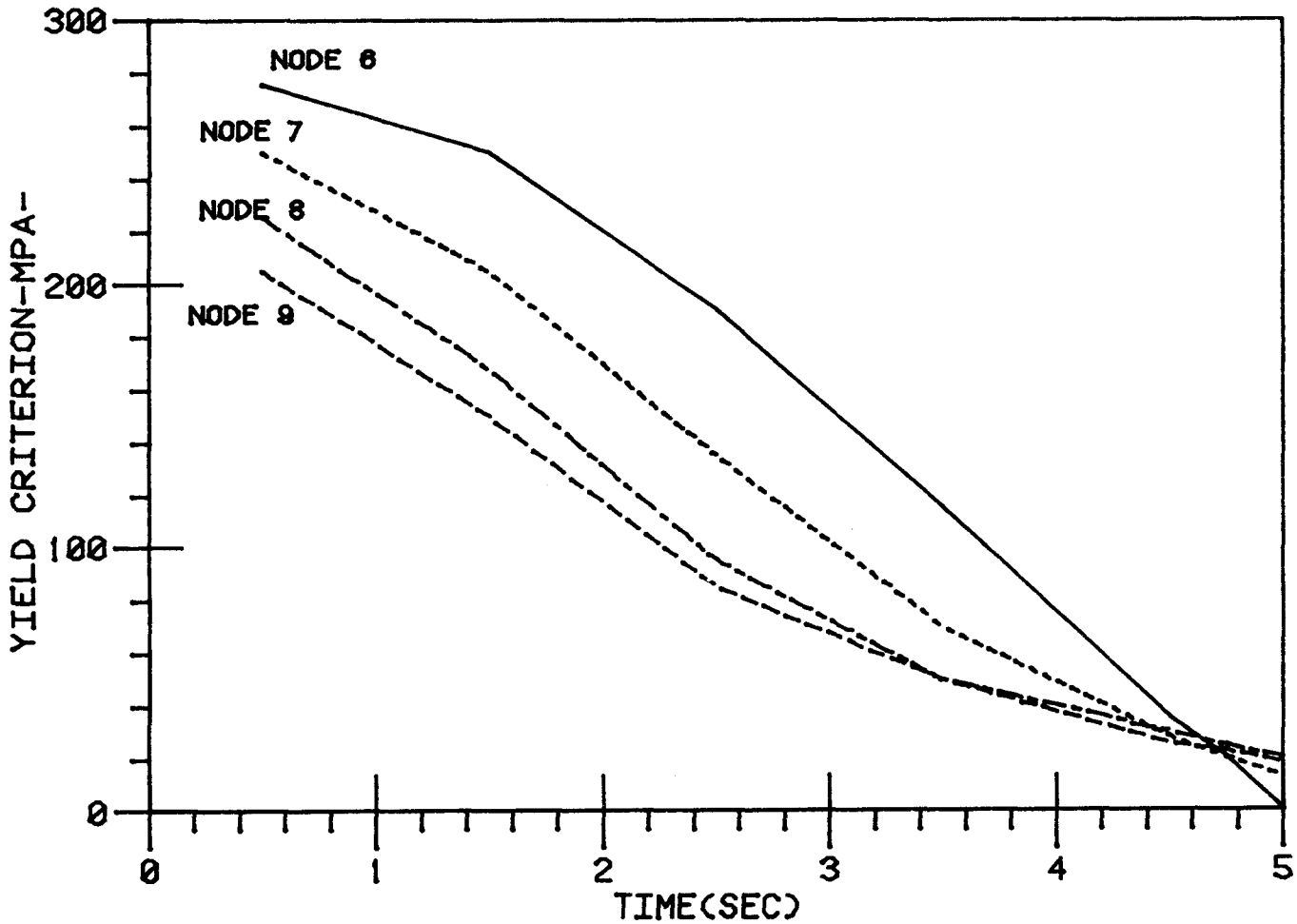

Figure 3.17. Tresca Yield Criterion in Clad (Case FP2).

pressure transient, may allow the clad temperature effect on the yield stress to become even more apparent. The failure location, in this event, may be calculated to be slightly higher in the core.

Another effect which is illustrated in these figures is the potential for failure of other core locations. Steady irradiation produces interaction pressures greater at the core extremities than at the midplane, because fuel swelling dominates. Transient irradiation produces mechanical interaction pressures larger at the core midplane, because cavity pressure and differential thermal expansion dominate. Case FP1 (Figure 3.18) shows that pre-stressing produces the next likely failure location at the bottom of the core. Case FP2 (Figure 3.19), however, shows a definite shift in this trend. The potential for failure of the core bottom (node 9) is less than that of the interval above the core midplane (node 7). Figures 3.18 and 3.19 show how the mechanical interaction pressure of node 6 progresses during the transient. In Case FP2 it dominates from start to finish. In the pre-stressed case, however, the interaction pressure must overcome a low steady-state value. Note that the interaction pressures of Case FP2 are zero until the fuel cracks and begins to contact the clad.

Figure 3.20 is a comparison of the clad outer hoop strain history at the failure location. It is seen here, also, that the transient strain tends to overcome the pre-transient irradiation-induced strain. The elastic strain is between 60% and 70% of the total strain at failure for the 0.005 $\Delta D/D$ permanent deformation criterion.

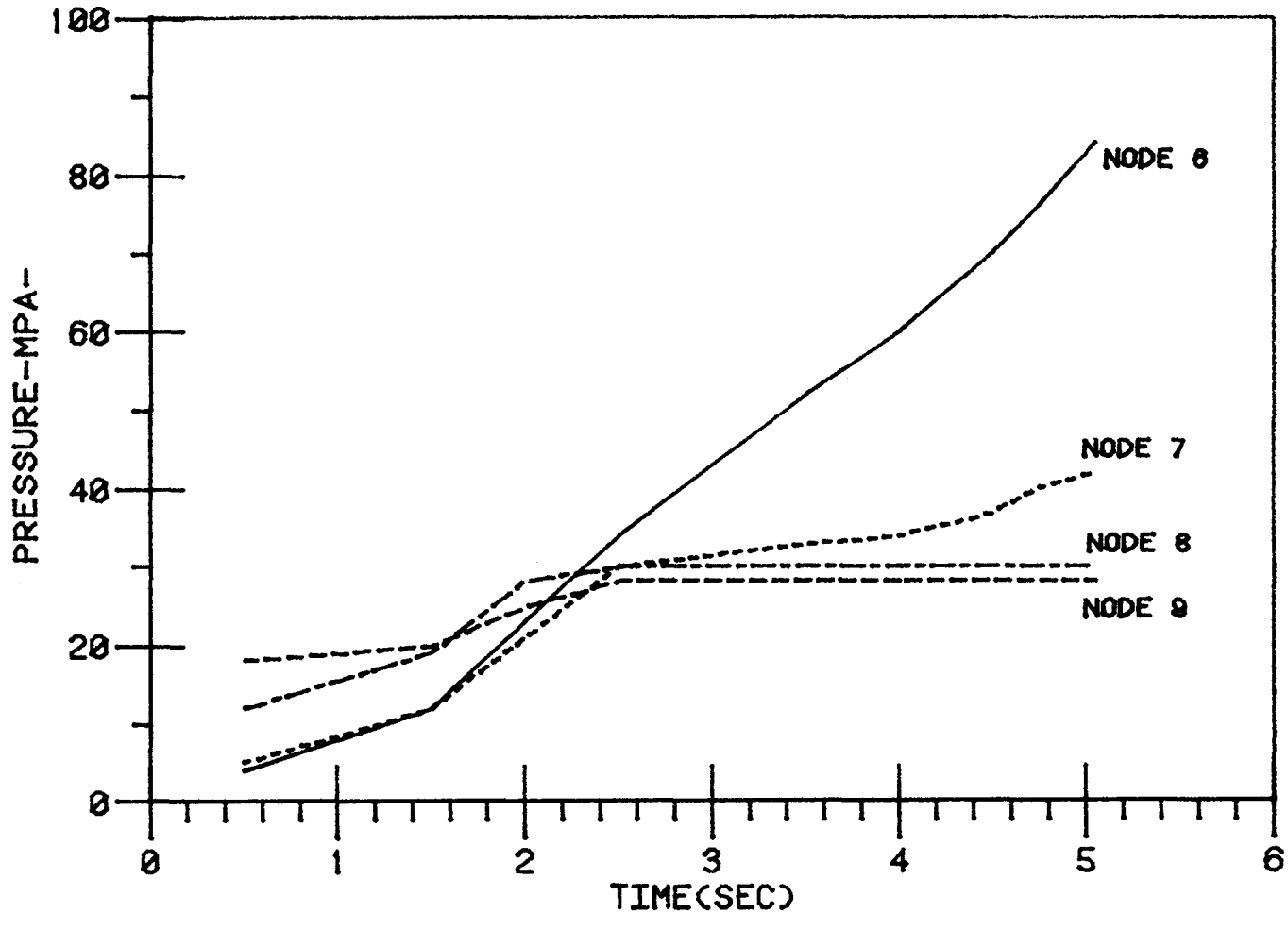

Figure 3.18. Fuel/Clad Mechanical Interaction Pressure (Case FP1).

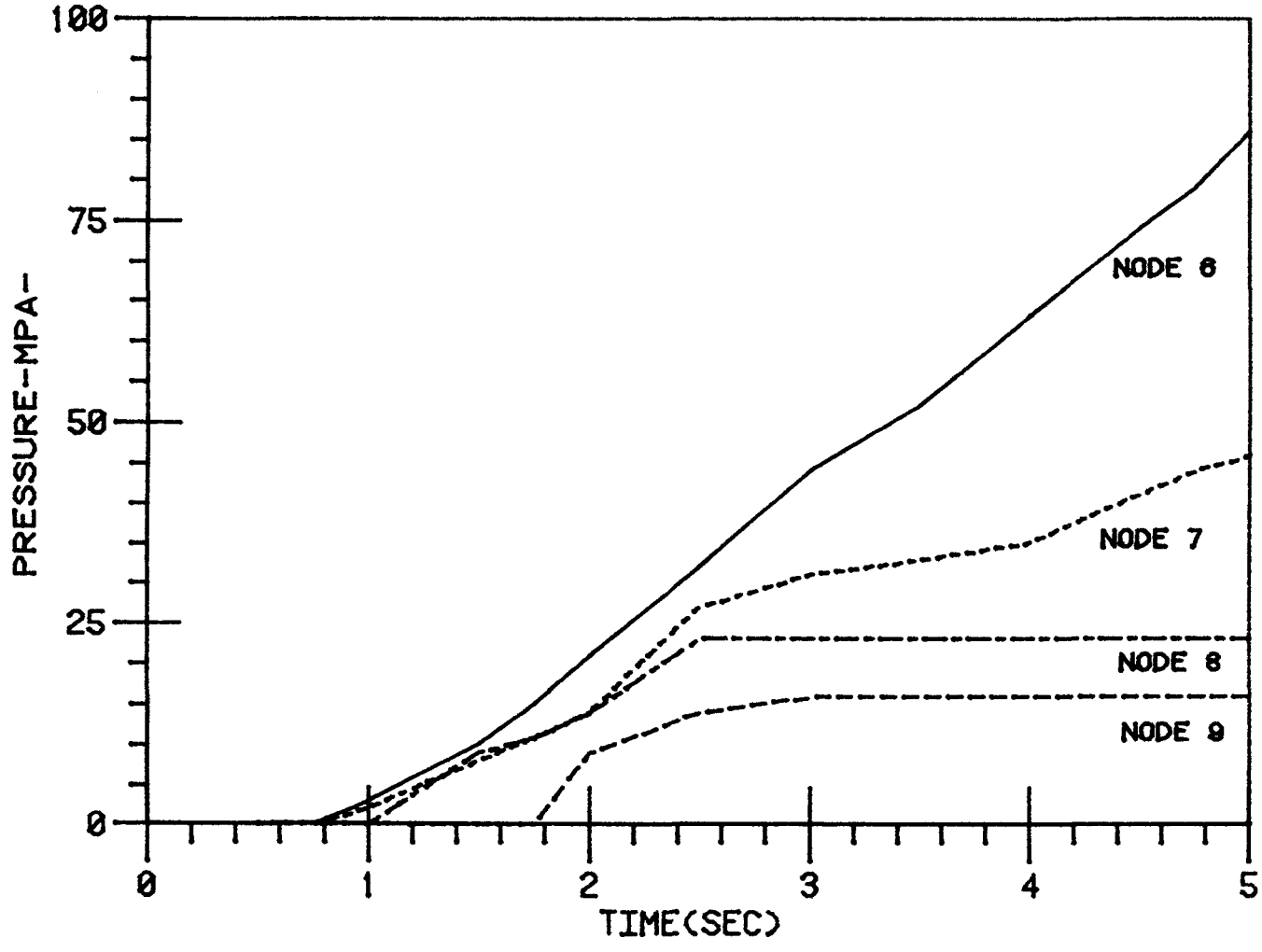

Figure 3.19. Fuel/Clad Mechanical Interaction Pressure (Case FP2).

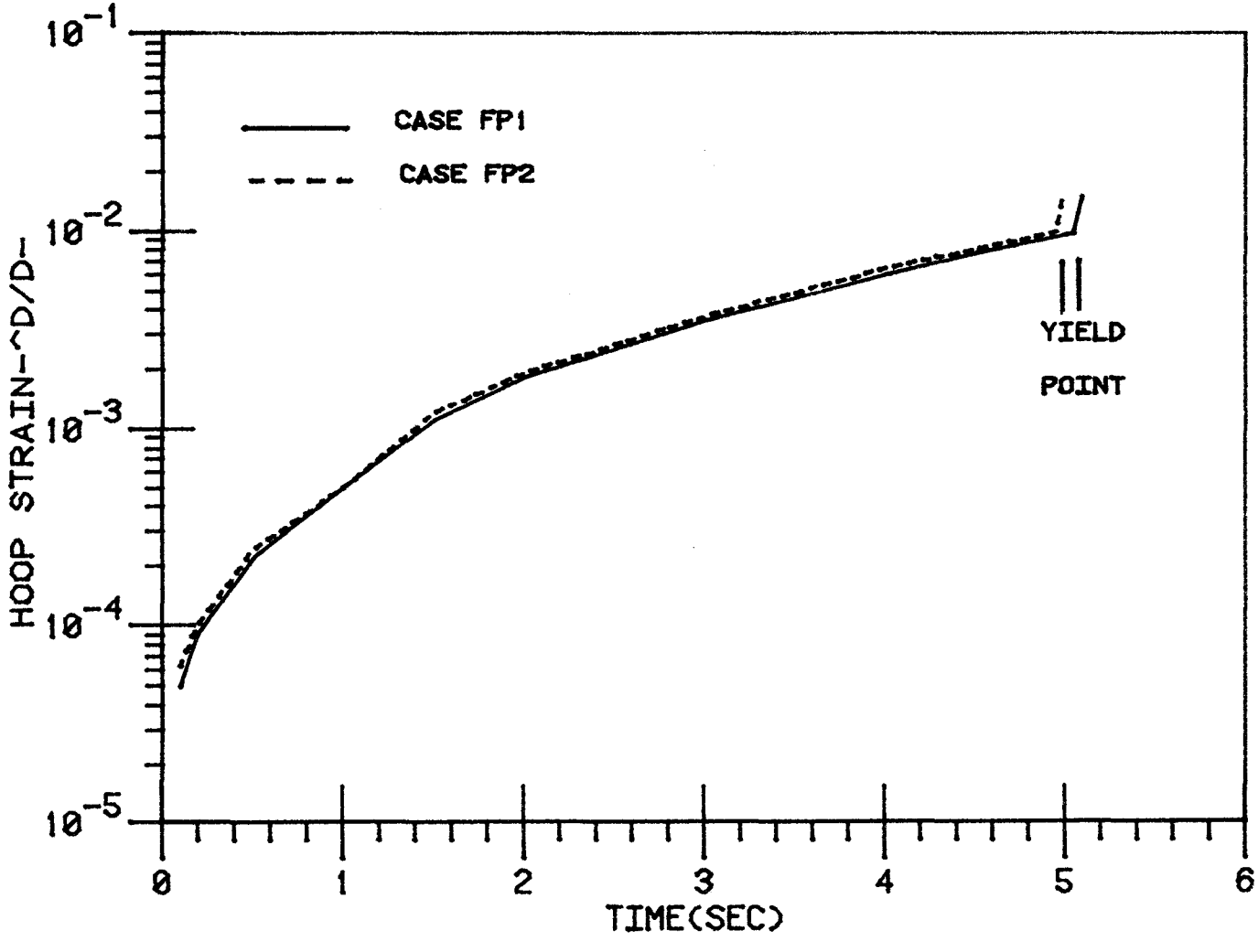

Figure 3.20. Outer Clad Hoop Strain at Failure Location.

Using this model, the major conclusions are:

1. The time of clad failure is governed by the time to reach clad yielding when the Tresca yield and permanent deformation failure criteria are used.
2. Clad pre-stressing due to steady-state irradiation is a secondary factor in determining failure location and time.
3. Pre-stressing produces a trend away from midplane failures because the steady-state stresses at the axial extremities of the core are larger than those at the midplane and are greatest at the bottom.
4. Transient-induced stresses tend to be larger at the midplane than at the axial extremities, tending to overcome the effects of the steady-state stress distribution.

3.4 References for Chapter 3.0

1. Kastenberg, W. E. and M. V. Frank, "Preliminary Analysis of the Transient Overpower Accident for CRBRP," UCLA-ENG-7557, July 1975.

2. Waltar, A. E. N. P. Wilburn, et.al., "An Analysis of the Unprotected Transient Overpower Accident in the FTR," HEDL-TME 75-50, Hanford Engineering Development Laboratory, June 1975.

3. Haas, P. M., T. Ginsberg, and T. P. Henry, "Analysis of Low Ramp TOP Accidents in the EOEC Core of the CRBR" Technical Note, BNL 21000, Brookhaven National Laboratory, November 3, 1975.

4. Rothman, A. B., et.al., "Review of TREAT Experiments in Support of Transient Overpower Analysis for Fast Reactor Safety, "CONF-740401, Beverly Hills, California, April 1974.

5. Rothman, A. B., et.al., "Results of Recent TOP and LOF Experiments in TREAT," Proc. of the Intl. Mtg. on Fast Reactor Safety and Related Physics, CONF-761001, Chicago, Illinois, October 1976.

6. Culley, G. E., et.al., "Fast Reactor Safety Implications of Recent Assessments of Fuel Pin Transient Behavior," Intl. Conf. on Fast Reactors for Safe and Reliable Operation, Karlsruhe, West Germany, October 1972.

7. Scott, J. H., et.al., "Microstructural Dependence of Failure in Mixed-Oxide LMFBR Fuel Pins," CONF-740401, Beverly Hills, California April 1974.

8. Baars, R. E., et.al., "Failure Threshold Correlation for Fast Reactor Transient Overpower Accident Analysis," Trans. Amer. Nuc. Society, Vol. 21, pp. 303-305, June 1975.

9. Baars, R. E., T. Hikido, and J. E. Hanson, "HEDL Empirical Correlation of Fuel Pin TOP Failure Thresholds - Status 1976." Proceedings of the Intl. Mtg. on Fast Reactor Safety and Related Physics, CONF-761001, Vol. IV, Chicago, Illinois, October 1976.

10. Wilburn, N. P., et.al., "Sensitivity of LMFBR Accident Analysis to Variations in an Expirical Fuel Pin Failure Criterion," Proc. of the Intl. Mtg. on Fast Reactor Safety and Related Physics, CONF-761001, Chicago, Illinois, October 1976.

11. Erdman, C. A., and P. M. Haas, "A Review of Methods for the Analysis of the TOP in LMFBR's," BNL 19877 (BNL/FRS 1) January 1975.

12. Atcheson, D. B. and R. R. Sherry, "A Mechanistic Approach to LMFBR Cladding Failure Prediction in Transient Overpower Experiments," Trans. Amer. Nuc. Society, Vol. 21, p. 302, June 1975.

13. Majumdar, D. and A. M. Judd, "Failure of Irradiated LMFBR Fuel Pins in a Transient Overpower Accident," Trans. Amer. Nuc. Society, Vol. 21, p. 302, June 1975.

14. Atcheson, D. B., R. R. Sherry, and K. J. Shimane, "Cladding Failure in TREAT Overpower Experiments: A Mechanistic Interpretation and its Implications for LMFBR Safety Analysis." Proc. of the Intl. Mtg. on Fast Reactor Safety and Related Physics, CONF-761001, Chicago, Illinois, October 1976.

15. Rumble, E. T., "A Hypothetical Overpower Excursion Model for Liquid Metal-Cooled Fast Breeder Reactors," Ph.D. Dissertation in Engineering, UCLA, University of California, Los Angeles, June 1974.

16. Peoppel, R. B., "An Advanced Gas Release and Swelling Sub-Routine," Proceedings of the Conference on Fast Reactor Fuel Technology, New Orleans, April 1971, pp. 311-326.

17. Dias, J. W., "Analysis of the Behavior of Fission Product Gas in Solid Fast Reactor Oxide Fuel Under Transient Heating Conditions," Ph.D. Dissertation in Engineering, UCLA, University of California, Los Angeles, July 1973.

18. Dias, J. W., and R. B. Peoppel, "Transient Swelling Studies with the Grass Code," Argonne National Laboratory, ANL-7992, 1973.

19. Estaves, R., "Fission Gas Behavior During Fast Thermal Transients," Ph.D. Dissertion in Engineering, UCLA, University of California, Los Angeles, January 1976.

20. Bogensberger, H. G., and C. Ronchi, "Effects Due to Fission Gas During Unprotected Overpower Transients in LMFBR's," Nuclear Technology, Vol. 29, April 1976, p. 73-85.

21. Kuczera, B., "Simulation of the Transient Behavior of LMFBR Fuel Pins Under Consideration of Special Burnup Phenomena Using the BREDA-II Code," Nuclear Engineering and Design, Vol. 31, No. 2, January 1975, pp. 294-307.

22. Kuczera, B., and P. Royl, "Application of Different Failure Criterion in Fuel Pin Modelling and Consequences for Overpower Transients in LMFBR's," Proc. of the 3rd SMIRT Conference, London, England, September 1975.

23. Bogensberger, H. G., et.al., "Analysis of LMFBR Overpower Accident, Including Fission Gas Effects in the Pre-disassembly and Disassembly Phase," Proc. of the Intl. Mtg. on Fast Reactor Safety and Related Physics, CONF-761001, Chicago, Illinois, October 1976.

24. Smith, L. L., and M. G. Stevenson, "Effect of Reactivity Insertion Rate on Fuel Pin Failure Threshold," Trans. Amer. Nuc. Soc., Vol. 17, November 1973, pp. 284-285.

25. Bohl, W. R., et.al., "An Analysis of Transient Undercooling and Transient Overpower Accidents Without Scram in the Clinch River Breeder Reactor," ANL/RAS 75-29, Argonne National Laboratory, July 1975.

26. Mast, P. K. and J. H. Scott, "Fuel Pin Failure Models and Fuel-Failure Thresholds for Core Disruptive Accident Analysis," Proc. Intl. Mtg. on Fast Reactor Safety and Related Physics, CONF-761001, Chicago, Illinois, October 1976.

27. Bard, F. E., et.al., "Analytic Models for Fuel Pin Transient Performance," Proc. Intl. Mtg. on Fast Reactor Safety and Related Physics, CONF-761001, Chicago, Illinois, October 1976.

28. Hunter, C. W., and R. L. Fish, "Deformation and Failure of Fast Reactor Fuel Cladding Specimens During High-Temperature Simulated Loss-of-Flow Transients," CONF-740401, Beverly Hills, California, April 1974.

29. Hunter, C. W., et.al., "Mechanical Properties During Simulated Overpower Transients of Fast Reactor Cladding Irradiated from 700-1000F," HEDL-TME 75-28, 1975.

30. Johnson, G. D., C. W. Hunter, and J. E. Hanson, "Fuel Cladding Mechanical Properties for Transient Analysis," Proc. of the Intl. Mtg. on Fast Reactor Safety and Related Physics, CONF-761001, Chicago, Illinois, October 1976.

31. Wald, J. W. and I. S. Levy, "LMFBR Fuel Pin Cladding Transient Performance Capabilities - An Analysis of FCTT Data," BNWL-2041, in publication.

32. Dillon, R. L. and I. S. Levy, Editors, "A State-of-the-Art Review of Degradation Processes in LMFBR Materials, Rev. 1, Vol. 1, August 1975," Section 7.3.2.

33. Kastenberg, W. E., "LMFBR Fuel Analysis, Task A: Oxide Fuel Dynamics," NUREG-0146, January 1977.

34. Frank, M. V., "Some Aspects of Fuel Rod Behavior During a Fast Reactor Overpower Transient," Ph.D. in Engineering, UCLA, University of California, Los Angeles, December 1977 (expected).

35. Sun, Y. and D. Okrent, "A Simplified Method of Computing Clad and Fuel, Stress and Strain During Steady State Irradiation," NUREG-0260, June 1977.

36. Frank, M. V., and W. E. Kastenberg, ANS Trans. 27, 1977, to be published.

37. Watanabe, A., and A. M. Judd, "A Computer Code for Predicting the Behavior of Oxide Fuel in Accidents," ANS Trans. 14:733, 1971.

38. Jankus, V. A., and R. W. Weeks, "LIFE 2, A Computer Analysis of Fast Reactor Fuel Element Behavior as a Function of Reactor Operating History," Proc. First Int'l Conf. on Structural Mechanics in Reactor Technology, Berlin, 1971.

39. Sun, Y. H., and D. Okrent, "On the Fuel-Clad Stress-Strain State at Beginning of a Transient," Proc. ANS Conf. Fast Reactor Safety, Chicago, 1976.

40. Lin, T. H., Theory of Inelastic Structures, John Wiley and Sons, New York, 1968.

41. Properties for LMFBR Safety, ANL-CEN-RSD-76-1 (Supplement 1), April 1976.

Blank Page

4.0 THERMAL LOADING CONSIDERATIONS OF FUEL PLATED OUT DURING TRANSIENT OVERPOWER ACCIDENTS

4.1 Introduction

Core disruptive accidents (CDA's) are generally broken up into several phases for computational ease and better mechanistic understanding of the complete accident. These phases generally include: the pre-dissassembly phase, the disassembly phase, the work energy phase and the post accident heat removal phase. For the loss of flow (LOF) accident, a "transition phase" has been added to examine potential recriticality during the transition between core disruption and long term coolability [1,2]. For the transient overpower accident, most of the research work has been centered upon the pre-disassembly phase and on the transition to core disruption in case hydrodynamic disassembly occurs. However, if hydraulic sweep-out of the fuel occurs, attention has only been given to the transition to nuclear shutdown.

The assumption of hydraulic sweepout of the fuel in the TOP accidents is highly questionable as many of the TREAT experiments, especially the Series H-4, H-5, and E-8 tests [3,4,5], have yielded substantial fuel freezing and channel plugging following fuel pin failure. The out of pile experiments conducted in Germany [6], to simulate TOP accidents in a seven pin bundle show the formation of a partial cooling channel blockage ($\approx$ 90%). Recently, a mechanistic method to study in-channel fuel freezing and plugging has been developed in References [7,8]. Based on this work [7,8], it is concluded that substantial fuel freezing and plugging of active core channels may occur after fuel pin failure. The amount and location of fuel plateout, however, has been found to be strongly dependent on the fuel particle size. The nature and location

of the blockages formed as a result of fuel plate-out is significantly different than assumed in the Clinch River Breeder Reactor PSAR [9], where the blockages have been assumed to be formed as a porous plug in the upper reflector region.

The presence of fuel in the active region of the core, especially near the upper mid-plane is of significant concern as these plugs may impede the flow of coolant through the core and also act as a source of positive reactivity. A deficient cooling due to reduced flow (assuming a constant pressure drop exists across the core) and increased heat generation rate in the fuel may lead an overpower transient accident into an undercooling accident, with a possibility of remelting, slumping and hydrodynamic disassembly. In this work, first a description of the type of blockages that may be formed by freezing of the semi-molten fuel particles on the wire wrap or when completely solidified particles get caught in the coolant channel, is given. Thereafter, the range of parameters for which freezing of molten fuel on the wire wrap may lead to melting of the wire wrap itself and the adjoining cladding are obtained. For the situations which do not lead to melting of the wire wrap or when the blockages are formed by solid particles, circumferential thermal loading on the cladding due to fuel plateout is considered. This in turn, yields information on the probability of high thermal stresses, along the periphery of the cladding and chances of local boiling in the channels.

4.2 Description of the Blockages

In the mechanistic model described in References [8,9,10], it is assumed that on pin failure, fuel is distributed uniformly around the pin periphery. The inchannel blockages are formed when the thin solid crust

of the semi-molten particles breaks open upon impact with a wire wrap, and subsequently the particles freeze on the wire wrap. To determine the amount of fuel that will stay on the wire wrap after impact, a sticking criteria is developed in Reference [10]. Use of this criteria to all of the cases considered [10], showed that all of the fuel will stay on the wire wrap after it plates out. Figure 4.1 shows the inchannel blockages that may be formed when semi-molten fuel plates out on the wire wrap.

The amount and location of the fuel that plates out on the wire wrap strongly depends on the particle diameter. A fraction of the ejected fuel that will plate out on the wire wrap is plotted in Figure 4.2 for fuel particles of diameter 250 μm, 500 μm and 1000 μm. In obtaining Figure 4.2, it is assumed that 20 gm of fuel and 0.015 gm of fission gas are ejected into the coolant channel linearly in 0.07 seconds. The conditions used at fuel pin failure and other input parameters are listed in Table 4.1. It is noted from Figure 4.2, that only about 6% of the ejected fuel will plateout if the fuel particle diameter is assumed to be 250 μm. The axial length of the fuel blockage so formed will be about 5 cm from the point of pin failure. However, 70% and 100% of ejected fuel will plateout within half pitch length of the wire wrap ($\sim$ 15 cm) if fuel particle diameters are assumed to be 500 and 1000 μm respectively.

The blockages formed by solid particles or semi-solidified particles that do not break open on impact with a wire wrap have also been studied by Wong [10]. His experimental set-up consisted of a seven-pin bundle enclosed in a 2.54 cm diameter glass tube. Stainless steel rods 0.635 cm in diameter were used to simulate fuel pins while 0.156 cm diameter stainless wire soldered to the steel rods acted as a wire wrap having a pitch of 30 cm. The experimental procedure consisted of placing glass

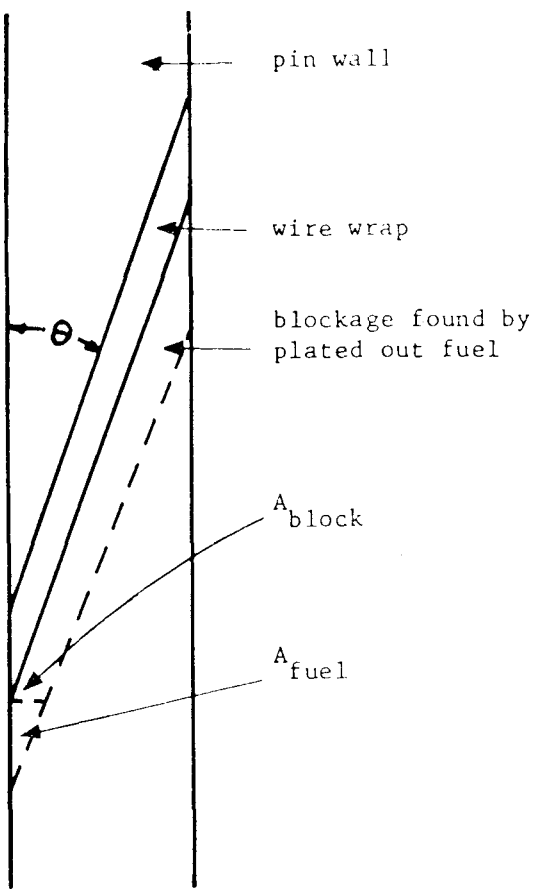

Figure 4.1 Blockages Formed by Freezing of Semi-Molten Fuel Particles.

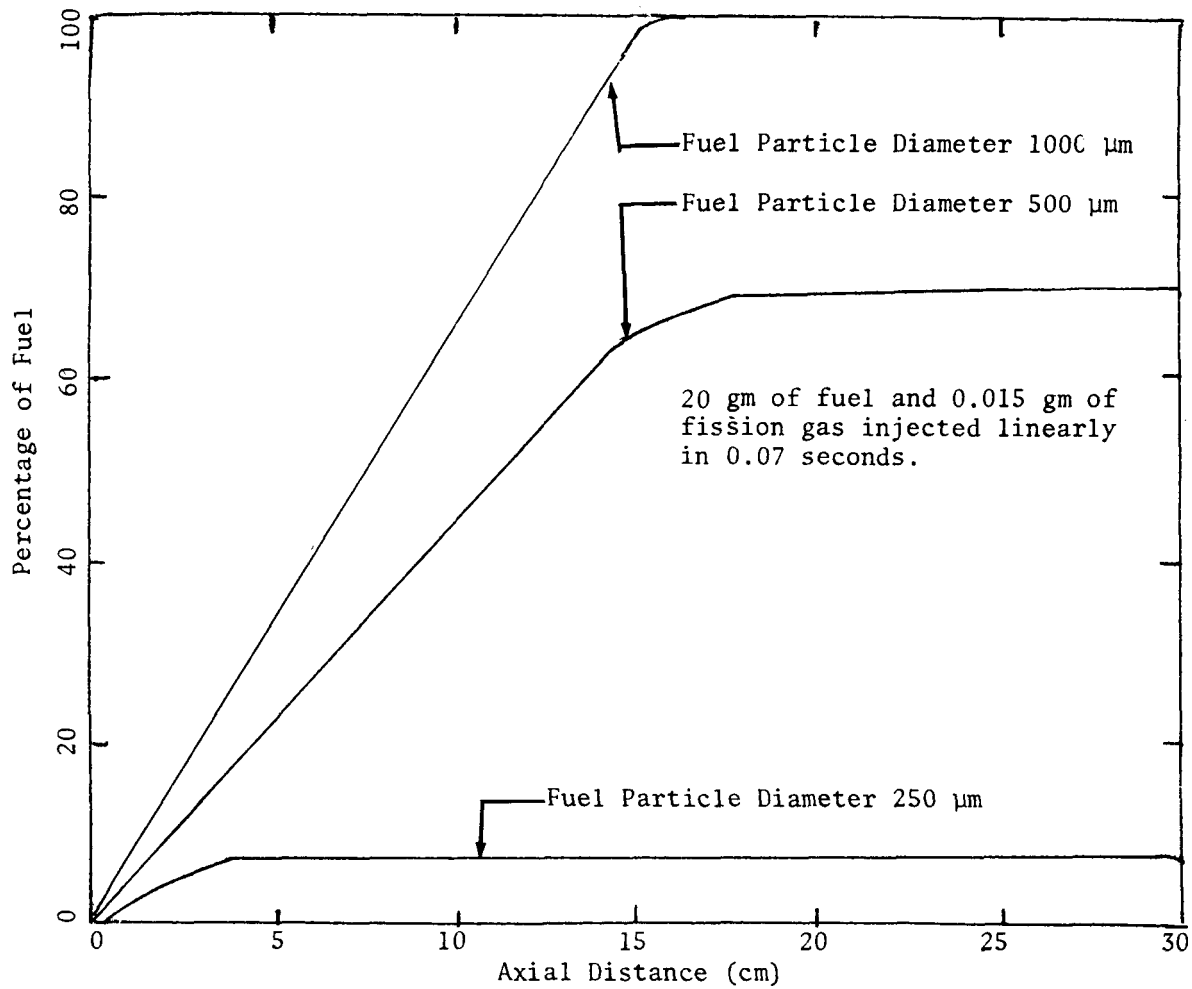

Figure 4.2 Fractional Plate out of Ejected Fuel as a Function of Axial Distance from the Point of Pin Failure.

Table 4.1 HOPE Predicted Conditions at Pin Failure and CRBR Input Parameters.

Reactivity ramp rate	2.4 cents/second
Burnup	5% atom burnup
Initial temperature of FCI zone	1,161° K
Initial pressure of FCI zone	5 atmospheres
Initial location of upper interface of FCI zone	112.96 cm
Initial location of lower interface of FCI zone	106.54 cm
Initial velocity of upper interface of FCI zone	763.54 cm/s
Initial velocity of lower interface of FCI zone	746.16 cm/s
Fuel ejection period	0.07 second
Rate of heat generation for fuel particles	$3.6 + 5(\text{time}) - 200(\text{time})^2$ x 808 W/c^3 for time < 0.1 second x 1,535 W/c^3 for time $\geq$ 0.1 second
Initial temperature of fuel particles	3,073° K
Location of top of active core	127 cm
Location of bottom of active core	35.56 cm
Location of top of fuel pin (includes upper reflector, fission gas plenum and upper blanket)	317.5 cm
Location of bottom of fuel pin (includes lower reflector and lower blanket)	-93.472 cm
Hydraulic diameter of coolant channel	0.3955 cm
Pressure at top of fuel pin	1.5 atmospheres
Pressure at bottom of fuel pin	8 atmospheres

beads of known amount and size on a screen placed below the fuel pin bundle and letting water flow through the screen at a desired rate. As water flows through the screen, it carries glass beads with it and a fraction of the glass particles is caught in the coolant channel, while the rest of the particles are swept out. The fraction of the particles retained in the coolant channel is obtained by subtracting the amount of particles swept out of the coolant channel from the total mass of particles placed on the screen. As seen from Figure 4.3, the amount of particles retained in the coolant channel is again found to be strongly dependent on the particle size. For example, when particles with diameter 800-800-1000 μm are placed on the screen, almost all of the particles are swept out of the coolant channel. But when the particle diameter is increased to about 1600 μm, only 30% of the particles are swept out.

Visual observations showed that generally two types of blockages were formed. In the inside channels, blockages were observed to be formed in columns. These blockages were initiated when a particle did not follow the flow path, but hit the wire wrap, and thereby blocked the flow path of the succeeding particles. Or, in some cases the particle diameter or the gap between two pins was such that the particle simply could not move through the passage provided for the coolant. In the outside channels, the blockages were observed to be formed in wedges. The wedge type blockages were formed by jamming of the particles travelling in the space between the fuel pin and the outside tube wall and the particles travelling along the wire wrap in the adjacent inner channel. Photographs of the inside channel and outside channel blockages are shown in Figure 4.4.

An attempt to determine the increase in pressure drop caused by the presence of these blockages in a seven-pin fuel assembly (effective

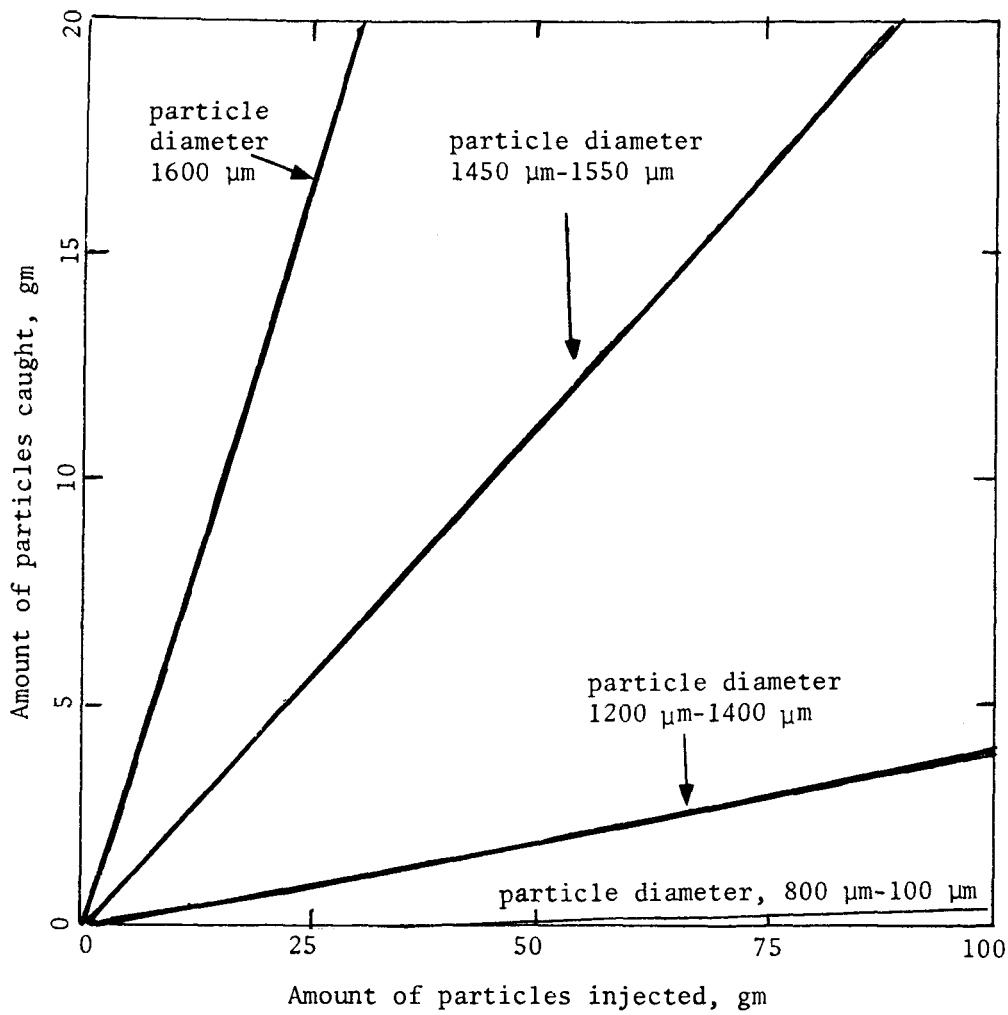

Figure 4.3 Amount of Particles Caught as a Function of Amount of Particles Injected.

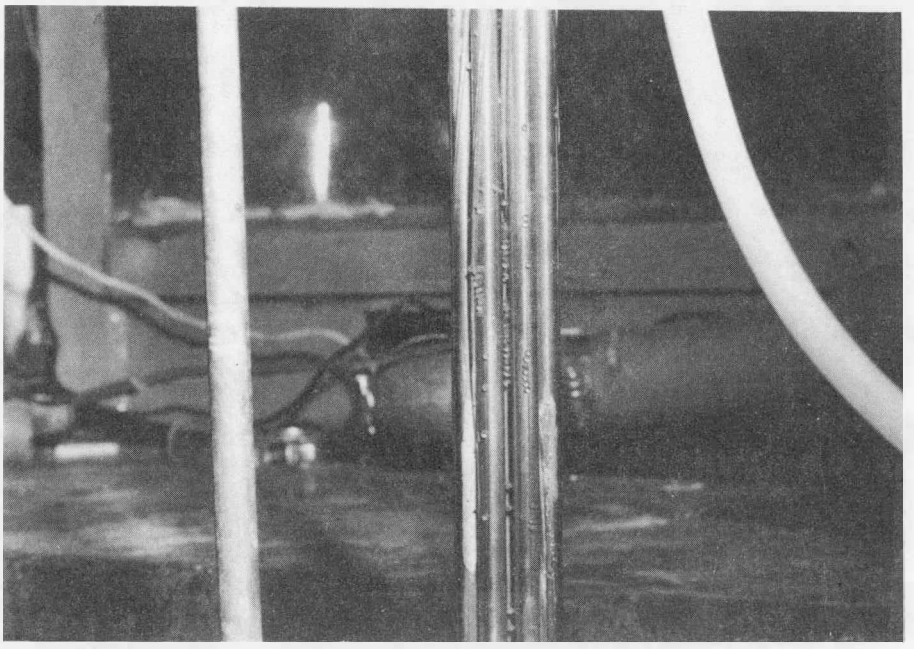

(a) Blockages Formed in Inside Channels.

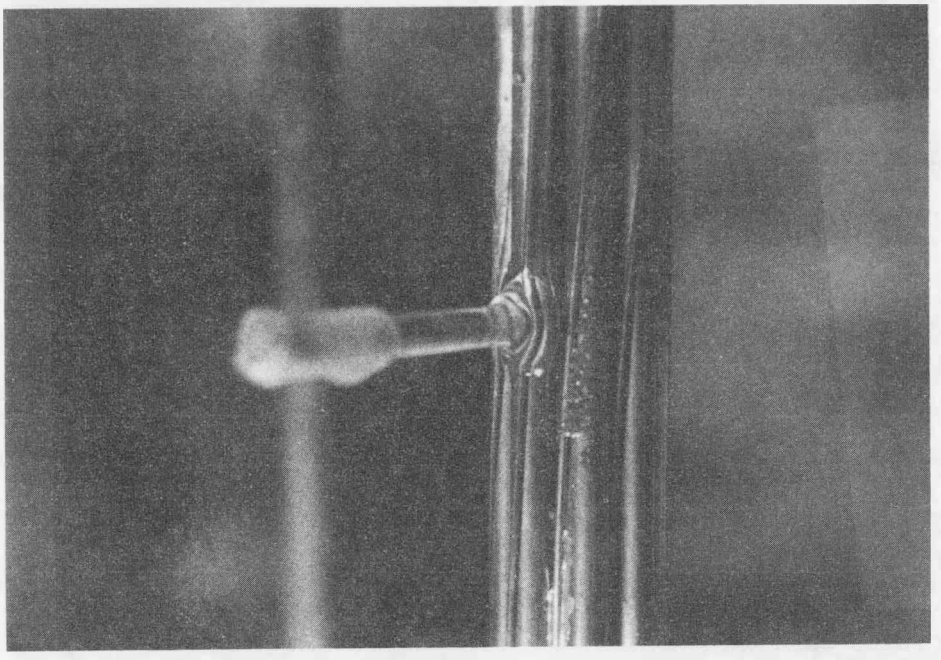

(b) Blockages Formed in Outside Channels.

Figure 4.4. Types of Blockages that May be Formed when Solidified Fuel Particles are Caught in the Coolant Channel.

height ≈ 1.0 meter) was also made by Wong [10]. The pressure drop was found to be strongly dependent on cross-sectional area of the coolant channel occupied by the blockage, but did not show a dependence on the diameter of the particles in the range of particle diameters studied. The additional pressure drop across the channel due to presence of these blockages smeared over the whole cross-section was correlated as

$$\Delta P = K \quad V^2/2 \qquad \text{kPa} \tag{1}$$

where

$$K = \left(C_1 + C_2 \cdot \frac{\text{Mass of particles retained in the channel}}{(\text{Density of the particles}) \cdot (\text{Length of the blockages}) \cdot \dfrac{1}{\text{Area of cross-section of the channel}}} \right) \Big/ V^{1/4}$$

In Equation (1), V is the unobstructed flow velocity in meters/sec. The constants C_1 and C_2 were experimentally determined to be 11.75 and 541, respectively. Direct application of Equation (1) to a real situation is questionable since Equation (1) is based on a seven-pin bundle data where enclosing tube wall plays a significant role. In a prototype, the can walls may have much less influence as the number of inner channels is considerably large. Nevertheless, Equation (1) provides a rough estimate of the pressure loss caused by solid particle blockages.

The above type of blockages which can also be formed when bare fuel pellets are broken up on exposure to liquid sodium, are not typical of CRBR but are generic to all types of fast reactors. Solid particle blockages in honeycomb lattice support similar to that intended for use in SNR-300 has been studied by Schultheiss [11]. It is desired that more work be carried out to determine the nature of these blockages for

the different type of grid spacers and under different bending conditions of the fuel pins. Effort should also be made to study the local flow and pressure drop across these blockages.

4.3 In Place Cooling of the Blockages Formed by Plated Out Fuel

After the semi-molten fuel particles hit the wire wrap and stick to it, the fuel will be in direct contact with the wire wrap and the adjoining cladding. Since the temperature of the fuel is much higher than the temperature of the wire wrap and cladding, heat will be transferred from the hot fuel to the wire wrap and cladding through the contact area. As more and more fuel plates out, the area transferring the heat to the wire wrap and cladding will become larger and larger and more energy will be transferred to the wire wrap and cladding. At the same time, energy will be lost by the wire wrap through convective heat transfer to the coolant at the surface area not covered by fuel and through conduction to the colder region of wire wrap and cladding (fin effect). After some time, the wire wrap and adjoining cladding may start to melt or remain solid depending on the balance between heat gained from fuel and heat lost to the coolant. If the wire wrap and adjoining cladding melt, it can lead to distortion of the wire wrap and movement of the fuel blockage. Figure 4.5 shows the relative location and direction of heat transfer between cladding, plated-out fuel and the wire wrap.

A theoretical model to determine the physical state of the wire wrap and the adjoining cladding has been developed in Reference [10]. In this model, it is assumed that

(i) The fuel covers only the lower half of the wire wrap.

(ii) The amount of fuel plate out and length of wire wrap covered by fuel are linear functions of time. The assumption of linear

The arrows ⟶, indicate direction of heat transfer

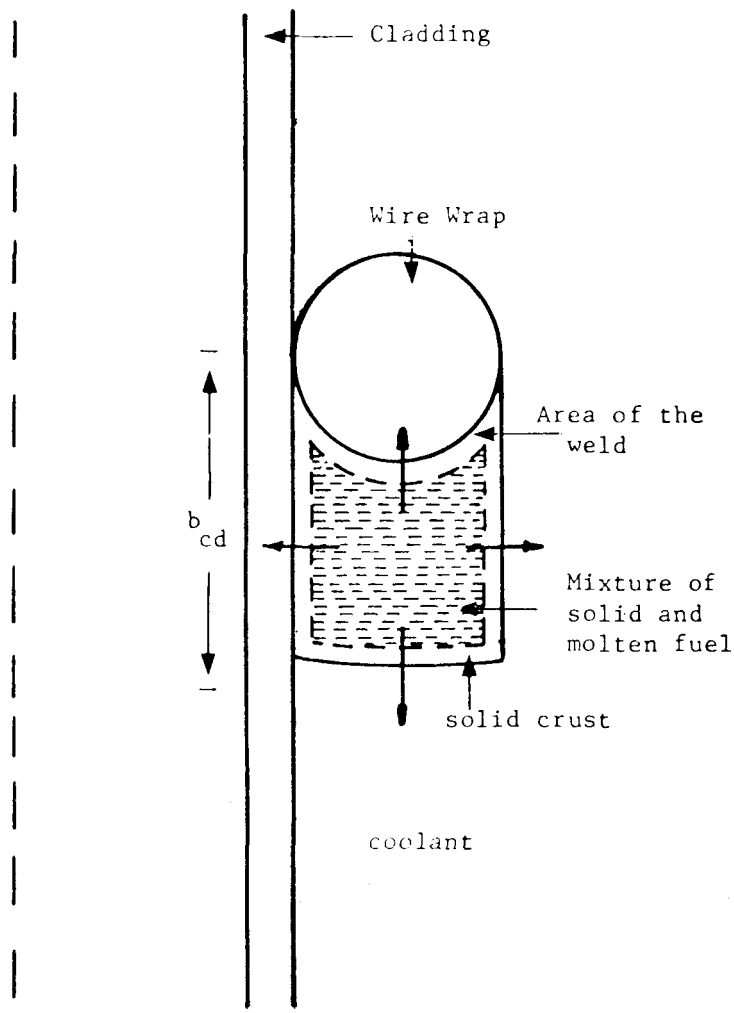

Figure 4.5 Relative Location of Cladding, Wire Wrap and Plate out Fuel.

plate out of the fuel is not consistent with the assumption of linear coverage of wire wrap by fuel. This assumption is not unrealistic, however, as it gives a slight overestimate of the amount of fuel plate out in the beginning and underestimate during the later period. For an instantaneous injection, the total time to fuel plate out is equal to the time taken by a fuel particle to travel an axial distance equal to half-pitch length from the fuel pin failure location. For a linear injection, the time taken by the fuel to cover the wire wrap is the sum of the injection time and the time needed for a particle to travel a distance equal to half-pitch length of the wire wrap.

(iii) The heat transfer coefficient at the fuel blockage-wire wrap interface and at the fuel blockage-cladding interface is based on transient conduction between two semi-infinite plates.

(iv) Because of item iii, the lumped capacity method is used to determine transient temperature of each of the wire wrap, fuel and the cladding adjoining the fuel blockage. This generally tends to overestimate the time at which all of the wire wrap will start to melt. In fact, melting of the outer surface of the wire wrap may start much earlier.

(v) The heat transfer between fuel and coolant affects only the physical state of the fuel and as such does not affect the analysis for the wire wrap. Also, for the time periods considered there was no possibility of melting of the fuel [12]. Thus, it has not been included in the overall analysis.

(vi) The heat transfer from fuel to the cladding is neglected because of uncertainty in the clad gap thickness and the heat generation rate in the fuel. This will result in over-estimation of the cladding

and the wire wrap melting time.

The coupled equation governing the transient temperature of the wire wrap has been solved numerically by Wong [10]. For the case when 20 gm of fuel and 0.015 gm of fission gas are assumed to be injected to the coolant channel linearly in 0.07 sec. and with other parameters at fuel pin failure as given in Table 4.1, the temperature of the wire wrap and adjoining cladding is plotted in Figure 4.6 as a function of time. When the fuel particle diameter is assumed to be 1000 μm, the wire wrap and adjoining cladding start to melt 0.02 seconds after pin failure and continue to do so until the end of the calculation (0.1 sec). The melting of wire wrap may lead to slumping of steel and fuel in the blockage or distortion and relocation of the wire wrap. The relocation process is very difficult to describe and as yet no effort has been made in that direction. However, when the fuel particle diameter is assumed to be 250 μm, the maximum temperature attained by the wrap and adjoining cladding is slightly less than the melting temperature of steel. After attaining the maximum value at 0.035, the temperature begins to drop. Near the melting temperature of steel, the wire wrap will be strengthless and may be displaced by the drag of the sodium coolant flowing past it.

The effect of the amount of fuel plate out, initial temperature of the wire wrap and the time independent physical state of the coolant on melting of the wire wrap and adjoining cladding is shown in Fig. 4.7. In Fig. 4.7, liquid sodium temperature has been chosen such that it represents the maximum subcooling of liquid sodium in the interaction zone when 20 gm of fuel is assumed to be injected into the coolant channel in 0.07 seconds. Similarly, sodium vapor temperature is the maximum

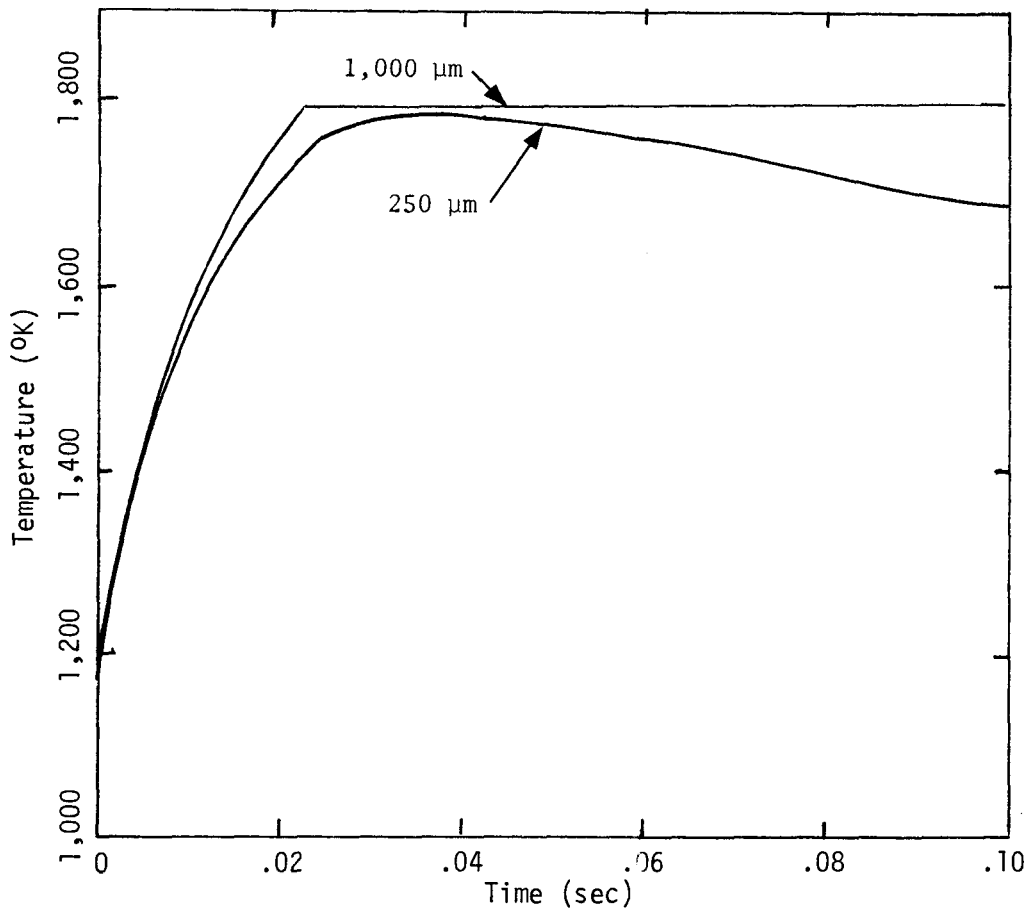

Figure 4.6 Temperature of Wire Wrap and Adjoining Cladding as a Function of Time.

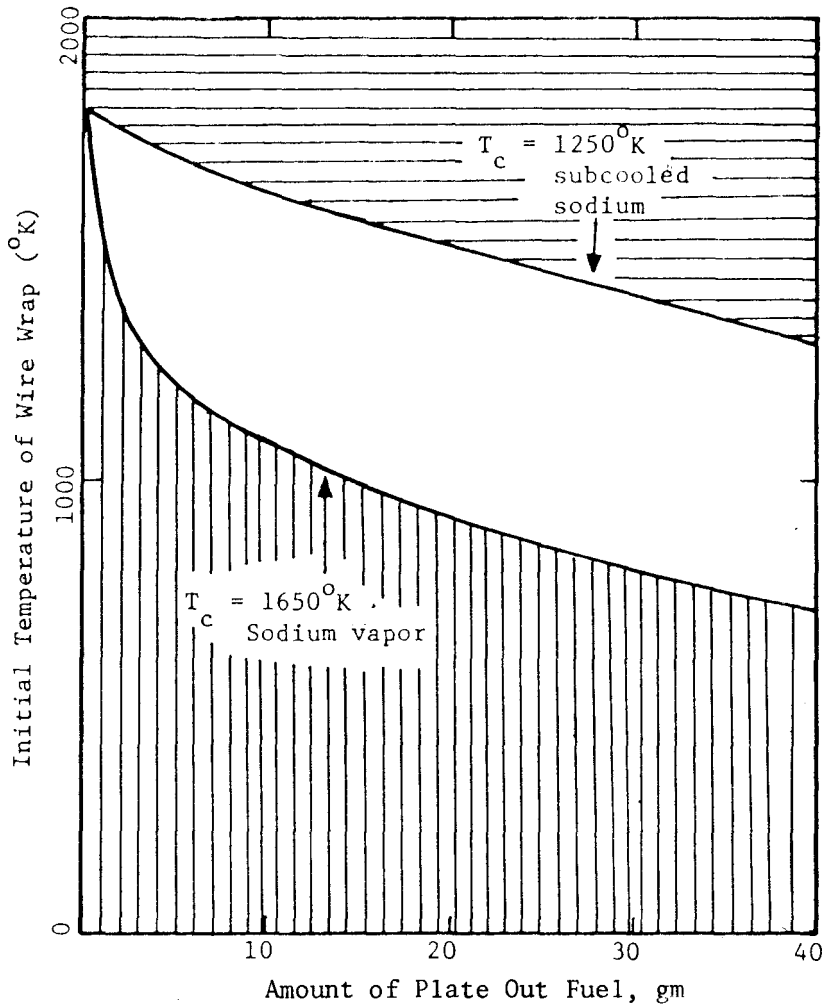

Figure 4.7 Melting Limit of Wire Wrap and Adjoining Cladding.

temperature of the interaction zone during vapor expansion. The shaded area below the lower curve indicates the conditions for which melting of the wire will not occur, whereas the shaded area above the upper curve represents the conditions which will lead to melting of the wire wrap. Generally, the conditions in the interaction zone during TOP accident would correspond to the unshaded region between the two curves. For a particular initial wire wrap temperature, the intercepts with the two curves of a horizontal line drawn parallel to the abscissa will give the minimum and maximum amount of fuel plate out that will lead to melting of the wire wrap.

4.4 Thermal Loading of the Stable Blockages

The thermal loading of fuel blockages which do not lead to melting of the wire wrap or cladding is considered in this section. The presence of solid fuel adjacent to the cladding will lead to preferential heat transfer and in turn large temperature variation along the periphery of the cladding. If local temperature anywhere along the cladding exceeds the saturation temperature of sodium, it can lead to inception of boiling in the channel. In order to determine the temperature distribution on the cladding surface, a two dimensional heat conduction equation is solved. To simplify the numerical solution without introducing much error, rectangular coordinates, instead of cylindrical coordinates are used. Figure 4.8 shows the relative location of the blockage and rectangular approximation of the cladding. The width of the blockage is assumed to be equal to the diameter of the wire wrap. For temperature independent thermophysical properties of the cladding, the transient conduction equation is written as

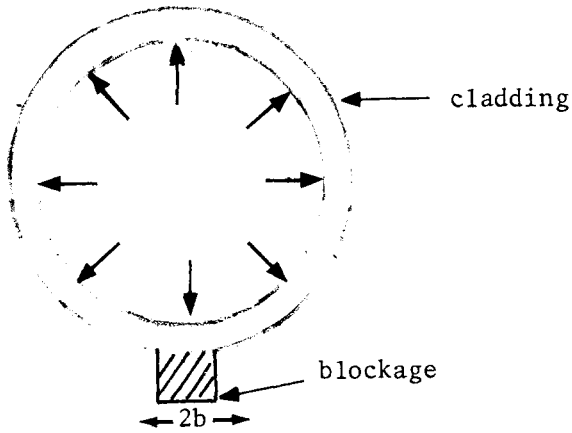

a. Relative Location of Blockage in Cylindrical Coordinates

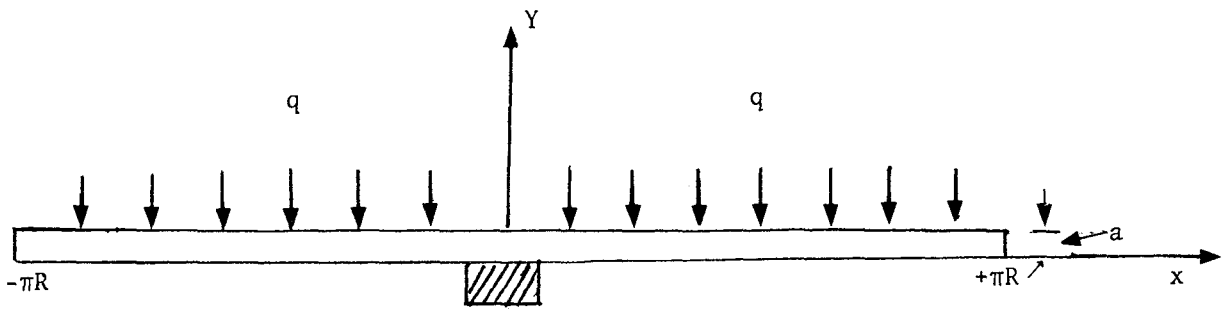

b. Relative Location of Blockage in Rectangular Coordinates

Figure 4.8 Peripheral Location of Fuel Blockage.

$$C_s \rho_s \frac{\partial t}{\partial t} = k_s \left(\frac{\partial^2 T}{\partial x^2} + \frac{\partial^2 T}{\partial y^2} \right) \tag{2}$$

The boundary conditions on equation (2) are:

$$k_s \frac{\partial T}{\partial y} = q \qquad y = a, \quad 0 \leq x \leq \pi R \tag{3}$$

$$k_s \frac{\partial T}{\partial y} = h(x,t)(T - To(x,t)) \qquad y = 0, \quad 0 \leq x \leq \pi R \tag{4}$$

$$\frac{\partial T}{\partial y} = 0 \qquad x = 0, \quad 0 \leq y \leq a \tag{5}$$

$$\frac{\partial T}{\partial y} = 0 \qquad x = \pi R, \quad 0 \leq y \leq a \tag{6}$$

and initial condition is:

$$T(x,y,0) = \frac{q}{k_s} y + \frac{q}{h(x)} + T_c \tag{7}$$

where q is the heat flux from fuel to the cladding. In this work q is assumed to be independent of x and time, while in reality it will be a function of both x and t. In equation (4), h(x,t) is the heat transfer coefficient and is defined as

$$h(x,t) = \left\{ \frac{k_s \alpha_s^{-\frac{1}{2}} \; k_f \alpha_f^{-\frac{1}{2}}}{\left(k_f \alpha_f^{-\frac{1}{2}} + k_s \alpha_s^{-\frac{1}{2}} \right)} \cdot \frac{1}{\sqrt{\pi t}} \right\} \quad \text{for } 0 \leq x \leq b \tag{8}$$

$$= \frac{k_c}{D_h} \left(5.2 + 0.018 \, P_e^{0.85} \right) \qquad \text{for } b < x \leq \pi R \tag{9}$$

The ambient temperature in equation (4) is defined as

$$T_o(x,t) = T_f \qquad \text{for} \quad 0 \leq x \leq b \tag{10}$$

$$= T_c \qquad \text{for} \quad b < x \leq \pi R \tag{11}$$

The above formulation ignores heat conduction in the axial direction and coolant and fuel blockage temperatures are assumed to be independent of time.

Equations (1-11) were solved numerically using a finite different scheme. Values of various physical parameters used in the calculations are listed in Table 4.2. Figure 4.9, shows the peripheral temperature distribution at a time when the temperature underneath the blockage is maximum. The calculations are made for both the axial average and the midplane power under transient overpower conditions $\left(q = 1.75\ q_{normal}\right)$ and for a sodium flow velocity of 6 meters/sec. It is noted that at normal flow velocity and average power, the cladding temperature outside of blockage will be less than the saturation temperature corresponding to normal operating pressure inside the core. Thus, for this case, inception of boiling in the channel is not expected. However, when the power is assumed to be 3 times the normal power $\left(\simeq 1.75\ q_{max}\right)$, the temperature at the edge of the blockage is significantly higher than the saturation temperature and possibility of initiation of boiling is quite high. Cladding peripheral temperature distribution under TOP conditions and normal power conditions for a flow velocity of 4 meters/sec. is shown in Figure 4.10. Again, it is noted that inception of boiling is possible only for blockages that are located near the midplane.

The time dependent temperature at the edge of the blockage subsequent to formation of the blockage is shown in Figure 4.11. It is observed

Table 4.2

Dimensions and Physical Properties Used

Thickness of cladding, a	.04 cm
Width of blockage, 2b	.2 cm
Length of cladding, $2\pi R$	2.0 cm
Pressure at top of fuel pin	1 atm
Pressure at top of core	3.23 atm
Pressure at bottom of core	4.29 atm
Saturation temperature of sodium at top of fuel pin	1150 K
Saturation temperature of sodium at top of core	1290 K
Saturation temperature of sodium at bottom of core	1330 K
Average bulk coolant temperature at 600 cm/sec, T_c	723 K
Average bulk coolant temperature at 400 cm/sec, T_c	759 K
Temperature of fuel blockage, T_f	2000 K
Heat transfer coefficient between coolant and cladding, h_c	13.9 W/cm^2K
Thermal conductivity of cladding, k_s	2076 W/cm K
Specific heat times density of cladding, $c_s\rho_s$.	4704 $w\text{-}sec/cm^3K$

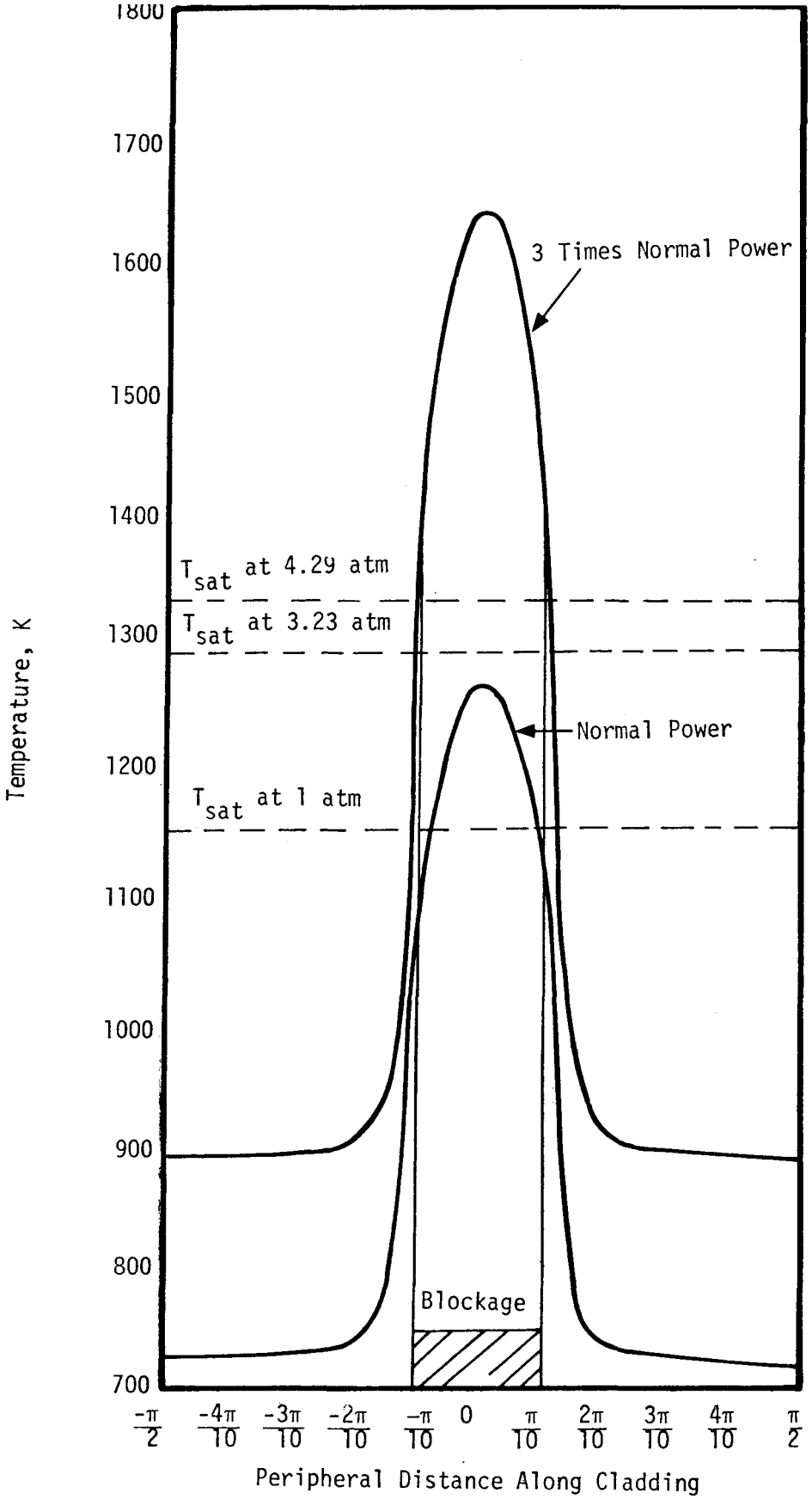

Fig. 4.9 Maximum Temperature Distribution Along Cladding for a Flow Velocity of 6 meters per second.

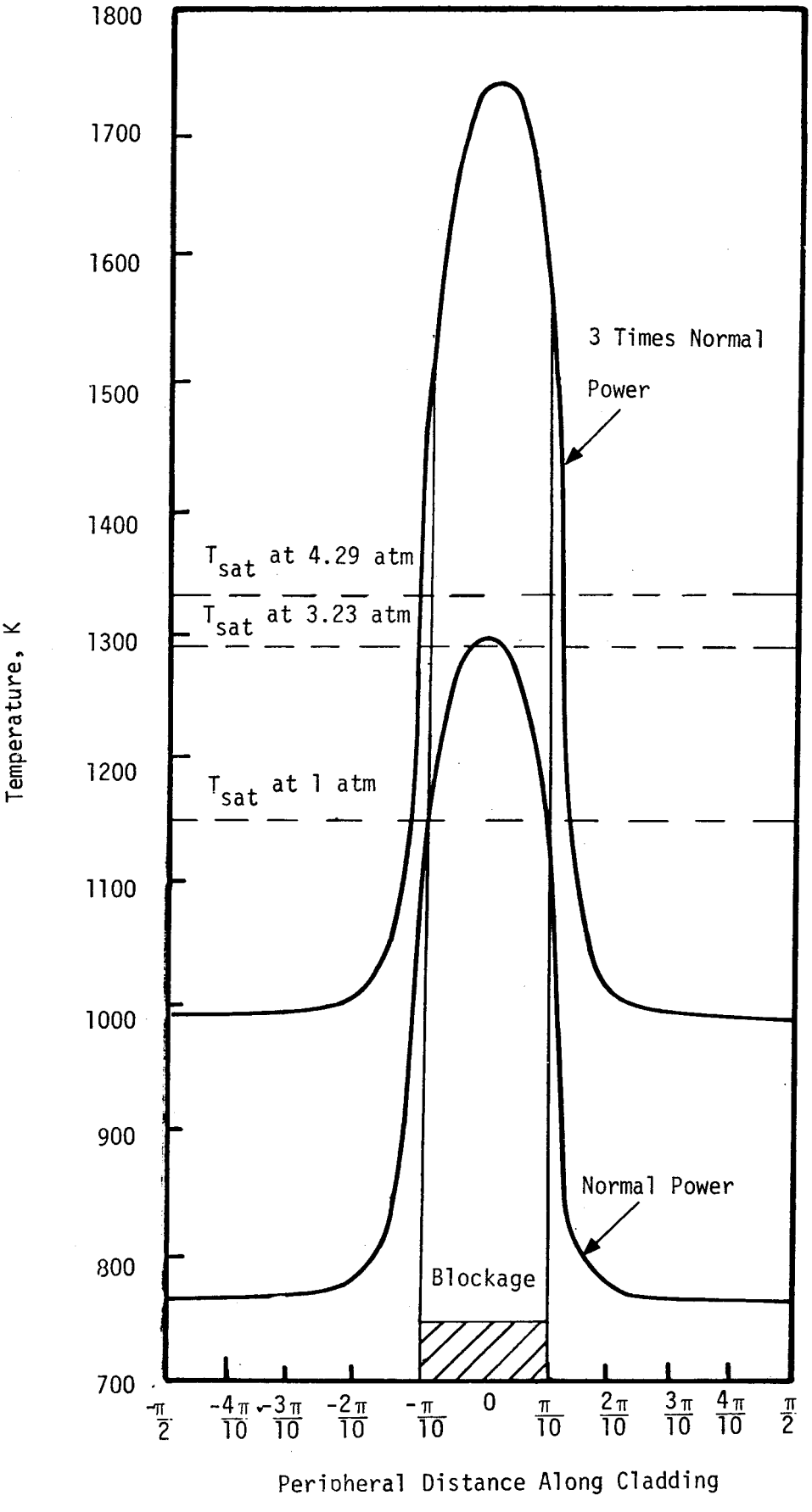

Fig. 4.10 Maximim Temperature Distribution Along Cladding For a Flow Velocity of 4 meters/sec.

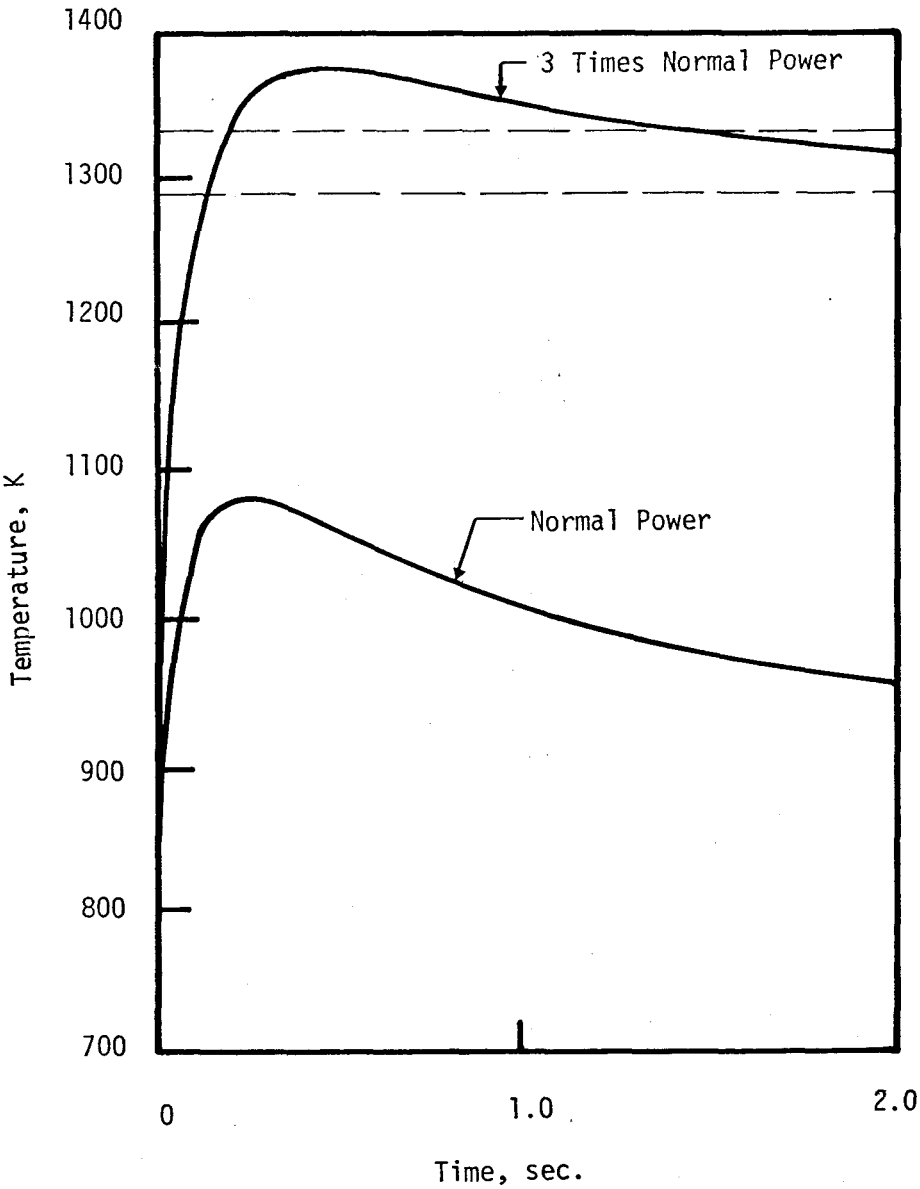

Fig.4.11 Cladding Surface Temperature at Edge of the Blockage as a function of time for a Normal Flow Velocity of 6 meters/sec.

that at 3 times normal power conditions ($\simeq 1.75\ q_{max}$) the temperature of the cladding near the edge of the blockage can be higher than saturation temperature of sodium for a considerable period of time. The work is being continued to include the dynamics of a vapor bubble growing at the edge of the blockage to determine if continued bubble growth can be sustained.

4.5 Conclusions

1. Two different types of blockages can form when semi-molten particles hit the wire wrap and freeze, and when solid fuel particles are caught in the coolant channels.
2. The size of the blockage and the amount of fuel in each blockage strongly depends on the size of the fuel particles and the amount of fuel injected into the coolant channel.
3. The blockages formed by solid particles result in large pressure drops across the blockages. The pressure drop is correlated with the dynamic head.
4. Under certain accident conditions, it is possible that the freezing of semi-molten fuel on the wire wrap may lead to melting and moving of the wire wrap.
5. A possibility of boiling at the corners of the cladding and the fuel exists. Calculations for the positive feedback reactivity due to the presence of in-channel blockages and boiling need to be performed.

4.6 References for Chapter 4.0

1. Boudreau, J. and J. F. Jackson, "Re-Criticality Considerations in LMFBR Accidents," Proc. of the Conference on Fast Reactor Safety, Beverly Hills, California, April 1974.

2. Jackson, J. F. et.al., "Trends in LMFBR Hypothetical Accident Analysis," Proc. of the Conference on Fast Reactor Safety, Beverly Hills, California, April 1974.

3. Wright, A. E., "Transient Overpower Test H4,ANL/RAS 74-30, November 1974.

4. Wright, A. E. et.al., "Transient Overpower Test H5 on FFTF-Type Intermediate Power Fuel," ANL/RAS 75-2, June 1975.

5. Rothman, A. B., C. E. Dickerman, R. K. Lo, R. G. Palm, L. A. Semenza, and H. U. Wider, "Results of Recent TOP and LOF Experiments in TREAT," Proceedings of International Meeting on Fast Reactor Safety and Related Physics, Chicago, Illinois, Vol. IV, p. 1625, 1976.

6. Bojarsky, E., H. Deckers, H. Drexler, S. Gross, H. Lehning, D. Piel, and H. Reiser, "Effects of Sodium Interaction in TOP Tests with Electrically Heated Fuel Pins," Proceedings of International Meeting on Fast Reactor Safety and Related Physics, Chicago, Illinois, Vol. IV, p. 1896, 1976.

7. Preliminary Safety Analysis Report, Clinch River Breeder Reactor, Project Management Corporation, 1975.

8. Dhir, V. K., K. W. Wong, and W. E. Kastenberg, "Mechanistic Study of Fuel Freezing and Channel Plugging During Fast Reactor Overpower Excursions," UCLA-ENG-7679, University of California, Los Angeles, August 1976.

9. Wong, K. W., V. K. Dhir, and W. E. Kastenberg, " A Study of Fuel Freezing and Channel Plugging During Hypothetical Overpower Transients," Proceedings of International Meeting on Fast Reactor Safety and Related Physics, Vol. IV, p. 1757, 1976.

10. Wong, K. W., "A Mechanistic Study of Fuel Freezing, Channel Plugging and Continued Coolability During Fast Reactor Overpower Excursions, NUREG-0310, July 1977.

11. Schultheiss, G. F., "Analysis of the Formation of Local Coolant Blockages in Sodium-Cooled Fast Breeder Reactors," EURFRN-1394, September 1976.

5.0 POTENTIAL FOR RECRITICALITY

5.1 Introduction

Core-disruptive accidents are usually assumed to be initiated by either a loss of flow (pump coast-down) or transient overpower accident (reactivity insertion) accompanied by failure to scram. Such accidents are generally characterized as energetic events and usually are assumed to occur on short-time scales. Because of the relative importance of different physical phenomena as well as computational convenience, the analysis of these accidents is carried out in various phases: predisassembly, disassembly, work-energy and post accident heat removal.

Increased understanding of the physical phenomena during the disassembly phase has resulted in the addition of a transition phase (between disassembly and work energy) for the loss-of-flow accident [1,2]. Some of the factors contributing to the inclusion of this transition phase are: 1) incoherencies in the disassembly leading to a less energetic hydrodynamic disassembly, 2) the prediction of the formation of plugs in the upper and lower axial blankets following the disassembly, and 3) the potential for recriticality should these plugs result in movement of fuel towards the core midplane. In the latter case, recriticality might be caused by fuel plugs re-melting, or by a change in heat transfer modes within the "bottled up" core.

Concurrent with studies of this transition phase is the study of alternate-accident scenarios. In particular, those with a slow progression of melting, but ultimately leading to core disassembly. Examples are the loss of heat sink accident [3] (with scram) and the

pipe-break accident (with and without scram) [4]. For these cases, some of the physical phenomena may be similar to that encountered in the transition phase for the loss-of-flow accident; e.g., the considerations for boiled-up mixtures.

For the transient overpower accident, scenarios can be envisioned which can lead to non-coolable conditions with resultant fuel melting, reconfiguration and potential criticality. One such scenario, that of local blockage formation followed by reduced coolability, was discussed in Chapter 4.0.

In this Chapter, the question of a transition phase for the transient overpower accident is discussed. First, some general aspects of scenarios which can lead to a recriticality are presented. This is followed by some criticality calculations for various reactor core re-configurations.

5.2 The Transition Phase for the TOP

As described in Chapter 3.0, fuel failures at or near the core midplane usually result in an energetic disassembly. This occurs because initial fuel motion is directed towards the midplane and the initial sodium voiding is at the core midplane. The positive reactivity ramp rates are large enough to cause a hydrodynamic disassembly [5-7].

Fuel failures which occur high in the core result in initial fuel motion which results in large negative reactivity ramp rates. Sodium voiding contributes very little neutronically because the initial voids occur near the top of the core where the worth is changing sign. If fuel sweepout is postulated and if the coolant flow is re-established, the accident is benign with little core

disruption expected to occur. The postulated sweepout causes neutronic shutdown.

As discussed in Chapter 4.0, recent experimental and theoretical evidence indicates that fuel blockages are a distinct possibility following fuel pin failure. This can result in the following:

1) less negative reactivity due to fuel motion is available for shutdown.
2) inadequate cooling may result causing remelting of the plug and/or further melting of intact clad and fuel in the core, and
3) collapse of the fuel plugs or fuel pins causing recriticality.

Such a series of events can be termed one type of transition phase for the transient overpower accident. Another type of transition phase may be initiated by a very mild transient overpower accident. As pointed out previously [8], initiating ramp rates between 1¢/sec and 10¢/sec cause failure to occur between 80 sec and 10 sec. Since the control rod being withdrawn is worth $3.20, there is still $2.00 left to be inserted. The amount of reactivity due to fuel sweepout in these cases is usually only about $2.00. Therefore, there is potentially a chance for a second overpower; this time beginning with a partially disrupted core which is subcritical.

In this case, more fuel failures would be required to occur. The time for these subsequent failures may be quite large, when compared with the first failures. For the 10¢/sec initiating ramp, the time to first failure is 12 seconds, while the time to subsequent failure is estimated to be 21 seconds. This may be ample time for a

transition phase to develop as well.

5.3 Potential Recriticality of a Disrupted Geometry

In an unprotected overpower transient or loss-of-flow accident, following the initiation phase, there may be a disrupted core geometry containing the molten pool of PuO_2 - UO_2. It is of interest to examine the potential for recriticality of a partially disrupted core geometry. Before attempting a coupled neutronics-hydrodynamics calculation which is likely to be time consuming, it is of interest to examine the range of criticality in a static manner. Based upon heat transfer calculations, various configurations can be postulated and static k-effective calculations made. In the present study, the potential for recriticality of a partially disrupted cylindrical geometry, in which there is a molten pool of UO_2 - PuO_2 in the central region, and extending radially up to a certain distance depending upon the number of rings of the molten subassemblies, is examined.

The pool extends axially from the bottom of the core geometry up to a certain height. The geometry of the disrupted core is two-dimensional as shown in Figure 5.1.

The recriticality calculations were made first with an approximate model using the one-dimensional diffusion code CAESAR and then with the two-dimensional diffusion code DIF2D.

One Dimensional Diffusion Calculations Using CAESAR

A series of one-dimensional (radial), multigroup diffusion calculations were performed. The k-effective of the partially disrupted geometry was calculated as a function of the number of molten rings of subassemblies, the amount of void present in the molten pool

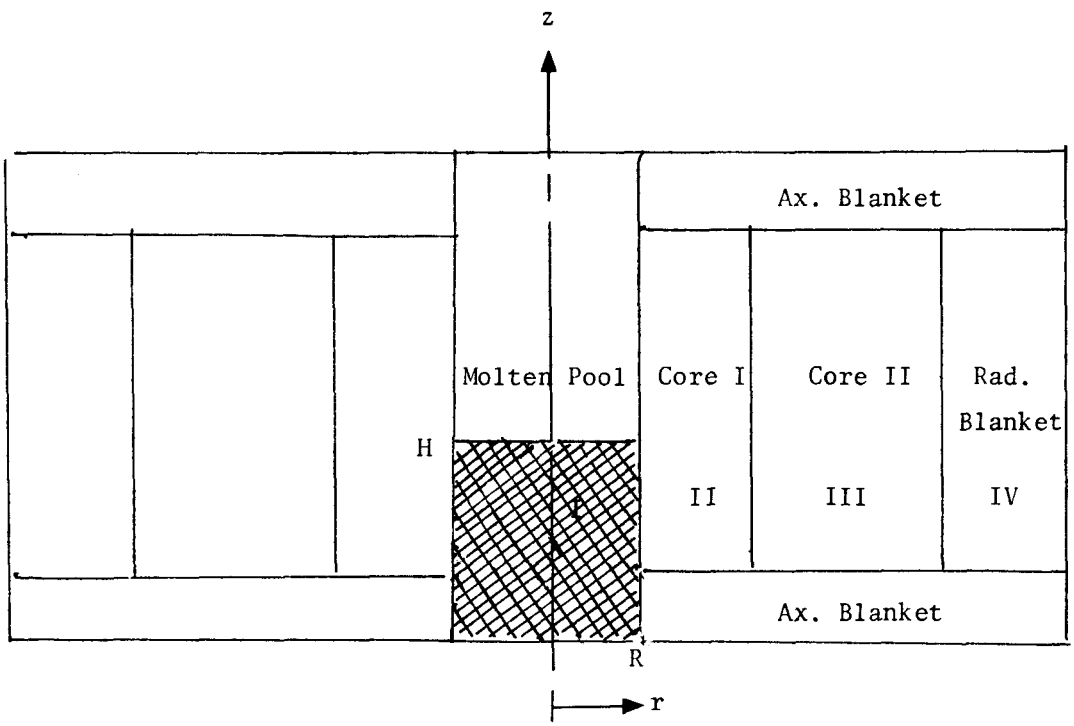

Figure 5.1 Partially Disrupted Core Geometry for Recriticality Studies.

and the height of the molten pool. In addition, calculations with and without molten steel were made.

Since the geometry is essentially two-dimensional (r-z), the axial leakage is accounted for by a radial dependent transverse buckling, Bz. For those radial regions, which had the intact geometry, the transverse leakage of the critical assembly was employed. For those radial regions, which have a molten pool, the transverse buckling is assumed to be

$$B_z^2 = (\pi/H)^2$$

where H is the height of the molten pool. The value of H was determined by conserving mass in the core and taking into account any void space present (i.e., should boiling occur). It should also be noted that the fission products were not accounted for neutronically (as in a Beginning of Life Core), except for the void space which could be considered to be trapped gaseous fission products if boiling does not occur.

For a Beginning of Life CRBR core configuration without poison, first a criticality search was made on the transverse buckling, while preserving radial dimensions. The steady state transverse buckling (in the axial direction) was obtained as $B_z^2 = 1.2759 \times 10^{-3}$ cm^{-2}.

Next, a series of one-dimensional k-effective calculations were made for the geometry of the CRBR with four regions. Region I contains molten UO_2 - PuO_2 with/without molten steel and/or voids and it radially extends up to a radius R, depending upon the number of rings of fuel subassemblies that are molten. It has a height H. Regions II, III and IV have the steady state compositions (i.e., Core I, Core II and

radial blanket, respectively) of the intact part of the core geometry.

Results of the Criticality Calculations for the One-Dimensional Model Using CAESAR.

In all calculations, since they are one-dimensional, an approximation is made for the transverse buckling, Bz. First, k-effective calculations were made using the steady state value of transverse buckling, Bz (1.2759×10^{-3} cm^{-2}) in all the four regions. Calculations were made for the different number of rings of molten subassemblies (i.e., different values of R, the radial extent of the molten pool) and the values are tabulated in Table 5.1. No steel or void were assumed to be present in the molten region.

Table 5.1

No. of Rings	2	4	6	8
k-eff	1.024	1.1219	1.2966	1.5424

The above calculations were then repeated for different heights H of the molten region (I) with transverse buckling in region I taken as $(\pi/H)^2$, while in other regions keeping the steady state value of the transverse buckling. The values are tabulated in Table 5.2 as a function of the number of rings of molten subassemblies.

Table 5.2

Height H (cm) \ No. of Rings	2	4	6	8
63.75	1.014	1.0906	1.2311	1.4408
50	1.0028	1.054	1.155	1.3240
40	0.988	1.0087	1.0625	1.1814
33	0.972	0.9605	0.9652	1.0332
30	0.9629	0.9339	0.9122	0.9532

Note that the k-effective values decrease as the height H of the molten pool is decreased. This is so, because with the reduced height H, the transverse leakage $B_z^2 \left[= \left(\pi/H\right)^2 \right]$ is larger in the molten pool and consequently k-effective is smaller. The trend of k-effective vs. the no. of rings of molten subassemblies (i.e., value of R) is not very clear, but in general we observe that if the geometry is supercritical (keff. > 1), then k-eff. increases with R and if it is subcritical, then it decreases with R. Thus, increasing the radial extent of the molten pool makes the geometry more supercritical or subcritical, if it is already so.

For a molten pool of PuO_2 - UO_2 with the composition of the steady state core I enrichment, the critical axial height for an infinite (radially) molten pool was determined to be 33 cms. The critical height of molten pool of PuO_2 - UO_2 with steady state volume fraction of steel present in it, was determined to be 48.4 cms.

Finally, the calculations were made to evaluate the effect of presence of voids and steel. Two cases were considered.

Case (i) Molten pool having 17.7% enrichment and a height of 35 cm. (i.e. active core)

Case (ii) Average (core and axial blanket) enrichment of 12.84% and a height of 49 cm.

For these two cases, calculations were made for k-effective in the presence of void, with 4 and 6 rings of molten subassemblies as follows:

a) 25% void with original height H

b) 50% void with original height H

c) 50% void with twice the height 2H

Note that cases a) and b) correspond to 25% and 50% of fuel, respectively, having blown out of the core, while in the case of c) the amount of fuel is conserved.

These calculations were repeated with steel present in the molten pool and the height H and the volume fractions adjusted accordingly. In all the cases, the height of the molten pool was never allowed to exceed that which gave the steady state transverse leakage. The results are tabulated in Table 5.3.

From this study, the following trends are observed. Without molten steel, the multiplication factor goes from sub- to super-critical at molten pool heights of 45 to 35 cms as the number of molten rings goes from 2 to 8. (The undisturbed active core height is 90 cms and has ten rings). Conservation of mass yields a height of 35 cms if the active core is allowed to melt and fill up the subassembly.

The criticality calculation is not sensitive to the void fraction if fuel is conserved. If fuel is assumed to be removed (i.e., blown off), then the presence of voids makes the core sub-critical. The addition of steel increases reactivity provided the height is increased conserving the mass. This has the effect of decreasing leakage. If the height is not increased, the parasitic absorption in steel causes the reactivity to decrease.

The calculations were made with one-dimensional diffusion theory and the values of k-effective. Hence, the exact transverse buckling in the molten pool is not known. In particular, if the steady state value of the transverse buckling is used for the molten

Table 5.3

Void Fraction \ No. of Rings	Case (i) 4 w/o Steel	Case (i) 4 with Steel	Case (i) 6 w/o Steel	Case (i) 6 with Steel	Case (ii) 4 w/o Steel	Case (ii) 4 with Steel	Case (ii) 6 w/o Steel	Case (ii) 6 with Steel
0% void orig. height	0.9760	1.0106	0.9964	1.0696	0.9873	0.99185	1.0222	1.03221
a	0.8975	0.9587	0.8385	0.96078	0.9339	0.96283	0.9124	0.97017
b	0.7869	0.8733	0.6214	0.78019	0.8444	0.90838	0.7292	0.85031
c	0.9763	0.9477	0.9967	0.9353	0.9871	0.90838	1.0223	0.85031

pool as in other regions, the values shown in Table 5.1 for the k-effective are obtained, which are the upper limits of their respective values since the transverse leakage is smallest. In the following section, we will see the results of some studies made for the partially disrupted geometry using a two-dimensional, multigroup diffusion theory code D1F2D.

Two-Dimensional Diffusion Calculations Using D1F2D

Two-dimensional multigroup diffusion code D1F2D was obtained from Argonne National Laboratory along with ENDFIV based, 27-group cross-section set library. The diffusion code package was incorporated into the UCLA computer system and it was checked successfully by doing criticality search of some sample geometries and checking the values obtained against those calculated using other methods.

The k-effective values were then recalculated (of those geometries containing molten pool of UO_2 - PuO_2), which were calculated before using the CAESAR code. We started with a BOL core and the intact geometry of the CRBR. First, we did a criticality search on the Boron poison in the inner core region of the reactor. The k-effective value of the resulting composition (after the Boron search), was obtained as 0.99882, which was taken as the starting, steady state k-effective value.

Next, we calculated the multiplication factor of a geometry with a molten pool of UO_2 - PuO_2 extending radially up to four rows of subassemblies (46.1 cms) and axially up to 63.0 cms in height, which contained the steel present in the original composition of the inner core. No void was considered to be present. The k-effective

value obtained was 1.01490, or the net k-effective above the steady state was [1.01490 - (1.00000 - 0.9882)] = 1.01608. The corresponding value obtained using the one-dimensional code CAESAR (and the approximate transverse buckling) was k-eff. = 1.0106 (see Table 5.3). The difference between the two calculated values is observed to be less than 0.6% for this case.

Next, we made a series of calculations for a similar geometry of a molten pool extending up to four rows of subassemblies (46.1 cms radially) to evaluate the effect of voids present. We repeated the calculations done before using CAESAR and tabulated in Table 5.3, entries a and b. In Table 5.4, we compare the values obtained by approximate one-dimensional calculation using CAESAR and the two-dimensional calculation using D1F2D.

Table 5.4

Void Fraction	CAESAR	D1F2D	(% Difference)
0% void	1.0106	1.01608	- 0.54%
25% void (a)	0.9587	0.91852	4.37%
50% void (b)	0.8733	0.90417	- 3.41%
75% void	—	0.89799	—

For no void present, the values differed by about 0.54%, while for the cases with 25% and 50% voids, the values differed by 4.37% and 3.41%, respectively, indicating a large deviation. One more calculation was made with the D1F2D code for 75% void fraction in the molten pool. In all cases, the heights of the molten pool were adjusted to conserve the fuel mass, but not exceeding the height of

the steady state core. The k-effective value for 75% void present was observed to be 0.89799, thus indicating a levelling-off of the k-effective value versus the % void in the molten pool.

Conclusions and Remarks

From the values tabulated in Table 5.4, it appears that it is worthwhile doing the more accurate, even though time consuming and expensive, two-dimensional diffusion calculations, since the values obtained by the approximate one-dimensional calculation can be off by as much as 5%.

Since the geometry and composition of the molten pool depends very much on such phenomena as the heat transfer to the solid steel wall surrounding the molten pool, absence or presence of a solid UO_2 crust, etc., the recriticality computations must be done in conjunction with the hydrodynamics and heat transfer calculations.

The Effect of Presence of Concrete on Recriticality

Finally, one set of calculations were done to determine the effect of hydrogen present in the concrete (in the form of H_2O) on the k-effective values of a molten pool surrounded by concrete.

Several calculations were made with varying percentage of H_2O present in the concrete and for varying percentage of concrete present in the molten pool for a simple slab geometry with two regions, one of molten UO_2 - PuO_2 (+ concrete) and the other of concrete. Calculations were done using the CAESAR code and Na (sodium) cross-sections were used for Ca and Mg. It was observed that the presence of H_2O had a substantial effect on the k-effective of the assembly. For the presence of 5-10% of H_2O in concrete, the difference in k-effective,

Δk was observed to be 5-25% of the value without H_2O. Since hydrogen acts as a moderator and thermalizes neutrons, the effect of its presence is to increase the k-effective value. Since the presence of hydrogen has a substantial effect on the recriticality of the assembly, it is imperative to make calculations taking into account hydrogen.

5.4 References for Chapter 5.0

1. Jackson, J. F. and J. E. Boudreau, "Trends in LMFBR Hypothetical Accident Analysis," Proc. ANS Fast Reactor Safety Conference, Beverly Hills, California CONF-740401, p. 1241, April 1974.

2. Majumdar, D. "A Review of the Transition Phase of Core-Disruptive Accidents in LMFBR's," BNL-NUREG-21797, August 1976.

3. Chan, C. K., T. K. Min and D. Okrent, "A Look at Alternate Core Disruption Accidents in LMFBR's," U.S. Nuclear Regulatory Commission, NUREG-0259, May 1977.

4. Bari, R. A., M. A. Klenin, W. T. Pratt, and Y. H. Sun, "Preliminary Assessment of the Meltdown Progression of the Loss of Heat Sink Accident with Scram in the Liquid Metal Fast Breeder Reactor," BNL-NUREG-23137, August 1977.

5. Heusener, G., G. Kessler, et. al., "Analysis of Hypothetical Accidents for SNR-300," KFK-1834, Nuclear Research Center, Karlsruhe, West Germany, September 1973.

6. Kuczera, B. and P. Royl, "Application of Different Failure Criterion in Fuel Pin Modelling and Consequences for Overpower Transients in LMFBR's," Proc. of the 3rd SMIRT Conference, London, England, September 1975.

7. Kastenberg, W. E. and M. Frank, "Preliminary Analysis of the Transient Overpower Accident for CRBRP," University of California, School of Engineering and Applied Science, UCLA-ENG-7557, July 1975.

8. Kastenberg, W. E., "LMFBR Fuel Analysis Task A: Oxide Fuel Dynamics," Final Report. USNRC,NUREG-0146, January 1977.

Blank Page

6.0 CONCLUSIONS

This report summarizes the results of studies conducted in support of the US Nuclear Regulatory Commission's review of the PSAR for the CRBRP. In particular, it deals with several areas of uncertainty in the analysis of the unprotected transient overpower accident (TOP). These areas of uncertainty include the time, place, and mode of fuel pin failure and several physical phenomena associated with transient overpower accidents initiated by slow or mild ramp rates. These include pre-failure fuel motion; fuel freezing, plugging, and plate-out following pin failure; and the potential for re-criticality.

A model for the calculation of pre-failure fuel motion for GCFR mixed oxide fuel pins with a prefabricated central void was modified for CRBRP-type fuel pins. The results of a set of single pin parametric studies indicate that internal fuel motion is more pronounced for slower heat-up rates. In addition, internal fuel motion is more pronounced for lower burnups.

Two fuel pin failure models were examined in this work. In the first, the "strain failure" criterion developed at PNL was fully implemented into the HOPE computer code at UCLA. The second was an extension of Sun's work on the calculation of steady-state stress and strain to the transient case. As a result of the first effort, it was concluded that the strain-failure model is not useable in its present form. This is because the curve-fits to the data are obtained from a limited number of experimental data points; therefore, the curves exhibit erratic and unrealistic behavior.

Using the extension of Sun's model for CRBR-type fuel pins, it was concluded that (a) the time of clad failure is governed by the time to

reach clad yielding when the Tresca yield and permanent deformation failure criteria are used, (b) clad pre-stressing due to irradiation is a secondary factor in determining failure location and time, (c) pre-stressing produces a trend away from midplane failure because the steady-state stresses at the axial extremities of the core are greater than those at the midplane, and (d) the transient-induced stresses tend to be larger at the midplane than at the axial extremities, thus tending to overcome the effects of the steady-state stress distribution.

Fuel freezing, plugging, and plate-out were also considered in this report. A description of the type of blockages that may be formed by the freezing of semi-molten fuel particles on the wire wrap, or when completely solidified particles get caught in the coolant channel, was presented. The amount of fuel and the length of the blockages were found to significantly depend on the size of the fuel particles and the amount of fuel injected into the coolant channel. The pressure drop across a blockage formed by solid particles was experimentally observed to be proportional to the dynamic head. The hydraulic and thermal coolant channel conditions leading to melting of the wire wrap when semi-molten fuel particles freeze on the wire wrap have been parametrically studied.

The results of the parametric calculations show that a good possibility of melting and relocation of the wire wrap under TOP conditions exists. For in-place coolable blockages the thermal loading on the cladding has also been studied and it is concluded that a possibility of the initiation of boiling at the corners of the blockages and the cladding exists. The reactivity feedback effect of the blockages and re-voiding of the channels during the progress of a transient overpower accident will be studied in the coming year.

Lastly, the potential for re-criticality in disrupted cores was considered. Several configurations were examined to determine the circumstances under which a molten core could reconfigure. It was shown that in the absence of molten steel, the multiplication factor goes from sub- to super-critical at molten pool heights of 45 to 35 cm as the number of molten rings goes from 2 to 8. The criticality calculation did not appear to be sensitive to voids if fuel was conserved. The addition of steel increases the reactivity provided that the height of the pool is increased, thereby conserving fuel mass. This has the effect of decreasing leakage. If the height is not increased, the parasitic absorption in steel dominates and causes a decrease in reactivity.

Several calculations for molten fuel-concrete mixtures were made. The major effect on the calculation was the amount of water present in the concrete. In the absence of the "mechanistic" value of water present, these calculations were not continued.